

Higher Fullerenes – Isolation, Halogenation and Structural Studies

Von der Fakultät Chemie der Universität Stuttgart
zur Erlangung der Würde eines Doktors der Naturwissenschaften (Dr.rer.nat)
genehmigte Abhandlung

Vorlegt von

Kalin Simeonov

aus Sofia
Bulgarien

Hauptberichter: Prof. Dr. M. Jansen

Mitberichter: Prof. Dr. T. Schleid

Tag der Prüfung: 02.04.2009

Max-Planck-Institut für Festkörperforschung, Stuttgart
2009

*Es gibt keinen Menschen der alles kann,
sowie es keinen gibt, der nichts kann.*

Table of Contents

1 Zusammenfassung	10
2 Abstract	15
3 General Introduction to the Fullerene Phenomenon	20
4 General Part	24
4.1 Methods and Equipment	24
4.1.1 Fullerene Production	24
4.1.2 Fullerene Extraction	28
4.1.3 Fullerene Separation - High Performance Liquid Chromatography	30
4.1.3.1 Basic Concepts of HPLC	30
4.1.3.2 Columns and Column Packings	37
4.1.3.3 Stationary Phase Selection – Motivation and Justification	39
4.1.3.4 HPLC Equipment	43
4.1.3.5 Special HPLC Operation Techniques	44
4.2 Analytic Methods – Characterization of Pristine Fullerenes and Fullerene Derivatives	46
4.2.1 Ultraviolet-Visible Spectrophotometry	46
4.2.1.1 Principles of UV/VIS Spectrophotometry	46
4.2.1.2 Spectrophotometers – the Design of HPLC Spectrophotometric Detectors	51
4.2.1.3 Light Absorption and Fullerenes	53
4.2.2 Matrix Assisted Laser Desorption Ionization – Time of Flight Mass Spectrometry	54
4.2.2.1 Theory behind the Time of Flight Analysis	55
4.2.2.2 Set-up of the Time of Flight Mass Spectrometer	57
4.2.3 Single Crystal X-ray Diffraction	58

4.2.3.1 Fundamental Relationships	59
4.2.3.2 Instrumentation	59
4.2.3.3 Data Collection and Results Presentation	61
4.3 Computations	62
4.3.1 Density Functional Theory	62
4.3.2 Hartree-Fock Method	63
4.3.3 Moeller-Plesset Perturbation Theory	64
4.3.4 Coupled Cluster Methods	64
5 Special Part	66
5.1 Opening Remarks	66
5.2 Isolation of Parent Fullerene Species – “Classical” and Alternative Approaches	68
5.2.1 Introduction	68
5.2.2 Isolation of D ₂ -C ₇₆ (1)	70
5.2.3 Isolation of D _{3h} -C ₇₈ (5), D ₂ -C ₈₀ (2), C ₂ -C ₈₄ , C _s -C ₈₄ (14), D ₂ -C ₈₄ and D _{2d} -C ₈₄ – Introduction of a New Mobile Phase for the Separation of Fullerene Species	71
5.2.4 An Alternative Route towards the Preparative Isolation of the Fullerene Isomers – D ₃ -C ₇₈ (1), C _{2v} -C ₇₈ (2) and C _{2v} -C ₇₈ (3)	75
5.2.4.1 Short Introduction to C ₇₈ -fullerenes – the First Multimembered Fullerene Family	75
5.2.4.2 Synthetic Approach towards the Chromatographic Isolation of Bulk Amounts of C ₇₈ -fullerene Isomers	76
5.2.4.3 The Motivation behind the Newly Developed Alternative Methodology	77
5.2.5 C ₂ -C ₈₂ – a Facile Route for Its Isolation	82
5.2.6 Conclusion	85
5.3 Structural Studies of Highly Chlorinated Fullerene Derivatives	86
5.3.1 Short Introductory Remarks	86

5.3.2 C₇₆(1)Cl₁₈.TiCl₄ – Structure Determination of the Chlorine Derivative of the Chiral D₂ Isomer of C₇₆	87
5.3.2.1 Synthetic Procedure	87
5.3.2.2 Crystallographic Data	87
5.3.2.3 Molecular Packing, Bond Distances and Aromatic Structure Formation	88
5.3.3 Crystal Structures of C₇₈(2)Cl₁₈.Br₂.TiCl₄, C₇₈(3)Cl₁₈, C₇₈(5)Cl₁₈	97
5.3.3.1 Synthesis of the Fullerene Halides	97
5.3.3.2 Crystallographic Data	98
5.3.3.3 Structural Features, Constitution Patterns and Extended Channels Formation	99
5.3.4 Crystal Structure of C₈₀(2)Cl₁₂	108
5.3.4.1 Synthetic Procedure	109
5.3.4.2 Crystallographic Data	109
5.3.4.3 C ₈₀ Cl ₁₂ – Structure Description	109
5.3.5 An Empirical Rationale of Halogen Atoms Addition Pattern in Higher Fullerenes	113
5.3.5.1 Steric Strain in Fullerenes	114
5.3.5.2 Addition Pattern of Chlorine Atoms in Higher Fullerenes	117
5.3.6 Unusual Short Intermolecular Halogen – Halogen Contacts in Chlorinated Derivatives of Fullerenes	124
5.3.6.1 Introduction to the Phenomenon of Intermolecular Halogen Interactions	125
5.3.6.2 Short Halogen – Halogen Contacts in C ₇₆ Cl ₁₈ , C ₇₈ Cl ₁₈ and C ₈₀ Cl ₁₂	126
5.3.6.3 Quantum Chemical Calculations and Binding Energies in Model Dimers	134
5.4 Closing Remarks	137
6 Literature	140
7 Appendix	151
7.1 Isolation of Individual Fullerene Isomers – Chromatograms	151

7.2 UV/VIS Spectra	156
8 Acknowledgements	162
9 List of Publications	163
10 Curriculum Vitae	164

Abbreviations

ASE	Accelerated Solvent Extraction
BP	Buckyprep
BP-M	Buckyprep-M
CC	Coupled Cluster
DE	Dimerization Energy
DFT	Density Functional Theory
hcp	hexagonal close packing
HOMO	Highest Occupied Molecular Orbital
HPLC	High Performance Liquid Chromatography
HTP	Height of Theoretical Plate
ICCB	Inter-pentagon Carbon-Carbon Bond
IPR	Isolated Pentagon Rule
IR	Infrared (Spectroscopy)
LUMO	Lowest Unoccupied Molecular Orbital
MALDI	Matrix-Assisted Laser Desorption Ionization
MP	Moeller Plesset
MS	Mass Spectrometry
NIR	Near Infrared
NMR	Nuclear Magnetic Resonance
NP-HPLC	Normal Phase HPLC
ODS	Octadecylsilyl
PHJ	Pentagon-Hexagon Junction
POAV	π-Orbital Axis Vector
RF	Radio Frequency
RP-HPLC	Reversed Phase HPLC
THJ	Triple Hexagon Junction
TOF	Time Of Flight
UV	Ultraviolet (Spectroscopy)
VIS	Visible (Spectroscopy)
VZT	Valence Triple Zeta

1 Zusammenfassung

Die vorliegende Arbeit kann in zwei Abschnitte unterteilt werden. Im ersten Abschnitt werden die chromatographischen Methoden, Systeme und Techniken diskutiert, mit denen im präparativen Maßstab isomerenreine Fullerenarten erhalten werden können. Folgende elf Fullerenisomere wurden in größerer Menge erhalten: $D_2-C_{76}(1)$, $D_3-C_{78}(1)$, $C_{2v}-C_{78}(2)$, $C_{2v}-C_{78}(3)$, $D_{3h}-C_{78}(5)$, $D_2-C_{80}(2)$, ein C_2-C_{82} , ein C_2-C_{84} , $C_s-C_{84}(14)$, ein D_2-C_{84} und ein $D_{2d}-C_{84}$. Von diesen wurde $D_{3h}-C_{78}(5)$ erstmals isoliert und seine Bildung während des induktiven Heizens von Graphit nachgewiesen. Es werden neuentwickelte und verbesserte Chromatographiesysteme vorgestellt, um den zeit- und kostenintensiven Trennungsprozess zu erleichtern. Die folgenden Schritte und Chromatographiesysteme wurden für die verschiedenen Fullerenisomere verwendet:

$D_2-C_{76}(1)$:

Preparativer Schritt (fraktionieren):

- a) Stationäre Phase – Buckyrep (20 × 250 mm, Nacalai Tesque Inc., Kyoto, Japan) b) Mobile Phase – Toluol-Hexan (4:1) c) Flußrate – 20 ml/min d) Säulentemperatur – 20°C e) Wellenlänge – 300 nm.

Semipräparativer Schritt (recycling HPLC):

- a) Stationäre Phase – Buckyrep (10 × 250 mm) b) Mobile Phase – Toluol-Hexan (4:1) c) Flußrate – 5 ml/min d) Säulentemperatur – 20°C e) Wellenlänge – 300 nm.

$D_{3h}-C_{78}(5)$, $D_2-C_{80}(2)$, C_2-C_{84} , $C_s-C_{84}(14)$, D_2-C_{84} und $D_{2d}-C_{84}$:

Preparativer Schritt (fraktionieren):

- a) Stationäre Phase – Buckyrep (20 × 250 mm) b) Mobile Phase – Toluol-Hexan (4:1) c) Flußrate – 20 ml/min d) Säulentemperatur – 20°C e) Wellenlänge – 300 nm.

Semipräparativer Schritt (recycling HPLC):

- a) Stationäre Phase – Buckyrep (10 × 250 mm) b) Mobile Phase – Toluol-Dichlormethan (1:1) c) Flußrate – 5 ml/min d) Säulentemperatur – 20°C e) Wellenlänge – 300 nm.

C₂-C₈₂

Preparativer Schritt (fraktionieren):

a) Stationäre Phase – Buckyprep (20 × 250 mm) b) Mobile Phase – Toluol-Hexan (4:1) c) Flußrate – 20 ml/min d) Säulentemperatur – 20°C e) Wellenlänge – 300 nm.

Semipräparativer Schritt (recycling HPLC):

a) Stationäre Phase – Buckyprep-M (4.6 × 250 mm, Nacalai Tesque Inc., Kyoto, Japan) b) Mobile Phase – Toluol-Methanol (4:1) c) Flußrate – 1 ml/min d) Säulentemperatur – 15°C e) Wellenlänge – 300 nm.

D₃-C₇₈(1), C_{2v}-C₇₈(2) und C_{2v}-C₇₈(3)

Die speziell für Fullerenseparation ausgelegten stationären Phasen bieten keine ausreichende Auflösung zwischen den C₇₈-Isomeren 1 und 2. Ebenso ist die kommerziell erhältliche Octadecylsilylphase, die üblicherweise für diesen Zweck verwendet wird, äußerst ineffizient. Dies rechtfertigt die Suche nach effizienteren Methoden, die präparative Mengen dieser Fullerene zu liefern. Hier wird ein alternativer Ansatz in diese Richtung vorgeschlagen. Die einzelnen Spezies werden isoliert, indem die Ausgangsmischung der Fullerene chemisch modifiziert wird (mit ICl). Anschließend werden die Derivate in der einstufigen Basislinien-Chromatographie aufgetrennt. Die entsprechenden Fulleren-Halogenide dissoziieren thermisch, die Ausgangssubstanzen werden isomerenrein erhalten. Der systematische Ansatz wird in folgender Abfolge dargestellt:

Preparativer Schritt (fraktionieren):

a) Stationäre Phase – Buckyprep (20 × 250 mm) b) Mobile Phase – Toluol-Hexan (4:1) c) Flußrate – 20 ml/min d) Säulentemperatur – 20°C e) Wellenlänge – 300 nm.

Die präparative C₇₈-Fraction enthält alle drei Isomere (1,2 and 3)

Semipräparativer Schritt (recycling HPLC):

a) Stationäre Phase – Buckyprep (10 × 250 mm) b) Mobile Phase – Toluol-Hexan (4:1) c) Flußrate – 5 ml/min d) Säulentemperatur – 20°C e) Wellenlänge – 300 nm.

Zwei Unterfraktionen werden erhalten – Unterfraktion **I** (Mischung der Isomere 1 und 2) und Unterfraktion **II** (Reines Isomer 3)

Synthese der Fullerenhalogenide:

Die Reaktion der Unterfraktion **I** und ICl in Chlorbenzol führt zur Entstehung der Fullerenhalogenide der Isomere 1 und 2.

Semipräparativer Schritt B:

Auftrennung der Fullerenhalogenide

a) Stationäre Phase – Buckyprep (10 × 250 mm) ausgestattet mit Buckyprep-Guard (10 × 20 mm, Nacalai Tesque Inc., Kyoto, Japan) b) Mobile Phase – Toluol c) Flußrate – 5 ml/min d) Säulentemperatur – 10°C e) Wellenlänge – 300 nm.

Die Ausgangsfullerene werden durch thermische Dissoziation der Fullerenhalogenide in isomerenreiner Form erhalten.

Der zweite Abschnitt der Arbeit behandelt Einkristalluntersuchungen der Kristallstrukturen folgender Fullerenhalogenide: $C_{76}(1)Cl_{18}$, $C_{78}(2)Cl_{18}$, $C_{78}(3)Cl_{18}$, $C_{78}(5)Cl_{18}$ und $C_{80}(2)Cl_{12}$.

Kristalle von $C_{2v}-C_{76}Cl_{18}$ in $C_{76}Cl_{18} \cdot TiCl_4$:

Orthorhombisch, Raumgruppe $Pbca$

$Z = 8$

$a = 11.5543(9) \text{ \AA}$

$b = 21.2875(17) \text{ \AA}$

$c = 47.168(4) \text{ \AA}$

Kristalle von $C_{2v}-C_{78}(2)Cl_{18}$ in $C_{78}(2)Cl_{18} \cdot Br_2 \cdot TiCl_4$:

Hexagonal, Raumgruppe $P6_3/mmc$

$Z = 2$

$a = 14.6910(13) \text{ \AA}$

$c = 17.0450(21) \text{ \AA}$

Kristalle von $C_{2v}-C_{78}(3)Cl_{18}$ in lösungsmittelfreiem $C_{78}(3)Cl_{18}$:

Hexagonal, Raumgruppe $P6_3/m$

$$Z = 2$$

$$a = 13.0202(16) \text{ \AA}$$

$$c = 18.7260(51) \text{ \AA}$$

Kristalle von D_{3h} - $C_{78}(5)Cl_{18}$ in lösungsmittelfreiem $C_{78}(5)Cl_{18}$:

Hexagonal, Raumgruppe $P6_3/m$

$$Z = 2$$

$$a = 13.0551(5) \text{ \AA}$$

$$c = 18.7620(14) \text{ \AA}$$

Kristalle von D_2 - $C_{80}(2)Cl_{12}$ in lösungsmittelfreiem $C_{80}Cl_{12}$:

Monoklin, Raumgruppe $C2/c$

$$Z = 4$$

$$a = 21.043(3) \text{ \AA}$$

$$b = 11.1665(14) \text{ \AA}$$

$$c = 21.510(3) \text{ \AA}$$

$$\beta = 106.235(2)^\circ$$

Die detaillierte Analyse der Kristalle sowie die molekulare Struktur der vorgestellten Verbindungen zeigen einige interessante Merkmale.

Auf Basis sorgfältiger Untersuchungen des Additionsusters von Chloratomen an allen fünf Fullerenhalogeniden wird ein Prinzip der höheren Fullerenreaktivität vorgeschlagen. Die Stabilität der chlorinierten Fullerene und die Selektivität der Chloraddition werden mit der Abnahme der sterischen Spannung im Produkt im Vergleich zum Ausgangsstoff erklärt.

Die genaue Analyse der fünf Kristallstrukturen führte zu der Entdeckung eines interessanten Phänomens, das den Fullerenhalogeniden offensichtlich generell innewohnt. In allen Strukturen wurde eine Anzahl kurzer intermolekularer Chlor-Chlor-Kontakte gefunden (in $C_{78}(2)Cl_{18}$, Br_2 , $TiCl_4$ existieren ebenso kurze Chlor-Brom-Kontakte). Es wurde die Annahme bewiesen, dass anziehende Wechselwirkungen zwischen den Chloratomen benachbarter Fullerene existieren und es wurde eine

angemessene Erklärung zu der Natur dieser Kontakte gegeben. Quantenchemische Berechnungen, die sowohl die Natur, als auch die Größenordnung dieser anziehenden intermolekularen Wechselwirkung weiter aufklären sollen, wurden begonnen.

2 Abstract

The present work might formally be subdivided into two sections. Within the frames of the first section, the chromatographic methods, systems and techniques used in obtaining of isomerically pure fullerene species in preparative amounts are widely discussed. The following eleven fullerene isomers have been obtained in bulk amounts: $D_2-C_{76}(1)$, $D_3-C_{78}(1)$, $C_{2v}-C_{78}(2)$, $C_{2v}-C_{78}(3)$, $D_{3h}-C_{78}(5)$, $D_2-C_{80}(2)$, a C_2-C_{82} , a C_2-C_{84} , $C_s-C_{84}(14)$, a D_2-C_{84} and a $D_{2d}-C_{84}$. Among these, $D_{3h}-C_{78}(5)$ has been isolated for the first time and its formation during the inductive heating of graphite confirmed. Newly developed and improved chromatographic systems are introduced in order to facilitate the laborious and resource-consuming isolation procedures. The following stages and chromatographic systems are utilized for the different fullerene representatives:

$D_2-C_{76}(1)$:

Preparative stage (fraction collection):

a) Stationary phase – Buckyprep (20 × 250 mm, Nacalai Tesque Inc., Kyoto, Japan) b) Mobile Phase – toluene-hexane (4:1) c) Flow rate – 20 ml/min d) Column temperature – 20°C e) Wavelength – 300 nm.

Semipreparative stage (recycling HPLC):

a) Stationary phase – Buckyprep (10 × 250 mm) b) Mobile Phase – toluene-hexane (4:1) c) Flow rate – 5 ml/min d) Column temperature – 20°C e) Wavelength – 300 nm.

$D_{3h}-C_{78}(5)$, $D_2-C_{80}(2)$, C_2-C_{84} , $C_s-C_{84}(14)$, D_2-C_{84} and $D_{2d}-C_{84}$:

Preparative stage (fraction collection):

a) Stationary phase – Buckyprep (20 × 250 mm) b) Mobile Phase – toluene-hexane (4:1) c) Flow rate – 20 ml/min d) Column temperature – 20°C e) Wavelength – 300 nm.

Semipreparative stage (recycling HPLC):

a) Stationary phase – Buckyprep (10 × 250 mm) b) Mobile Phase – toluene-dichloromethane (1:1) c) Flow rate – 5 ml/min d) Column temperature – 20°C e) Wavelength – 300 nm.

C₂-C₈₂

Preparative stage (fraction collection):

- a) Stationary phase – Buckyprep (20 × 250 mm) b) Mobile Phase – toluene-hexane (4:1)
- c) Flow rate – 20 ml/min d) Column temperature – 20°C e) Wavelength – 300 nm.

Semipreparative stage (recycling HPLC):

- a) Stationary phase – Buckyprep-M (4.6 × 250 mm, Nacalai Tesque Inc., Kyoto, Japan)
- b) Mobile Phase – toluene-methanol (4:1) c) Flow rate – 1 ml/min d) Column temperature – 15°C e) Wavelength – 300 nm.

D₃-C₇₈(1), C_{2v}-C₇₈(2) and C_{2v}-C₇₈(3)

The inability of the specially designed for fullerene separation stationary phases to provide reasonable resolution between C₇₈ isomers 1 and 2, as well as the inefficiency of the commercially available octadecylsilyl phases commonly used for that purpose have justified the search for more efficient methodologies capable of delivering preparative amounts of these two fullerenes. Herein, an alternative approach in this direction is suggested. The isolation of the individual species is achieved through chemical modification (with ICl) of the initial fullerene mixture followed by the one-step baseline chromatographic separation of their derivatives. Through thermal dissociation of the respective fullerene halides, the parent species are obtained in isomerically pure form. The systematic procedure is represented by the following sequence:

Preparative stage (fraction collection):

- a) Stationary phase – Buckyprep (20 × 250 mm) b) Mobile Phase – toluene-hexane (4:1)
- c) Flow rate – 20 ml/min d) Column temperature – 20°C e) Wavelength – 300 nm.

The preparative C₇₈-fraction contains all three isomers (1,2 and 3)

Semipreparative stage A (recycling HPLC):

- a) Stationary phase – Buckyprep (10 × 250 mm) b) Mobile Phase – toluene-hexane (4:1)
- c) Flow rate – 5 ml/min d) Column temperature – 20°C e) Wavelength – 300 nm.

Two subfractions are obtained – subfraction **I** (mixture of isomers 1 and 2) and subfraction **II** (pure isomer 3)

Synthesis of fullerene halides:

A reaction between subfraction **I** and ICl in chlorobenzene results in the generation of the fullerene halides of isomers 1 and 2.

Semipreparative stage B:

Separation of fullerene halides

a) Stationary phase – Buckyprep (10 × 250 mm) equipped with Buckyprep-Guard (10 × 20 mm, Nacalai Tesque Inc., Kyoto, Japan) b) Mobile Phase – toluene c) Flow rate – 5 ml/min d) Column temperature – 10°C e) Wavelength – 300 nm.

The parent fullerenes are obtained in isomerically pure form through thermal dissociation of the respective fullerene halides.

The second section of the present work deals with the single crystal X-ray studies of the crystal structures of the following fullerene halides: $C_{76}(1)Cl_{18}$, $C_{78}(2)Cl_{18}$, $C_{78}(3)Cl_{18}$, $C_{78}(5)Cl_{18}$ and $C_{80}(2)Cl_{12}$.

Crystals of C_{2v} - $C_{76}Cl_{18}$ in $C_{76}Cl_{18} \cdot TiCl_4$:

Orthorhombic, space group $Pbca$

$$Z = 8$$

$$a = 11.5543(9) \text{ \AA}$$

$$b = 21.2875(17) \text{ \AA}$$

$$c = 47.168(4) \text{ \AA}$$

Crystals of C_{2v} - $C_{78}(2)Cl_{18}$ in $C_{78}(2)Cl_{18} \cdot Br_2 \cdot TiCl_4$:

Hexagonal, space group $P6_3/mmc$

$$Z = 2$$

$$a = 14.6910(13) \text{ \AA}$$

$$c = 17.0450(21) \text{ \AA}$$

Crystals of C_{2v} - $C_{78}(3)Cl_{18}$ in solvent free $C_{78}(3)Cl_{18}$:

Hexagonal, space group $P6_3/m$

$$Z = 2$$

$$a = 13.0202(16) \text{ \AA}$$

$$c = 18.7260(51) \text{ \AA}$$

Crystals of D_{3h} - $C_{78}(5)Cl_{18}$ in solvent free $C_{78}(5)Cl_{18}$:

Hexagonal, space group $P6_3/m$

$$Z = 2$$

$$a = 13.0551(5) \text{ \AA}$$

$$c = 18.7620(14) \text{ \AA}$$

Crystals of D_2 - $C_{80}(2)Cl_{12}$ in solvent free $C_{80}Cl_{12}$:

Monoclinic, space group $C2/c$

$$Z = 4$$

$$a = 21.043(3) \text{ \AA}$$

$$b = 11.1665(14) \text{ \AA}$$

$$c = 21.510(3) \text{ \AA}$$

$$\beta = 106.235(2)^\circ$$

Detailed analyses of the crystal, as well as the molecular structures of the reported compounds have shown some interesting features.

On the basis of careful examinations of the addition patterns of chlorine atoms in all five fullerene halides, a proposal of a principle of higher fullerene reactivity has been made. The stability of the chlorinated fullerenes, as well as the selectivity of chlorine addition is explained by the relief in steric strain in the products compared to that in the parent species.

The thorough analyses of the five crystal structures have resulted in the discovery of an interesting phenomenon apparently intrinsic to fullerene halides in general. The presence of numerous short intermolecular chlorine-chlorine contacts has been encountered in all structures (in $C_{78}(2)Cl_{18} \cdot Br_2 \cdot TiCl_4$ also short chlorine-bromine contacts exist). The assumption that attractive interactions between the chlorine atoms belonging to neighboring fullerene molecules exist has been proven and a reasonable explanation for the contacts' nature given. Quantum chemical calculations aiming at further elucidation

of the nature, as well as the magnitude of these attractive intermolecular forces have been initiated.

3 General Introduction to the Fullerene Phenomenon

Certainly, one of the most exciting and important to humankind chemical elements is carbon. Until recently, for synthetic chemists, elemental carbon as starting material had played a minor role. This situation changed dramatically when the family of known allotropes of carbon, graphite and diamond became enriched by another member - the fullerenes. In contrast to graphite and diamond with their extended solid state structures, fullerenes are spherically shaped molecular species detectable in solutions as well as in the gas phase (Figure 1).

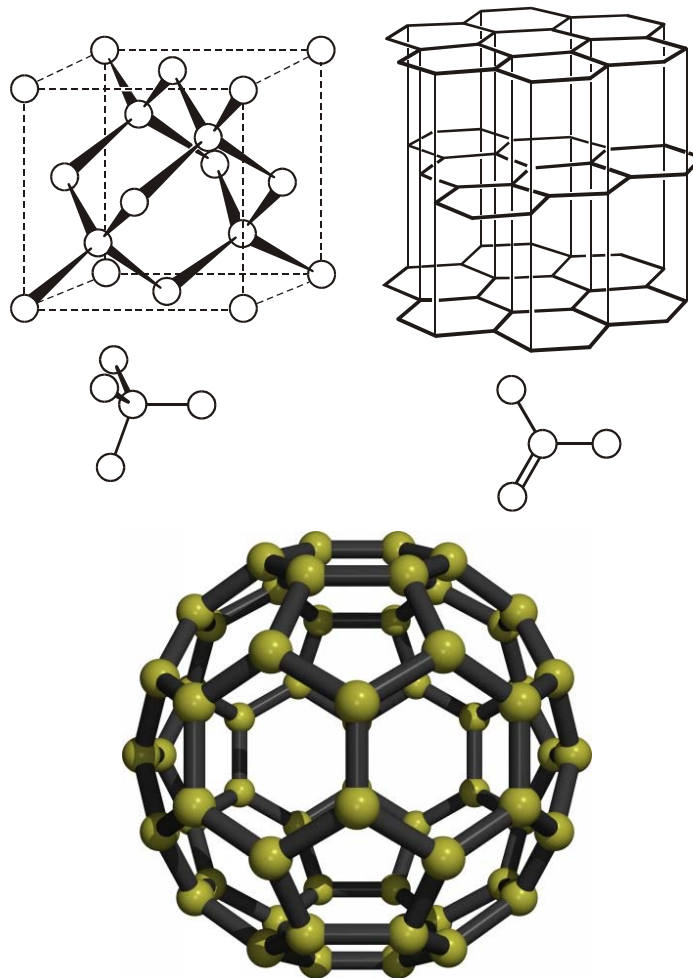


Figure 1 Different allotropic modifications of carbon: Diamond with its sp^3 hybridized carbon atoms, graphite (sp^2 hybridized carbon atoms in each layer) and C_{60} fullerene

The fullerene molecules are closed-shell all-carbon bodies containing only pentagons (exactly 12) and hexagons (see Figure 2). Hollow-cage molecules were mentioned for the first time as long ago as 1966.^[1] A number of theoretical speculations on the rationality of even-numbered all-carbon frameworks based on the truncated polyhedra followed over the next decades.^[2-4]

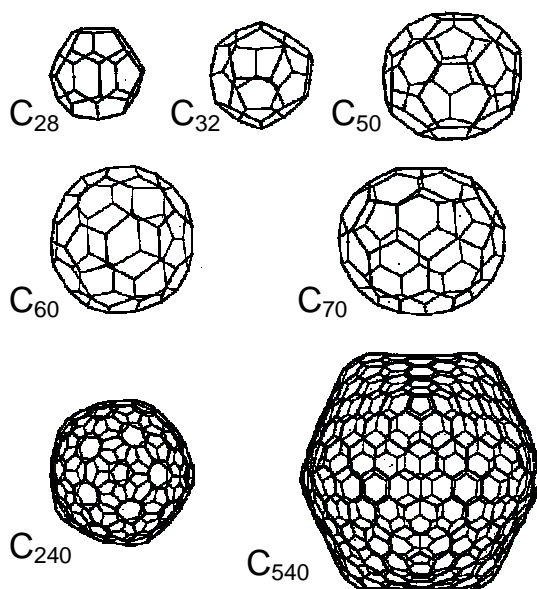


Figure 2 Different fullerene representatives

The first experimental evidence of the existence of such a molecular species, a closed-cage molecule consisting of sixty carbon atoms, came together with the proposal of its structure by Kroto, Heath, O'Brien, Curl, and Smalley in 1985.^[5] Later on, in 1990, this proposal was confirmed by Krätschmer, Lamb, Fostiropoulos, and Huffman who reported a method for the bulk production of C_{60} through resistive heating of graphite along with its IR spectroscopic structure determination – an icosahedral molecule closely representing the shape of a soccer ball.^[6] These fundamental findings provoked the interest of chemists, physicists and material scientists on C_{60} to such an extent that in the following years there hardly existed another molecule so intensively investigated. And indeed, the vast majority of the existing fullerene literature is devoted to the chemical and physical properties of C_{60} and its derivatives, with comparatively little emphasis on other

fullerenes. The reason for this is mainly because C_{60} is the most abundant fullerene in graphitic soot.^[6] However, with the introduction of other fullerene species, for instance C_{70} isolated from the other products of the carbon-arc synthesis by column chromatography,^[7] as well as C_{76} ,^[8] C_{78} ,^[9,10] C_{84} ,^[10,11] etc, it became clear that each member of the large fullerene family deserves individual attention.

Presumably, the systematic study of the “homologous series” of fullerene species would have been much easier if a vast number of isomers of individual cages did not exist. For example, for a cage constituted of 50 carbon atoms, 271 structural isomers are possible.^[12] The numbers grow progressively with increasing the carbon content. However, paying the tribute to elevated steric strain, hence the decreased cage stability, caused by fusing two or more pentagons, has led to the establishment of the so called “isolated pentagon rule”(IPR).^[13,14] According to this rule only cages with separated pentagons can exist, diminishing by this the number of acceptable structural isomers for each individual fullerene. Therefore, the first possible configuration obeying that rule can be constructed of not less than sixty carbon atoms - C_{60} possesses one stable isomer (I_h-C_{60}). Notwithstanding the fact that the next smallest fullerenes after C_{60} complying with the IPR (C_{70} , C_{72} and C_{74}) possess only one IPR-isomer each, generally with increasing the carbon content increases also the possibility to implement more than one structure for each consecutive member of the homologous series.^[12-14] Thus, two IPR-isomers exist for C_{76} , five for C_{78} , seven for C_{80} , nine for C_{82} , etc.^[12] This purely geometrical contrivance considerably reduces the number of available structures.

To provide ground for thorough investigation of the chemical and physical properties of individual fullerene isomers, an important requirement must be satisfied: the target species need, as minimum, be soluble in conventional solvents. However, far not all fullerenes are soluble. The insolubility of fullerene isomers has been attributed to their covalently linked polymeric nature, which is believed to be a result of the small (or zero) HOMO-LUMO gaps of some individual species (HOMO – highest occupied molecular orbital, LUMO – lowest unoccupied molecular orbital).^[15,16] The latter additionally reduces the amount of recoverable from the graphitic soot fullerenes. In other words, only the stable, IPR obeying and with comparatively large HOMO-LUMO gaps isomers of different cages are to be found in fullerene extracts. The apparent simplicity is

unfortunately deceptive. The thorough study of the properties of each individual fullerene isomer requires its isolation from the crude fullerene mixture beforehand. The available separation procedures mainly based on laborious and in many cases ineffective chromatographic techniques have resulted in the isolation of some fullerene species in pure form.

In order to anticipate specific properties from each individual fullerene cage, one should possess above all the complete structure information including connectivity pattern, bond distances and angles, electronic structure, etc. Although combining restraints such as IPR and the presence of only five- and six-membered rings in the molecule with NMR studies usually provides confirmation of the fullerene species constitution, a direct method of structure determination such as X-ray crystallography is envisaged to solve the query of single-isomer recognition.

The objectives of this work are to demonstrate means for obtaining preparative amounts of isomerically pure higher fullerenes (fullerenes consisting of more than 70 carbon atoms) as well as the elucidation of their connectivity patterns through single crystal X-ray analyses of the fullerene chlorine derivatives.

4 General Part

This part is devoted to the general concepts of the methods as well as the peculiarities of the equipment used for synthesis, extraction and isolation of fullerene species. The analytical techniques employed for characterization of pristine fullerenes and fullerene derivatives (through single crystal X-ray analyses) are discussed too.

4.1 Methods and Equipment

The methods most widely used in production, extraction and separation of fullerenes are briefly described. Strong emphasis is put on the special equipment employed in separation of fullerene species as well as on the specific chromatographic techniques needed in order to obtain isomerically pure fullerenes.

4.1.1 Fullerene Production

Since the discovery of fullerene species by Kroto et al. in 1995,^[5] different synthetic routes for fullerene production have been proposed. The very beginning has been set up by Smalley's device initially developed for investigating compounds and clusters formed from refractory elements, which is shown in Figure 3.^[17-19] The target is a graphite disk which is rotated slowly to provide a fresh vaporization surface. The vaporization laser, a 5-ns pulse at 532 nm of about 30 – 40 mJ, is focused onto the surface of the graphite. The pulsed nozzle passes helium over this vaporization zone (inner pressure \approx 10 atm). The vaporized material is caught up in the helium gas flow, mixed with it, and cooled by it. The cooling vapor then begins to condense into clusters.^[20]

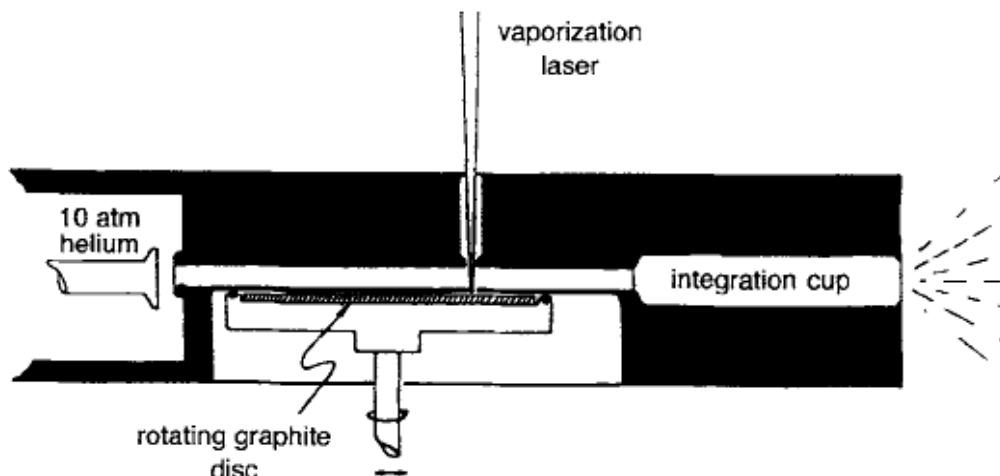


Figure 3 Smalley's device for investigating compounds or clusters formed from refractory elements (the figure is replicated from Ref. [20])

The fullerenes discovery has actually occurred when under the right conditions in Smalley's device, C_{60}^+ has become the "super magic number" in the TOF- (time of flight) mass-spectra among the other far less prominent carbon clusters.

The above described synthetic procedure, however, has not shown capable of delivering plausible amounts of fullerene material, making the demand of another method for bulk production of the all-carbon closed-caged molecules requisite. Half a decade after the fundamental discovery of the C_{60} -cluster, Krätschmer et al. developed such a method based on resistive heating of graphite.^[6] Basically, the original apparatus used for the first production of fullerenes consisted of a bell jar as recipient, connected to a pump system and a gas inlet (Figure 4). In the interior, two graphite rods are kept in contact. One of them is sharpened to a conical point, while the end of the other is flat. Both graphite rods are connected to copper electrodes. Under constant helium pressure of approximately 140 mbar, voltage is applied and the electric current passing through the rods dissipates its power heating the narrow point of contact. At temperatures of approximately 2500-3000°C, smoke develops at the contact zone, which consecutively being transported by convection away from the heat zone cools at the jar walls.

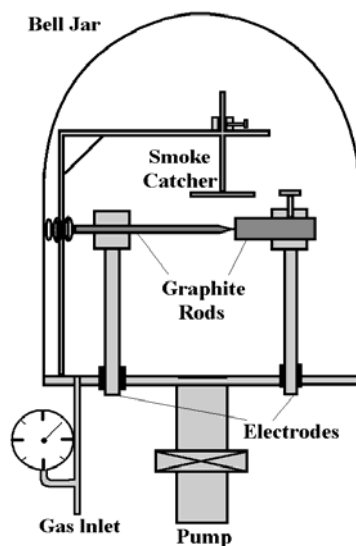


Figure 4 The fullerene generator originally used by Krätschmer et al.^[6]

Many modifications of this apparatus has been realized improving the synthetic parameters to a certain extend. A similar setting but based on alternative heating of the graphite rods has been proposed by Smalley and coworkers.^[21] Here, the rods are kept in close proximity but not in a direct contact resulting in the generation of an electric arc rather than resistive heating when a voltage is applied between the two electrodes. This technique is known as contact-arc vaporization of graphite because the rods are kept so close together as to mimic a contact (see Figure 5).^[22-27]

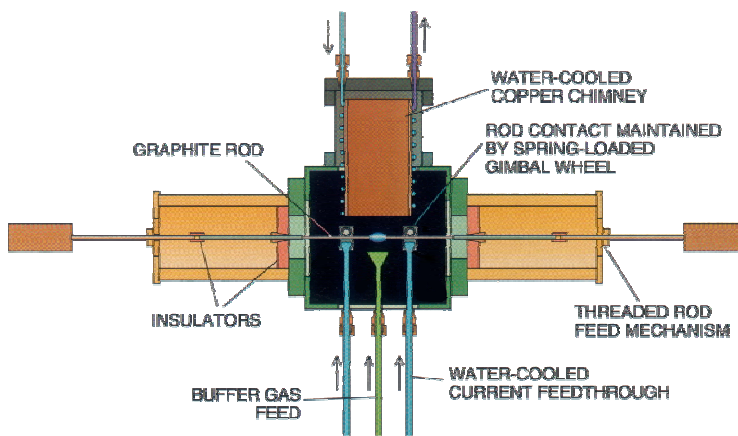


Figure 5 Schematic diagram of a graphite rod contact-arc fullerene generator

The fullerene soots used for the purpose of this work have been generated through inductive heating of graphite (along the radio-frequency (RF) route), the full details of which have been previously reported.^[28,29] Evaporation of graphitic bodies in a helium atmosphere generates fullerene-containing soot that condenses on the cold glass wall of the reaction tube. This method permits a continuous operation by keeping the graphite body in the heating zone. The graphical representation of the RF furnace is given in Figure 6.

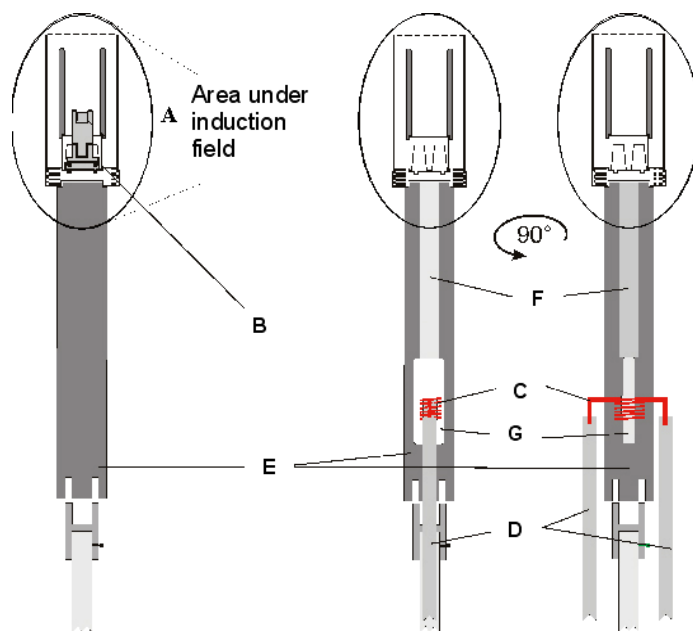


Figure 6 RF-furnace, where: A – the area under induction field; B – graphite crown; C – heating resistance; D – power supply for the resistance; E – boron nitride support column; F – tunnel; G – cavity for the resistance;

Besides the thus far described synthetic approaches, a few alternative methods have been proposed, which do not fall in the scope of this work and are not paid particular attention. The most prominent among them are the fullerene synthesis in combustion and fullerene formation from hydrocarbons.

4.1.2 Fullerene Extraction

For the concrete needs of this work, two different extraction methods have been used in order to obtain fullerenes in solution. The first one is based on the classical soxhlet extraction. The general make-up of the soxhlet apparatus is presented in Figure 7.

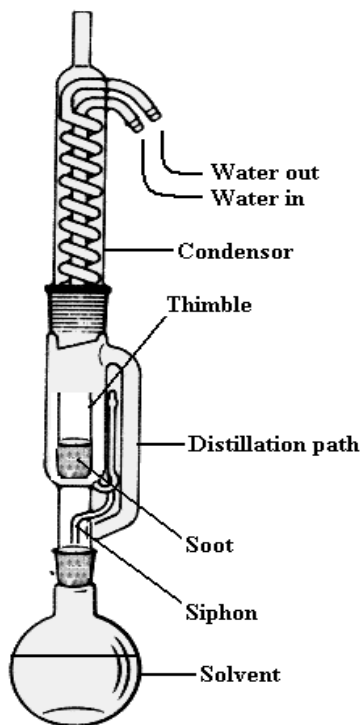


Figure 7 Schematic representation of the Soxhlet extractor

Normally, the graphitic soot containing different fullerene species is placed inside a thimble made from thick filter paper, which is loaded into the chamber of the Soxhlet extractor. The solvent is refluxed in such a way that the vapor travels up a distillation arm and floods into the chamber housing the extraction thimble. The condenser ensures that solvent vapor cools and flows back down into the chamber housing the thimble. The desired compounds will then dissolve in the hot solvent. When the Soxhlet chamber is almost full, it automatically empties through a siphon arm, with the solvent dripping back down to the distillation flask. This cycle is allowed to repeat many times. After the

extraction the solvent is removed, yielding the extracted compounds. The non-soluble portion of the solid (mainly graphitic particles) remains in the thimble.

The second extraction technique is based on the so called accelerated solvent extraction (ASE). For that purpose, a Dionex ASE 100 (Dionex Corporation, USA) extractor is used. The construction of the extractor is shown in Figure 8.

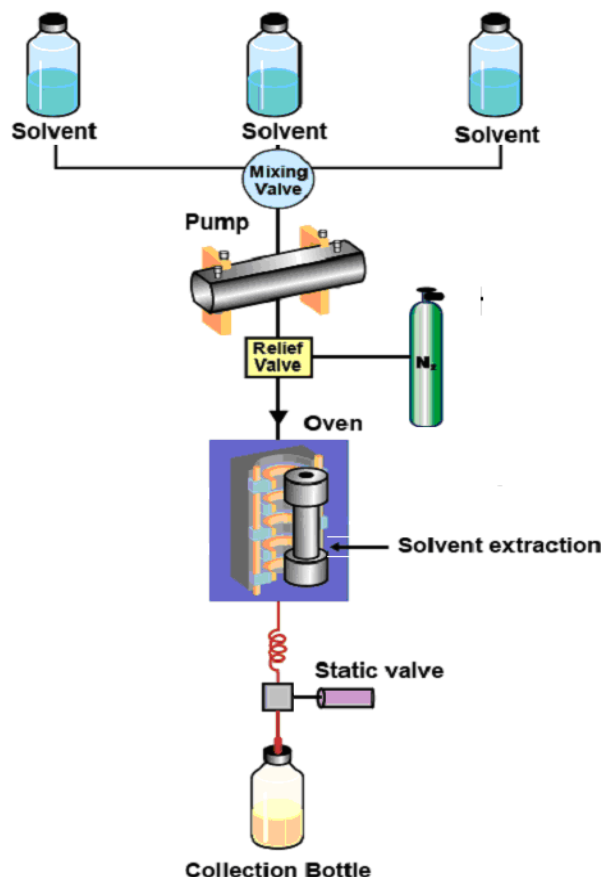


Figure 8 ASE 100 set-up

ASE 100 operates by compressing the extraction solvent (or a mixture of solvents) through an extraction cell containing the solid sample. The sample cell is heated by direct contact with the oven. The extraction is performed by suffusing the sample cell with the hot solvent. When the extraction is complete, compressed nitrogen moves all of the solvent from the cell to the collection container.

4.1.3 Fullerene Separation - High Performance Liquid Chromatography

The method of fullerene separation chosen for the aims of this work is based on high performance liquid chromatography (HPLC). The following section describes in short the basic HPLC concepts, presents the array of column packings used for the separation of fullerene species and gives a short overview on the assembly of the concrete chromatographic equipment.

4.1.3.1 Basic Concepts of HPLC

HPLC is basically an improved form of column chromatography.^[30-32] Instead of a solvent dripping down the column under gravity, it is forced through applying high pressures. HPLC permits the use of much smaller particles for the column packing material which gives a much greater surface area for interactions between the stationary phase and the analytes flowing through it. This allows a much better separation of the mixture components. The separation process is actually based on the different distribution of the mixture components between two phases, a stationary phase and a mobile phase. Those components residing preferentially in the stationary phase are retained longer in the system than those that are distributed selectively in the mobile phase. As a consequence, solutes are eluted from the system as local concentrations in the mobile phase in the order of their increasing distribution coefficients with respect to the stationary phase. The distribution coefficient is given by:

$$K = \frac{C_s}{C_m}$$

where C_s is the concentration of the analyte in the stationary phase, whereas C_m is its concentration in the mobile phase. Therefore, an effective separation between two components can be achieved only when they have different distribution coefficients with respect to the same stationary and mobile phases. Along the indispensable difference in distribution coefficients of the different solutes, the chromatographic system (mobile and

stationary phase selection) must provide for minimal spreading of each solute band (dispersion) so that the eluted bands are discrete. The latter strongly depends on the optimal physical properties of the column (column dimensions, particle diameter, mobile phase velocity etc.)

The basic parameter in chromatography is the analyte retention. The classical way to determine the chromatographic retention of a concrete solute is to measure the time elapsed between the injection and the maximum of the detector response. This parameter is called “retention time”. Retention time, T_R is inversely proportional to the mobile phase flow rate. The product of retention time and eluent flow rate is called “retention volume”. The retention volume, V_R represents the volume of the eluent flowed through the column while eluting a particular component. Component V_R might be split into two parts: reduced retention volume (the volume of the eluent that passed through the column while the component was residing in the stationary phase) and dead volume (the volume of the eluent that passed through the column while the component was moving with the liquid phase). The second part is equal to the volume of the liquid phase in the column and it will be the same for any component eluted on this column. Retention volume is independent of the flow parameters, but it depends on the geometrical parameters of the column. The fundamental retention parameter is the ratio of the retention volume and dead volume, k :

$$k = \frac{V_R}{V_0}$$

where V_0 is the dead volume of the column. Historically, a slightly different retention parameter, called capacity factor, k' was introduced by the analogy with the liquid partitioning theory and widely accepted in chromatographic practice. The capacity factor is given by the expression:

$$k' = \frac{V_R - V_0}{V_0}, \text{ or } k' = \frac{T_R - T_0}{T_0}$$

where T_0 is the retention time of an unretained solute (dead time). The capacity factor is dimensionless and independent on any geometrical parameters of the column or HPLC system.

An important characteristic of the chromatographic system is the column efficiency. After injection, the initially narrow chromatographic band broadens during its movement through the column. The higher the column band broadening, the smaller the number of components that can be separated. In other words, the peak width is an indication of how good or efficient the column is. The peak width is dependent on a number of parameters such as the column length, flow rate, particle size, etc. The column efficiency can be presented by the expression:

$$N = a \left(\frac{T_R}{W} \right)^2$$

where N is the number of theoretical plates (the term “theoretical plate” comes from the analogy with the distillation theory), a is a constant depending on the method used in measuring W , and W is the peak width at a given peak height. In practice, it is accepted to measure peak width either at the base line or at the half height. If the half height is selected, the value of a is equal to 5.54, and the expression for the number of theoretical plates has the shape:

$$N = 5.54 \left(\frac{T_R}{W_{1/2}} \right)^2$$

where $W_{1/2}$ is the peak width at half height. The number of theoretical plates depends on the column length: the longer the column, the larger the plate number. Therefore, the plate height term has been introduced to measure how efficiently the column has been packed:

$$h = \frac{L}{N}$$

where h is the height of the theoretical plate (HTP) and L is the column length. Therefore, the lower the plate height, the more efficient the chromatographic column. Besides the column efficiency and the capacity factor, two other important parameters define the quality of the chromatographic system – selectivity and resolution. Selectivity is the ratio of the capacity factors of two neighboring peaks in the chromatogram. Selectivity represents the separation power of a particular stationary phase with respect to the concrete compounds and is given by:

$$\alpha = \frac{k'_2}{k'_1}$$

where α is the selectivity and k'_1 and k'_2 are the capacity factors of the two compounds. This parameter is independent of the column efficiency; it only depends on the nature of the components, eluent composition, and stationary phase surface chemistry. In general, if the selectivity of two components is equal to 1, then there is no way to separate them by improving the column efficiency.

Resolution is the second parameter describing the separation capability of the complete chromatographic system relative to the particular components of the mixture. By convention, resolution, R is expressed as the ratio of the distance between two adjacent peak maxima to the mean value of the peak widths at the base line:

$$R = 2 \frac{V_{R2} - V_{R1}}{W_1 + W_2}$$

If the peaks are approximated to symmetric triangles and if R is equal to or more than 1 then components are completely separated. If R is less than 1, then components are overlapped. By using the expressions for the capacity factor and column efficiency the equation for R could be transferred to the form:

$$R = \frac{\sqrt{N}}{2} \frac{k'_2 - k'_1}{k'_1 + k'_2 + 2}$$

Thus far introduced parameters fully assess the separation abilities of a concrete chromatographic system with respect to a particular mixture of compounds. To evaluate one of the most important characteristics of the chromatographic system, the column efficiency known also as band broadening, in 1956 J.J. Van Deemter introduced an equation which combined the three principal sources of band broadening; multiple path of an analyte through the column packing, molecular diffusion and effect of mass transfer between phases. Generally, Van Deemter's equation represents the dependence of the HTP on the mobile phase linear velocity.

The velocity of mobile phase in the column may vary significantly across the column diameter, depending on the particle shape, porosity, and the whole bed structure (packing), leading to band broadening. The dependence of HTP on the packing characteristics is given by the expression:

$$H_p = 2\lambda d_p$$

where H_p is the HTP arising from the variation in the zone flow velocity, d_p is the particle diameter (average), and λ is a constant which is close to 1. This shows that H_p may be reduced (efficiency increased) by reducing the particle diameter. The coefficient λ depends on the particle size distribution, thus the narrower the distribution, the smaller λ .

It is well-known that molecules disperse or mix due to diffusion. The longitudinal diffusion (along the column long axis) leads to band broadening of the chromatographic zone. This process may be described by the equation:

$$H_d = 2 \frac{\gamma D_m}{v}$$

where H_d is the HTP descending from the longitudinal diffusion, D_m is the analyte diffusion coefficient in the mobile phase, γ is a factor which is related to the diffusion restriction by the column packing and v is the flow velocity. It is obvious that the higher the eluent velocity, the lower the diffusion effect on the band broadening. Molecular diffusion in the liquid phase is about five orders of magnitude lower than that in the gas phase, thus this effect is almost negligible with the standard HPLC flow rates.

Mass transfer is the most questionable parameter. For the modern types of packing materials it may combine two effects: adsorption kinetics and mass transfer (mainly due to diffusion) inside the particles. 95% of all modern packing materials consist of spherical, totally porous rigid particles with average diameter of 5 μm and pore diameter of 100 \AA . Ratio of the particle to the pore diameter is 500/1. There is no pressure induced flow inside the particle, and molecules can move there only by diffusion. Adsorption kinetics is almost negligible compared to the diffusion inside the particles, and band broadening may be written in form:

$$H_m = \omega \frac{d_p^2}{D_m} v$$

where H_m is HTP dependent on the particles characteristics and ω is a coefficient determined by the pore size distribution, shape, and also particle size distribution. This equation describes the linear dependence of HTP on the flow rate. The slower the velocity, the more uniformly analyte molecules may penetrate inside the particle and the less the effect of different penetration on the efficiency.

Combining the three equations in one results in an expression representing the total band broadening; therefore the sum of all of them will give the total column plate height:

$$H = H_p + H_d + H_m$$

The expanded form will be:

$$H = 2\lambda d_p + 2 \frac{\gamma D_m}{v} + \frac{\omega d_p^2}{D_m} v, \text{ or } H = A + \frac{B}{v} + Cv$$

The second expression is more commonly used in practice. **A**, **B** and **C** are constants derived from the extended form. Different components have different dependencies of HTP on the flow rate on the same column. This shows that the component nature, type of surface interactions and perhaps other parameters have an influence on the column efficiency related to the particular component. The plot shown below (Deemter plot) highlights the contribution of each term of the Deemter equation.

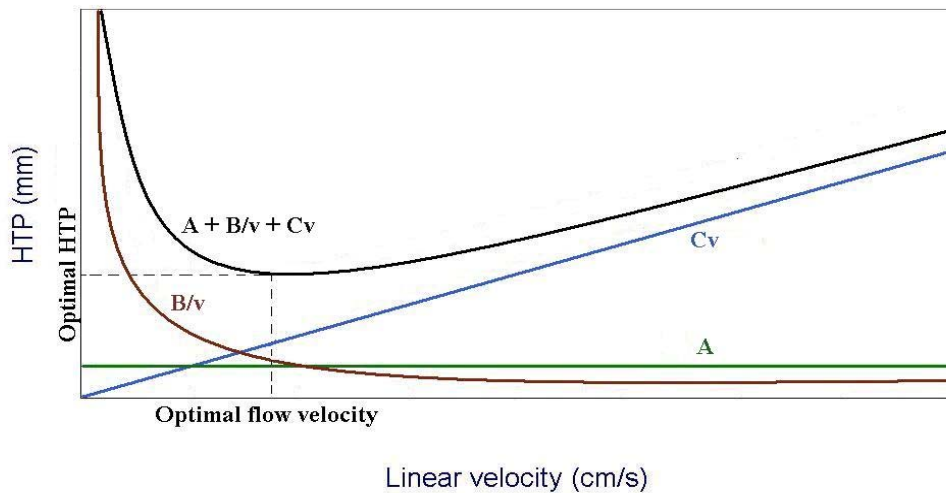


Figure 9 Van Deemter plot

The **A** term is independent of velocity and represents the so called “Eddy” mixing. It is smallest when the packed column particles are small and uniform. The **B** term represents axial diffusion or the natural diffusion tendency of molecules. This effect is diminished at high flow rates and so this term is divided by v . The **C** term is due to kinetic resistance to equilibrium in the separation process. The greater the flow rate, the more a molecule on the packing tends to lag behind molecules in the mobile phase. Thus this term is

proportional to v . The most significant conclusion from this relationship is that an optimal eluent flow rate can be found where the column efficiency will be the best.

4.1.3.2 Columns and Column Packings

HPLC adsorbent (stationary phase) is the material which after being packed in the column actually retains (adsorbs) the analytes and produces the separation. Only the surface of the stationary phase actually participates in the chromatographic retention process. Thus, chromatography is a dynamic interface phenomenon.

Porous silica is the most widely used packing material in HPLC. Its chemical composition could be expressed as $\text{SiO}_2 \cdot x\text{H}_2\text{O}$, which means that water is chemically bound in non-stoichiometric amount. The specific retention behavior of solutes at given eluent composition is governed mainly by the chemical nature of the silica surface. The following different types of adsorption sites on the surface of the fully hydroxylated silica are recognized (Figure 10).

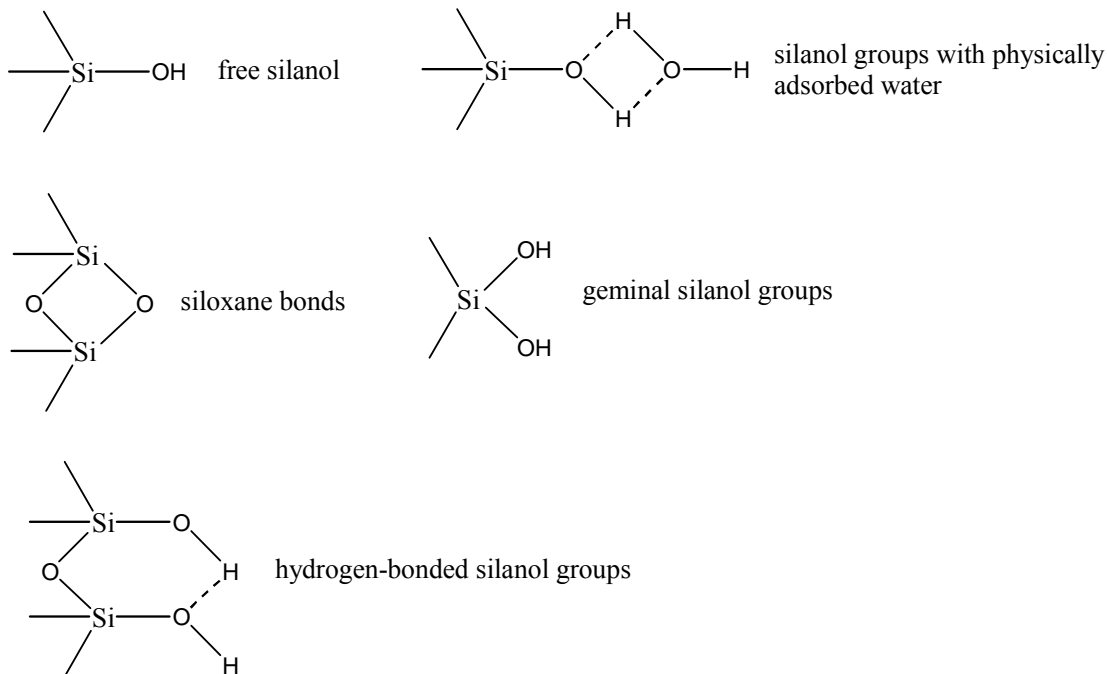


Figure 10 Adsorption sites in hydroxylated silica

Most of the chromatographic properties of the silica surface are related to the interactions with silanol groups, although siloxane and hydrogen bonded silanols may also contribute to the surface activity.

The HPLC columns are usually packed with small silica particles, preferably spherical in shape. The particles are always presented by some degree of size distribution. Most LC packing materials have a Gaussian type of particle size distribution, so the position of the maximum is the mean particle diameter, while the standard deviation represents the distribution width. In HPLC practice, the less the particle size distribution the more uniform the packing in the chromatographic column, and the more efficient the column itself.

Besides the particle size distribution, another very important adsorbent parameter is the pore size and pore size distribution. Adsorbent surface area is the factor directly affecting the analyte retention. Pore size defines the ability of the analyte molecules to penetrate inside the particle and interact with its inner surface. This is especially important because the ratio of the outer particle surface to its inner one is about 1:1000. The surface molecular interaction mainly occurs on the inner particle surface.

Historically, using unmodified silica as the packing material and nonpolar organic solvents as the mobile phase was defined as “normal-phase” chromatography (NP). The usual application of NP chromatography is the separation of hydrophobic compounds. These compounds do not show strong interaction with the highly polar stationary phase and could be eluted from the column relatively fast.

The chromatographic technique which utilizes nonpolar adsorbent surface (modified silica surface) and polar eluent has been named “reversed-phase” HPLC (RP-HPLC). Since the time when reversed-phase packing materials became commercially available, the number of applications using RP-HPLC has substantially grown, and nowadays it is the most widely used HPLC mode. A very rich variation of species could be attached to the silica surface. These are different organofunctional groups (R). R may represent substituents of various functionality such as aliphatic or aromatic hydroxyl, amine, carbonyl, nitril etc. The functional group R can be directly linked to the surface silicon atom, such that a Si–R bond forms. This type of surface modification is usually very laborious and does not result in a stable surface modification. Another type of bonding is

the Si–O–R. This bond is known as an ester bond. The Si–O–Si–R bonding is obtained by treatment of the silica surface with organosilanes (R_nSiX_{4-n}), where X is the reactive group such as halogen, ethoxy or methoxy. This type of bonding is the most widely used in modern HPLC. The reaction of monochlorosilane with the silica surface leads to the attachment of only one alkylsilane ligand to one silanol group. The type of layer which involves the formation of a monomolecular organic layer on the silica surface is called “monomeric bonding”. Polymeric phases can be prepared by reacting silica with di- or trichlorosilane in the presence of trace amount of water. The two different bonded layers are represented in Figure 11.

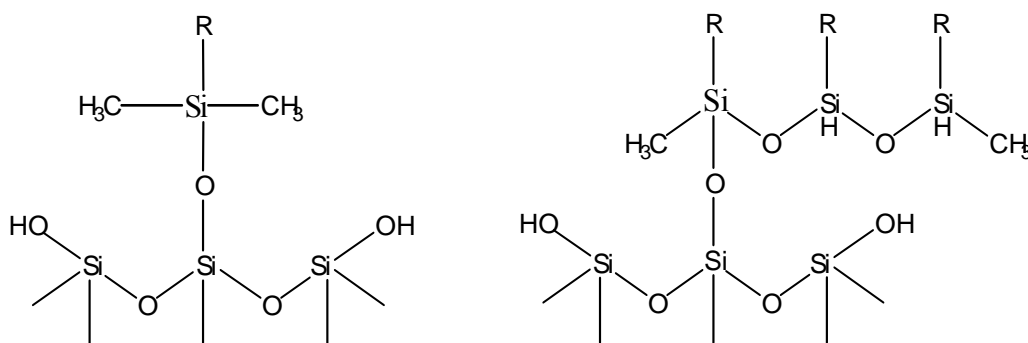


Figure 11 Schematic representations of monomeric and polymeric bonded layers

4.1.3.3 Stationary Phase Selection – Motivation and Justification

For the aims of this work five different types of packing material have been used. All of them are intellectual property of Nacalai Tesque Inc., Kyoto, Japan.

Two different RP-C₁₈ columns, one monomeric and one polymeric type, are used in the course of this work. The more special, designed mainly for separation of fullerene species 5–PYE, Buckyprep (BP), and Buckyprep-M (BP-M) columns have packings the structures of which are shown in Figure 12.

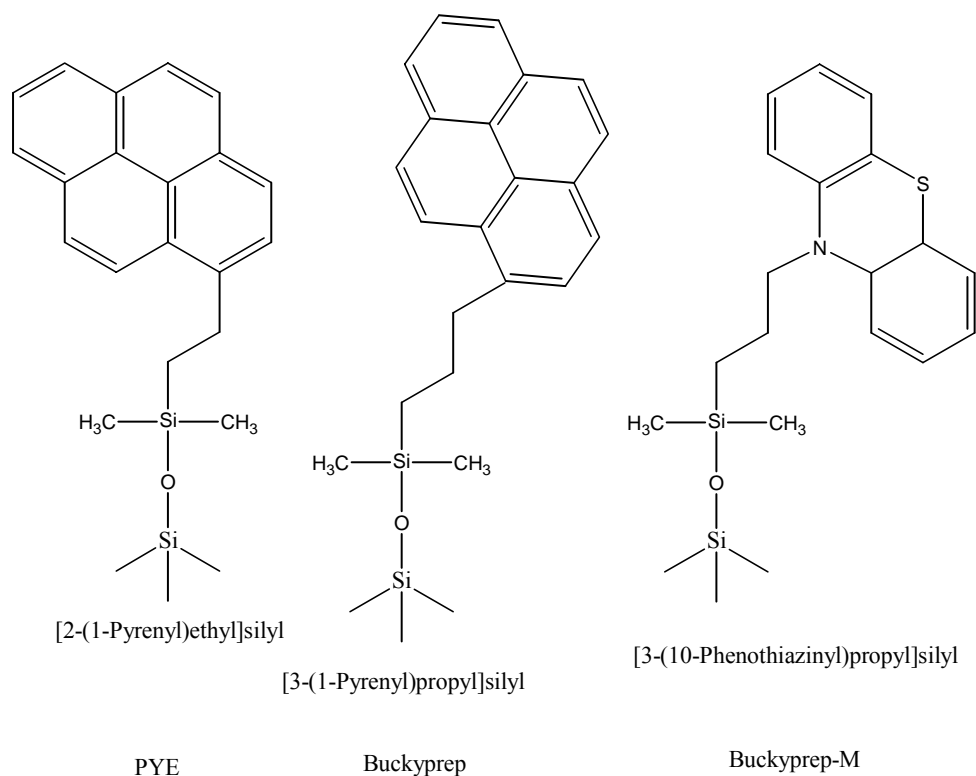


Figure 12 Different stationary phases for fullerene separation

The conventional C₁₈ RP bonded stationary phases are widely used for the separation of fullerene species.^[33-35] RP bonded phases provide satisfactory resolution for C₆₀, C₇₀ and higher fullerenes based mainly on molecular recognition mechanism.^[36,37] The results obtained with both monomeric and polymeric types of stationary phases suggest that the monomeric C₁₈-bonded phases with higher carbon content (i.e. higher surface coverage) exhibit good separation power for C₆₀ and C₇₀ fullerenes. The polymeric types exhibit limited retention values for these solutes, although some types show a better shape selectivity for some higher fullerenes.^[37] The latter justifies the predominant usage of polymeric phase throughout the course of this thesis when C₁₈-RP HPLC was selected as a parameter of the separation process. In other words, monomeric phases separate the analytes according to molecular size, while polymeric ones can additionally distinguish shape differences but offer limited retention for bulky analytes. This fact is explained by the rigid net of closely disposed alkyl additives (bonded to the silica support), the distances between which frequently are shorter than the average size of the fullerene

molecule, leading to exclusion phenomena. This exclusion is especially pronounced under ambient and elevated temperatures (the temperature regions most usually employed for chromatographic separations). A graphical representation of the possible phase ordering/disordering under different temperatures and the subsequent analyte exclusion is shown in Figure 13.

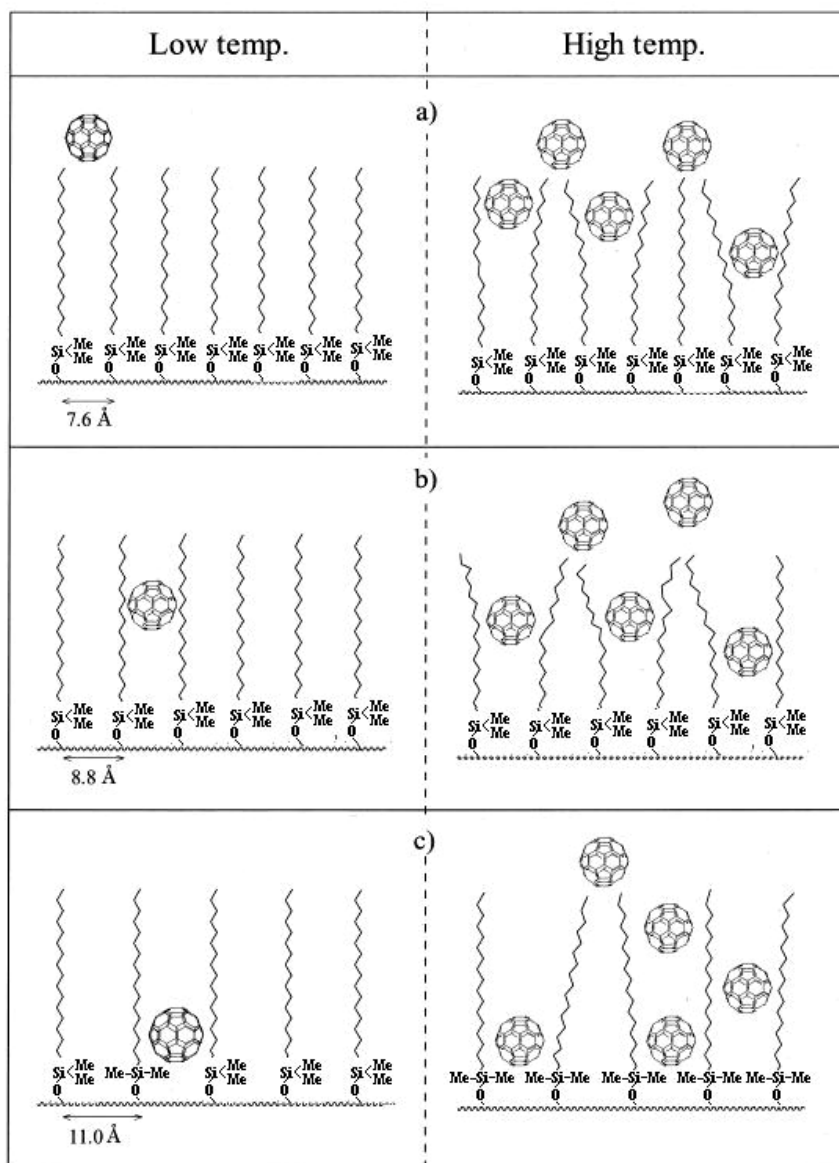


Figure 13 Retention model of C_{60} on C_{18} phases with different surface coverage. Left: at low temperatures; Right: at ambient and/or elevated temperatures. The average ligand intervals are shown too.^[37]

A closer look at the figure shows that besides the temperature, a crucial role for the effective interaction between the fullerene molecule and the stationary phase ligands plays the average distance between adjacent alkyl chains (the surface coverage). The strongest interaction, hence the highest retention parameters with respect to a specific fullerene cage show those phases which exhibit a “perfect match” between the average ligand separations and the molecular diameter of the respective fullerene molecule.

The maximal retention parameters with respect to C₆₀ and C₇₀ fullerenes using different chromatographic systems (different combinations of mobile and C₁₈-stationary phases) have been observed under decreased temperatures of about -30, -40°C.^[36,37] Increasing the temperature above these values significantly decreases the interaction between the adsorbent and the analytes (due to the conformational change in the stationary phase discussed above), thus negatively influencing the retention parameters. The resulting low loadability of C₁₈-RP phases makes them unsuitable for preparative separation and isolation of fullerene species.

For the preparative isolation of fullerenes, the specially designed for that purpose 5 PYE, BP, and BP-M columns have been selected mainly due to their high loadability and comparatively satisfactory resolution with respect to some higher fullerenes (all three columns have shown incapable in resolving fullerene cages higher than C₈₄). Preparative scale separation can be achieved with a 250 mm x 4.6 mm analytical column for any of the three bonded stationary phases. The type of chromatography with this array of phases is considered to be RP, irrespective of the mobile phase being a nonpolar solvent or solvent mixture (usually toluene and/or mixture of toluene and hexane are used as the mobile phases). Since all three columns employ chemically bonded silica phases (Figure 12), no special operation techniques are required. Here in contrast to conventional C₁₈-RP phases the emphasis is put on intermolecular $\pi - \pi$ interaction between the stationary phase ligands and the respective fullerene molecules. The BP-M column is originally designed for the separation and of metallofullerenes (endohedral fullerenes), but for the needs of this work it has been employed in the isolation of empty cage fullerenes.

4.1.3.4 HPLC Equipment

Basically, three different HPLC set-ups have been used in the course of the chromatographic part of this work.

The “standard analytic HPLC” from the Prominence series of Shimadzu (Shimadzu Corporation) consists of the following units: Solvent delivery system (pump) LC-20AT, degasser DGU-20A₅, column oven CTO-20AC, diode array detector SPD-M20A, communication bus module CBM-20A and a manual injector Rheodyne 7725i. The software used for data collection and manipulation is LC solutions version 1.21 SP1 (Lab Solutions, Shimadzu Corporation).

The set-up used for the semi-preparative needs is presented in Figure 14.

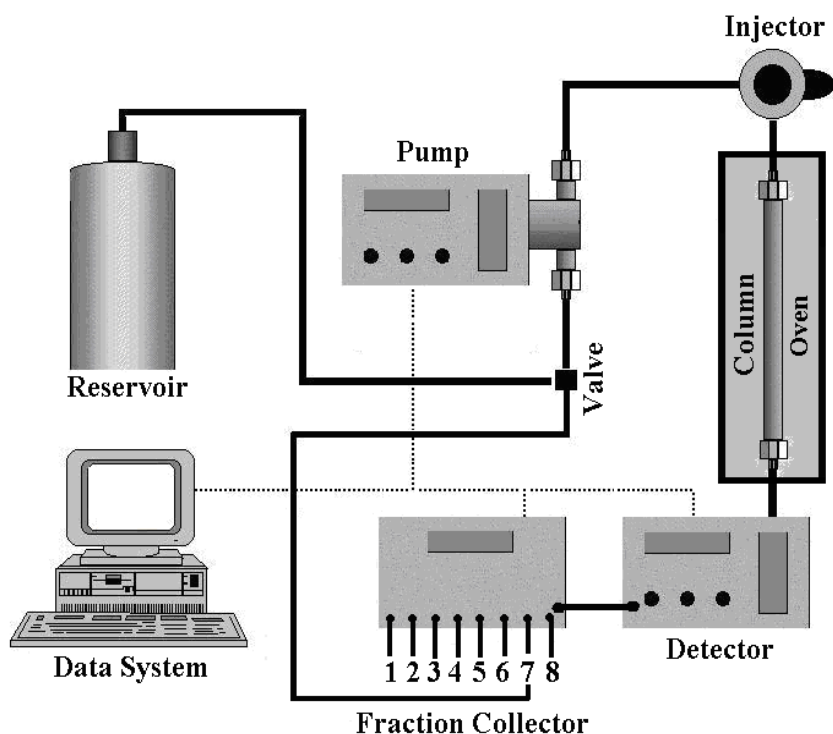


Figure 14 Schematic representation of the semi-preparative equipment

It consists of the following modules: Solvent delivery system Sykam S-1021 (Sykam GmbH, Germany), column thermo controller Sykam S-4011, sample collector Sykam S-6340, multi-wavelength detector Jasco MD-1515 (Jasco GmbH, Germany) and a manual

injector Rheodyne 7725i. Borwin PDA (Jasco GmbH) is the software packet used for the data management.

The preparative system consists of the following components: Solvent delivery system Sykam S-1121, column thermo controller Sykam S-4011, sample collector Sykam S-6340, ultraviolet/visible light (UV/VIS) detector Shimadzu SPD-20A, injector, selector, and the same software package used with the semi-preparative set-up. A schematic representation of the modular-type equipment is shown in Figure 15.

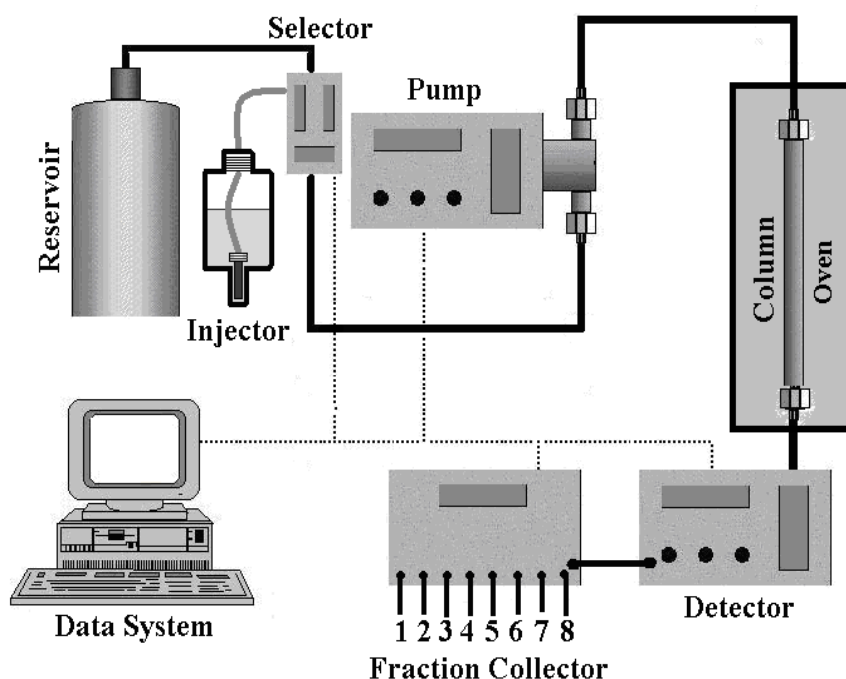


Figure 15 Preparative HPLC equipment

4.1.3.5 Special HPLC Operation Techniques

The preparative separation of fullerene species has been exclusively performed with a BP column with dimensions 250 x 20 mm. The equipment shown in Figure 15 has been programmed to automatically perform fraction collection overnight, saving a valuable amount of operation time. One cycle comprises of ten consecutive injections, where each injection goes on for 45 minutes of fraction collection and 5 minutes of column equilibration. The overall continuance is about 500 minutes with constant eluent flow rate

of 20 ml/min. Since mainly toluene (Acros, HPLC-grade with purity < 99.9%) has been used for the preparative chromatographic steps, the approximate amount of ten liters of solvent has been spent for every cycle. To reduce the drastic amounts of expensive solvent consumed, bi-distillation procedure has been performed after each preparative cycle. As can be seen from Figure 15, the filtrated fullerene extract is loaded into the improvised sample injector, from where depending on the command given to the selector unit is being introduced into the column. The selector unit chooses the flow that should be fed into the column between the reservoir (loaded with the mobile phase) and the injector container. Different fractions containing one or more fullerene species are collected with the help of the fraction collector in separate containers. Approximately three grams of fullerenes can be separated with one cycle on the preparative-scale HPLC. The higher fullerene fractions obtained after the initial preparative step contain more than one fullerene species. Since not much can be done in adjusting the separation ability of the chromatographic system (the choice of stationary and mobile phases is rather restricted), another technique must be developed in order to acquire isomerically pure fullerene species. Here, this is achieved by employing the so called recycling approach. A closer look into Figure 14 reveals that the seemingly identical to the preparative set-up semi-preparative equipment has one prominent difference; figuratively depicted as collector's channel 7, the outflow from the detector instead of being directed to any of the other outlets (the fraction containers or the waste channel) is reintroduced into the column for another separation. Depending on the degree of separation achieved after the second introduction, the same procedure might be repeated many times until the desired result is obtained. The valve on Figure 14 is nothing more but a mechanical connector feeding the outflow back into the chromatographic column. When any of the other channels is open, the mobile phase is sucked from the reservoir and the system operates as a conventional HPLC.

4.2 Analytic Methods – Characterization of Pristine Fullerenes and Fullerene Derivatives

In this chapter, the principles as well as some operation techniques of the main analytical methods used for the characterization and identification of fullerene species are briefly discussed. These include ultraviolet-visible (UV/VIS) spectrophotometry, matrix-assisted laser-desorption ionization – time of flight (MALDI-TOF) mass-spectrometry (MS), and single-crystal X-ray diffraction used for the analyses of fullerene monocrystals.

4.2.1 Ultraviolet-Visible Spectrophotometry

Fullerenes, generally, possess very prominent and characteristic electronic absorptions in the near-ultraviolet/visible/near-infrared (UV/VIS/NIR) region of the electromagnetic spectrum. For the needs of this work UV/VIS spectrophotometry has been used to identify fullerene species in solution.

4.2.1.1 Principles of UV/VIS Spectrophotometry

The visible region of the spectrum comprises photon energies from 36 to approximately 72 kcal/mol, and the near ultraviolet region, out to 200 nm, extends this energy range to 143 kcal/mol.^[38] Ultraviolet radiation having wavelengths less than 200 nm is difficult to handle, and is rarely used as a routine tool for structural analysis of analytes in solution. A diagram showing the various kinds of electronic excitation that may occur in organic molecules is shown in Figure 16. Of the six transitions outlined, only the two lowest energy ones (left-most, colored blue) are achieved by the energies available in the 200 to 800 nm region. As a rule, energetically favored electron promotion will be from HOMO to LUMO, and the resulting species is called an excited state. When sample molecules are exposed to light having an energy that matches a possible electronic transition within the molecule, some of the light energy will be absorbed as the electron is promoted to a higher energy orbital. An optical spectrometer records the wavelengths at which

absorption occurs, together with the degree of absorption at each wavelength. The resulting spectrum is presented as a graph of absorbance (**A**) versus wavelength (λ). Absorbance usually ranges from 0 (no absorption) to 2 (99% absorption).

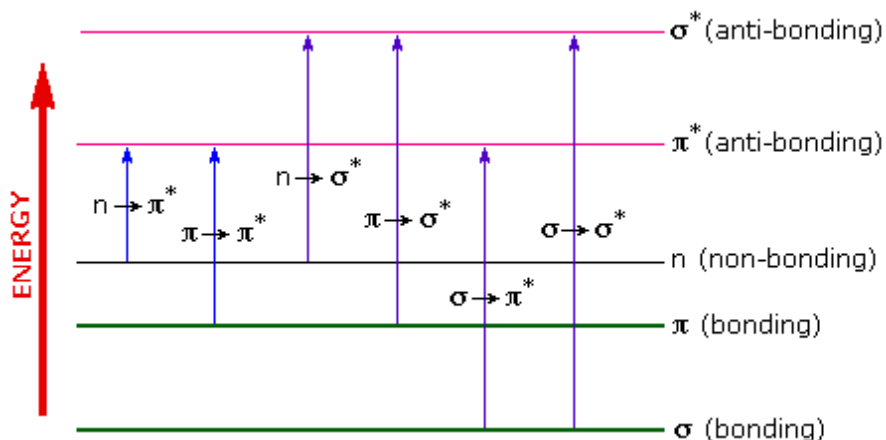


Figure 16 Diagram showing different electronic transitions in an organic molecule. Only the leftmost two (depicted in blue) are used in UV/VIS spectrophotometry for routine analyses

For the absorbance of a sample to be proportional to the number of absorbing molecules in the spectrometer light beam (e.g. their molar concentration in the sample cuvette), it is necessary to correct the absorbance value if the spectra of different compounds are to be compared in a meaningful way. The corrected absorption value is called "molar absorptivity", and is particularly useful when comparing the spectra of different compounds. Molar absorptivity (ϵ) is defined as:

$$\epsilon = \frac{A}{c.L}$$

where **A** is absorbance, **c** is the sample concentration in moles/liter and **L** is the length of light path through the sample in cm (cuvette width).

Molecular moieties capable of absorbing light in the 200 to 800 nm region are π -electron functions and hetero atoms having non-bonding valence-shell electron pairs. Such light absorbing groups are referred to as chromophores. Some simple chromophores and their

light absorption characteristics are given in Table 1. The oxygen non-bonding electrons in alcohols and ethers do not give rise to absorption above 160 nm. Consequently, pure alcohol and ether solvents may be used for spectroscopic studies. The presence of chromophores in a molecule can be documented by UV/VIS spectroscopy, but the failure of most instruments to provide absorption data for wavelengths below 200 nm makes the detection of isolated chromophores problematic. Fortunately, conjugation generally moves the absorption maxima to longer wavelengths, so conjugation becomes the major structural feature identified by this technique.

Table 1 Examples of substituted with different chromophores benzene and the respective λ shifts depending on the solvent used

Chromophore R =	λ_1 (nm)	λ_2 (nm)	Solvent
Unsubstituted C ₆ H ₆	204	256	Cyclohexane (C)
OH	210.5	270	Water (W)
O ⁻	235	287	W
OCH ₃	217	269	W
SH	236	269	Hexane (H)
NH ₂	230	280	W
NH ₃ ⁺	203	254	W
NO ₂	252	280	H
CHO	244	280	Ethanol (E)
COCH ₃	240	278	E
CO ₂ H	230	270	W
CO ₂ ⁻	224	268	W
CN	224	271	W
F	204	254	E
Cl	209.5	263.5	W

Br	210	261	W
I	207	257	W
CH ₃	207	261	W
CH=CH ₂	244	282	E
C≡C-C ₆ H ₅	236	278	H

Molar absorptivities may be very large for strongly absorbing chromophores and very small if absorption is weak. The magnitude of ϵ reflects both the size of the chromophore and the probability that light of a given wavelength will be absorbed when it strikes the chromophore.

From the polyene spectra displayed in Figure 17, it is clear that each additional double bond in the conjugated π -electron system shifts the absorption maximum about 30 nm in the same direction. Also, the molar absorptivity ϵ roughly doubles with each new conjugated double bond. When describing shifts in absorption, the terms defined in Table 2 are used.

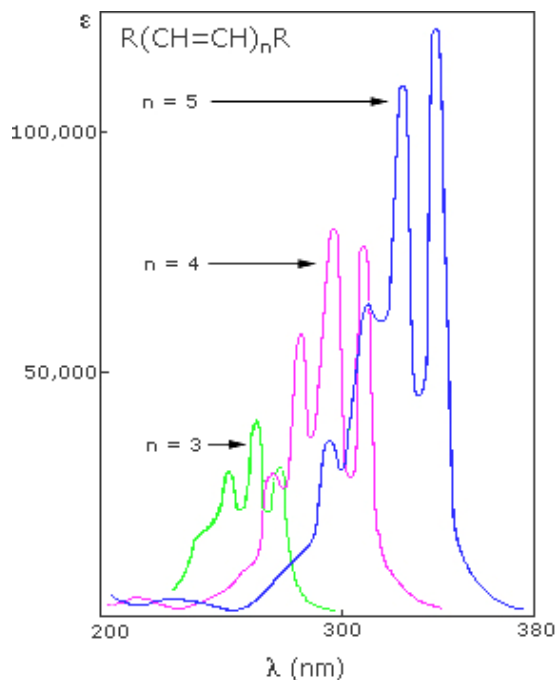


Figure 17 UV spectra of polyenes showing changes in ϵ and λ depending on the number of double bonds (n = number of double bonds)

Table 2 Different terms describing the change in λ and ϵ

Nature of Shift	Descriptive Term
To Longer Wavelength	Bathochromic
To Shorter Wavelength	Hypsochromic
To Greater Absorbance	Hyperchromic
To Lower Absorbance	Hypochromic

Thus, extending conjugation generally results in bathochromic and hyperchromic shifts in absorption. The appearance of several absorption peaks or shoulders for a given chromophore is common for highly conjugated systems, and is often solvent dependent. This fine structure reflects not only the different conformations such systems may assume, but also electronic transitions between the different vibrational energy levels possible for each electronic state. Vibrational fine structure of this kind is most pronounced in vapor phase spectra, and is broadened and obscured in solution.

To understand why conjugation should cause bathochromic shifts in the absorption maxima of chromophores, the relative energy levels of the π -orbitals need to be considered. When two double bonds are conjugated, the four p-atomic orbitals combine to generate four π -molecular orbitals (two are bonding and two are antibonding). In a similar manner, the three double bonds of a conjugated triene create six π -molecular orbitals, half of them bonding, half antibonding. The energetically most favorable $\pi \rightarrow \pi^*$ excitation occurs from the highest energy bonding π -orbital (HOMO) to the lowest energy antibonding π -orbital (LUMO).

The diagrams illustrated in Figure 18 represent the excitation for an isolated double bond (only two π -orbitals), for a conjugated diene, and triene, respectively. In each case the HOMO is colored blue and the LUMO is colored magenta. Increased conjugation brings the HOMO and LUMO orbitals closer together. The energy (ΔE) required to promote the electron is therefore less, and the wavelength that provides this energy is increased correspondingly.

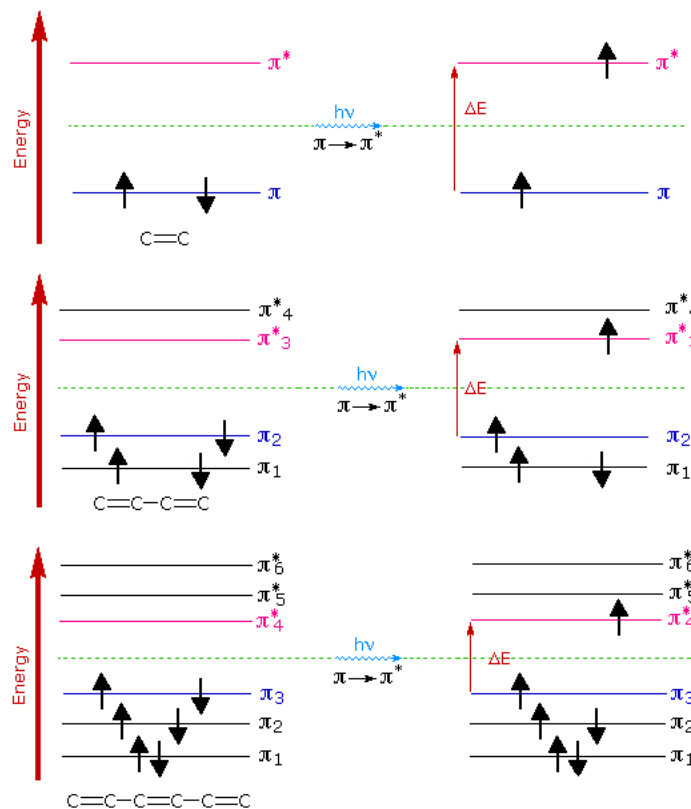


Figure 18 Diagram showing the effect of conjugation on the change in energy (ΔE) for isolated double bond, diene and triene when transitions from HOMO to LUMO orbitals are considered

Many other kinds of conjugated π -electron systems act as chromophores and absorb light in the 200 to 800 nm region. These include unsaturated aldehydes and ketones and aromatic ring compounds.

4.2.1.2 Spectrophotometers – the Design of HPLC Spectrophotometric Detectors

The multi-wavelength detectors employ light sources that emit light over a wide range of wavelengths (deuterium lamps operate in the UV region 180 – 370 nm). Employing an appropriate optical system (a prism or diffraction grid), light of a specific wavelength can be selected for detection purposes. Light of a specific wavelength might be chosen where a solute has an absorption maximum to provide maximum sensitivity. Alternatively, the absorption spectra of the eluted substances could be obtained for identification purposes

by scanning over a range of wavelengths. The latter procedure, however, differs with the type of multi-wavelength detector being used. There are two basic types of multi-wavelength detectors, the dispersion detector and the diode array detector, the latter being the more popular.

In the dispersive instrument, the light is dispersed before it enters the sensor cell and thus virtually monochromatic light passes through the cell. A diagram of the multi-wavelength dispersive UV/VIS detector is shown in Figure 19.

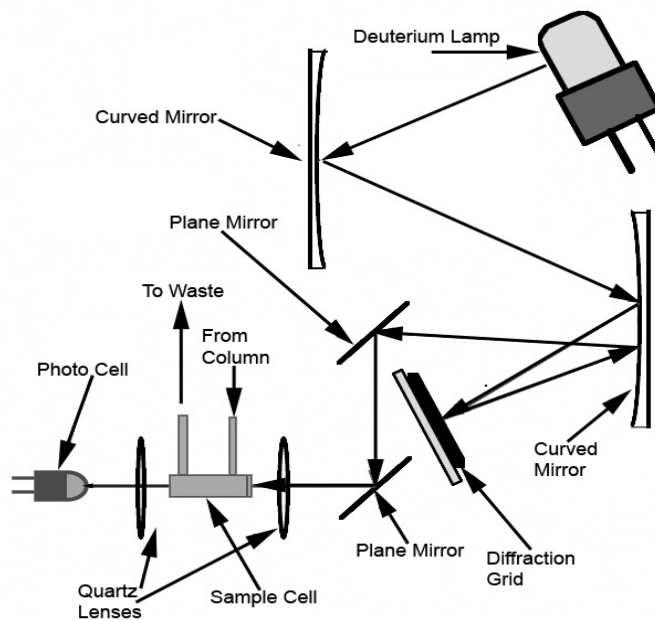


Figure 19 Set-up of the multi-wavelength dispersive detector

The diode array detector operates quite differently. Light of all wavelengths generated by the deuterium lamp and the lamp which generates light in the visible range of the electromagnetic spectrum is passed through the cell and then dispersed over an array of diodes. Thus, the absorption at discrete groups of wavelengths is continuously monitored at each diode. A diagram of the diode array detector is shown in Figure 20.

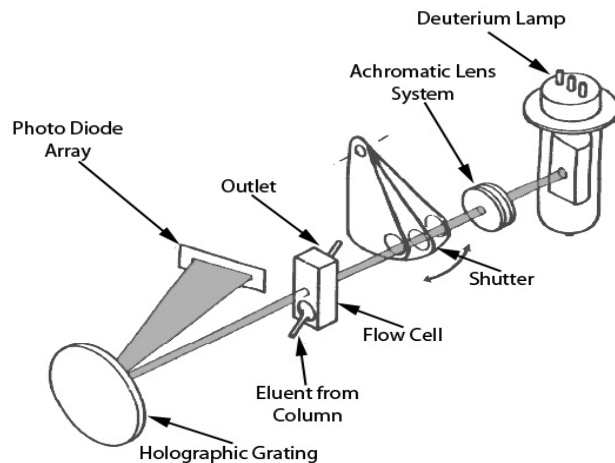


Figure 20 Set-up of the diode array detector

4.2.1.3 Light Absorption and Fullerenes

The electronic absorption spectra of C_{60} and C_{70} , given here simply as an example, are characterized by several stronger absorptions between 190 and 410 nm as well as by some forbidden transitions in the visible part of the spectrum.^[39] Their UV/VIS spectra are presented in Figures 21 and 22.

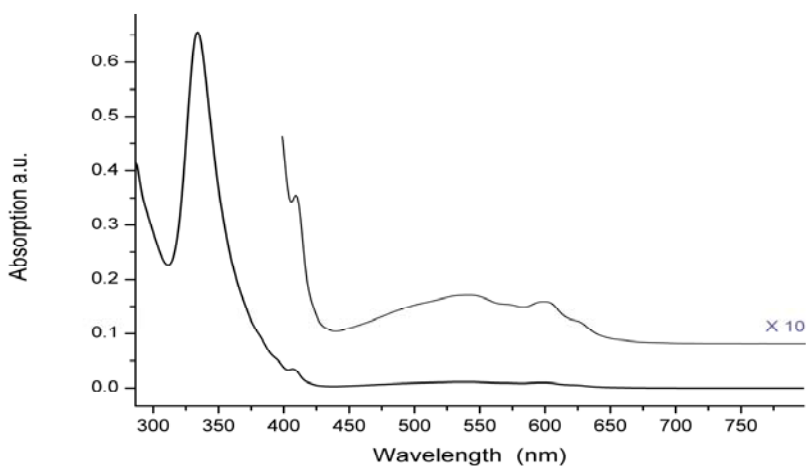


Figure 21 UV/VIS spectra of C_{60} in toluene

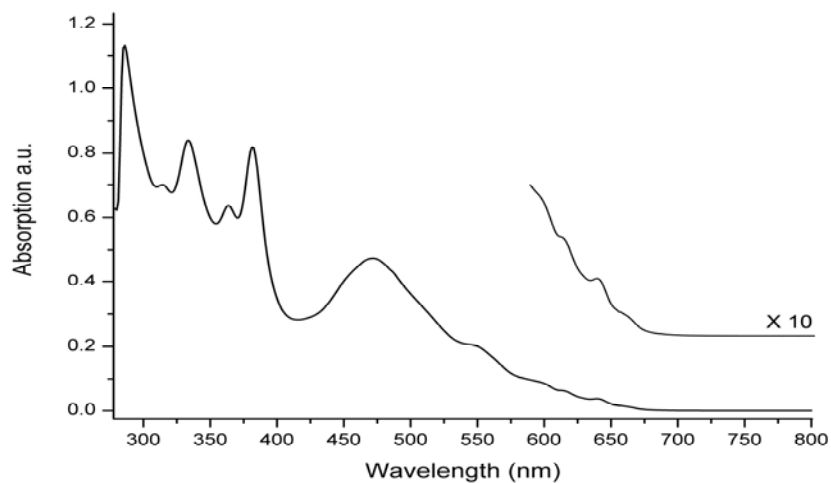


Figure 22 UV/VIS spectra of C_{70} in toluene

For C_{60} , the assignment of the transitions has been carried out on the basis of theoretical calculations.^[40,41] The absorptions between 190 and 410 nm are due to allowed $\pi - \pi^*$ transitions, whereas those between 410 and 620 nm are due to orbital forbidden singlet-singlet transitions. The latter absorptions are responsible for the purple color of C_{60} and the red color of C_{70} .

4.2.2 Matrix Assisted Laser Desorption Ionization – Time of Flight Mass Spectrometry

One of the frequently used analytical techniques in fullerene research, especially when complex fullerene extracts are analyzed, is the MALDI – TOF MS. The main reasons for selecting this type of mass spectrometry are: Laser ionization is a soft type of ionization, the method provides a broad mass range, the data acquisition is rather fast, the MALDI – TOF appliances are easy to use and maintain (for example no additional supply of gases is required) and it provides high sensitivity, superior mass resolution and accuracy.

4.2.2.1 Theory behind the Time of Flight Analysis

After ionizing the atoms, the respective ions are accelerated by an electric field such that an arbitrary ion possesses the same kinetic energy as any other ion with the same charge. What actually happens when the ion is accelerated into the time-of-flight tube by the voltage, U is that its potential energy, E_p converts to kinetic energy. The potential energy of the charged particle is proportional to its effective charge, z and U :

$$E_p = zU$$

The kinetic energy, E_k given by the equation,

$$E_k = \frac{1}{2}mv^2$$

where m is the mass of the particle and v is its linear velocity, is equal to the potential energy meaning that:

$$zU = \frac{1}{2}mv^2$$

The velocity of the particle inside the tube can be determined since the length of its path (d) is known and the time of its flight (t) can be measured. Therefore:

$$v = \frac{d}{t}$$

By substituting the value of v , the following equation is obtained:

$$zU = \frac{1}{2}m\left(\frac{d}{t}\right)^2$$

Rearranging that equation so that the flight time is expressed by everything else gives:

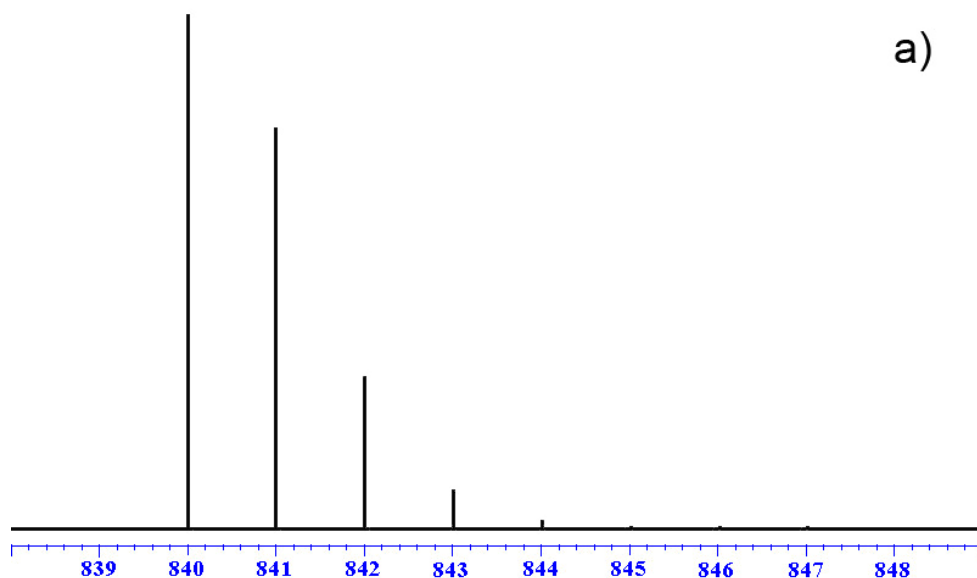
$$t^2 = \frac{d^2}{2U} \frac{m}{z}, \text{ or } t = \frac{d}{\sqrt{2U}} \sqrt{\frac{m}{z}}$$

The factor $\frac{d}{\sqrt{2U}}$ represents a constant that in principle does not change when a set of ions are analyzed in a single pulse of acceleration. The last equation can thus be given as:

$$t = k \sqrt{\frac{m}{z}}$$

where **k** is a proportionality constant representing factors related to the instrument settings and characteristics.

Additional information for the elemental composition of a concrete molecule (molecular ion) under investigation might be obtained from its isotopic distribution pattern. The relative intensities of individual peaks theoretically should provide the exact elemental composition. For example, from the mass to charge ratio of 840 of a molecular ion (the first most intensive signals in both mass spectra in Figure 23), except C₇₀-fullerene one might as well expect a species with the composition C₆₂O₆. However, comparing the relative intensities of the signals, the difference between both compositions here can be easily recognized.



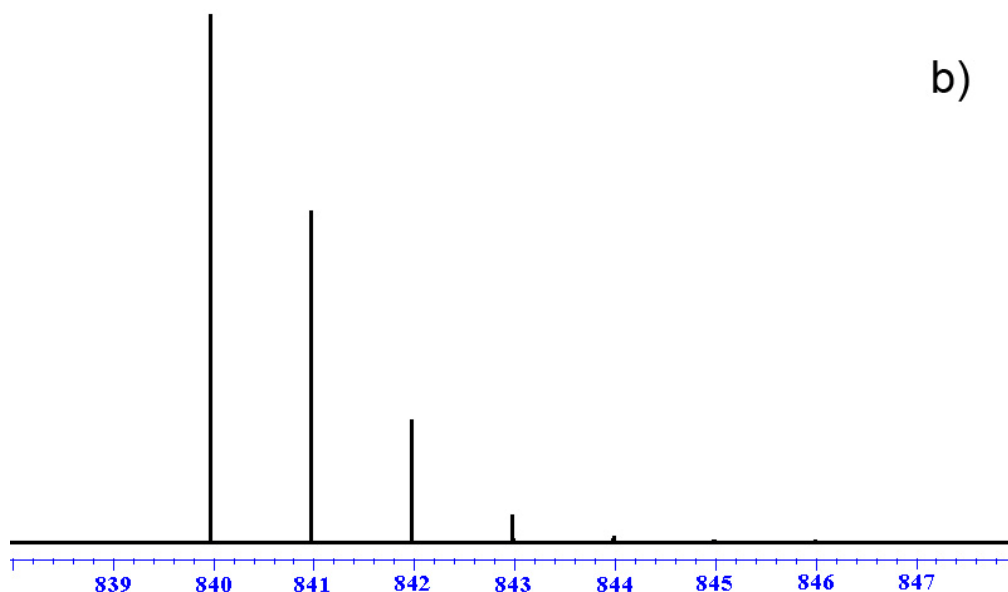


Figure 23 Calculated isotopic distribution patterns of C₇₀-fullerene (a) and a molecule with composition C₆₂O₆ (b). The relative intensities of the signals can be used to differentiate between both species

4.2.2.2 Set-up of the Time of Flight Mass Spectrometer

The ionization of the sample being analyzed is triggered by a laser beam (ArF – laser). Sometimes, a matrix is used to protect the analyzed molecule from being destroyed by the direct laser beam and to facilitate vaporization and ionization (if the matrix is avoided the technique might well be called LDI, i.e. laser desorption ionization only). The type of a mass spectrometer most widely used with MALDI is the TOF MS, mainly due to its large range of mass detection. The TOF measurement procedure is also ideally suited to the MALDI process since the pulsed laser takes individual “shots” rather than working in continuous operation. A TOF MS consists of a mass analyzer and a detector.

The TOF mass analyzer can be a linear flight tube or a reflectron. The reflectron is used to correct the kinetic energy distribution in the direction of ion flight. The reflectron uses an electrostatic field to reflect the ion beam toward the detector. The more energetic ions penetrate deeper into the reflectron, and take a slightly longer path to the detector. Less energetic ions of the same charge and mass will only penetrate a short distance into the

reflectron and take a shorter path to the detector. The detector is placed at the focal point where ions of different energies focused by the reflectron strike at the same time. A schematic representation of the reflectron TOF MS is shown in Figure 24.

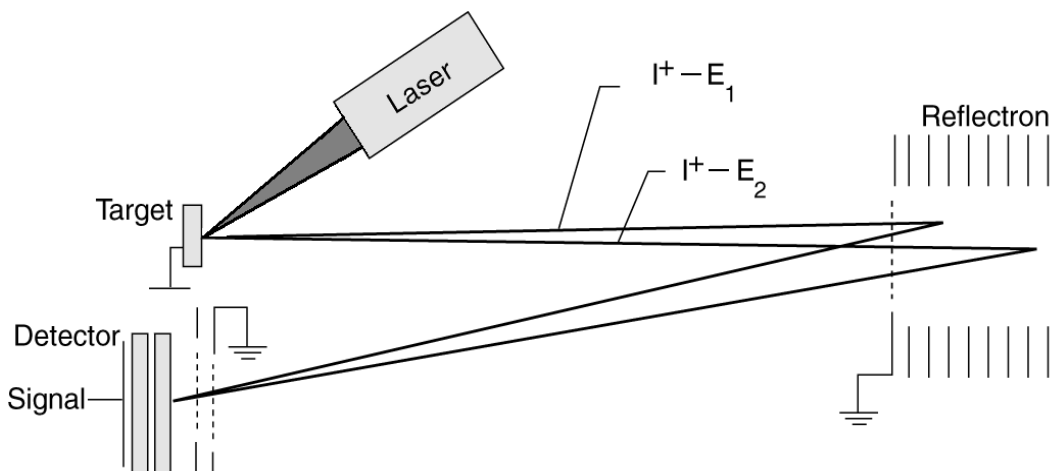


Figure 24 Schematic chart of LDI TOF MS showing the simultaneous arrival at the detector of two ions (I^+) possessing equal m/z ratios but different kinetic energies (E_1 and E_2)

The TOF MS detectors generally consist of a micro-channel plate detector and a fast analog-to-digital convertor.

The MALDI TOF MS used during the course of this thesis is Bruker Reflex IV (Bruker Daltonics, Germany).

4.2.3 Single Crystal X-ray Diffraction

Single crystal X-ray diffraction is a non-destructive analytical method which delivers information about the lattice structure of crystalline substances, including unit cell parameters, bond-lengths, bond-angles, etc. Directly related is single-crystal refinement, where the data generated from the X-ray analysis is interpreted and refined to obtain the crystal structure.

4.2.3.1 Fundamental Relationships

X-ray diffraction is based on the constructive interference of monochromatic X-rays and the crystalline sample. These X-rays are generated by a cathode ray tube, filtered to produce monochromatic radiation, collimated to concentrate, and directed toward the sample. The interaction of the incident rays with the sample produces constructive interference (thus a diffracted ray) when conditions satisfy Bragg's Law;

$$n\lambda = 2d \sin\theta$$

where the wavelength of the electromagnetic radiation (λ) is related to the diffraction angle (θ) and the lattice spacing in the crystalline sample (d). These diffracted X-rays are then detected, counted and processed. By changing the geometry of the incident rays, the orientation of the centered crystal and the detector, all possible diffraction directions of the lattice are attained.

Usually, crystal structures contain several thousand unique reflections, the spatial arrangement of which is referred to as a diffraction pattern. Indices (hkl) may be assigned to each reflection, indicating its position within the diffraction pattern. This pattern has a reciprocal Fourier transform relationship to the crystal lattice and the unit cell in real space. This step is referred to as the solution of the crystal structure. After the structure is solved, it is further refined using the least-squares techniques.

4.2.3.2 Instrumentation

X-ray diffractometers consist of three basic elements; an X-ray tube, a sample holder, and an X-ray detector. X-rays are generated in a cathode ray tube by heating a filament to produce electrons, accelerating the electrons toward a target by applying a voltage, and impact of the electrons with the target material. When electrons have sufficient energy to dislodge inner shell electrons of the target material, characteristic X-ray spectra are produced. These spectra consist of several components, the most common being K_{α} and

K_{β} . K_{α} consists, in part, of $K_{\alpha 1}$ and $K_{\alpha 2}$. $K_{\alpha 1}$ has a slightly shorter wavelength and twice the intensity as $K_{\alpha 2}$. The specific wavelengths are characteristic with respect to the target material. Filtering, by foils or crystal monochromators, is required to produce monochromatic X-rays needed for diffraction. $K_{\alpha 1}$ and $K_{\alpha 2}$ are sufficiently close in wavelength such that an average of the two is used. Molybdenum is the most common target material for single crystal diffraction, with $\text{Mo}_{K_{\alpha}}$ radiation = 0.7107\AA . These X-rays are collimated and directed onto the sample. When the geometry of the incident X-rays impinging the sample satisfies the Bragg's Equation, constructive interference occurs. Figure 25 represents schematically the set-up of a single crystal X-ray diffractometer with four degrees of freedom (the rotation angles 2θ , ω , ϕ and χ):

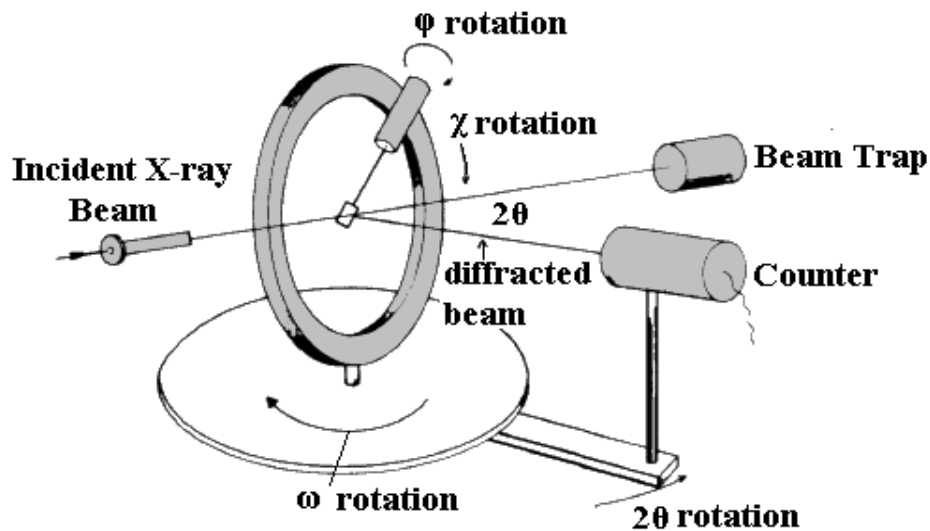


Figure 25 Single crystal X-ray diffractometer

Those X-rays which are not diffracted are either transmitted through the crystal or reflected off the crystal surface. A beam stop is located directly opposite the incident beam to block transmitted rays and prevent burn-out of the detector. Reflected rays are not picked up by the detector due to the different angles involved. Diffracted rays at the correct orientation are then collected by the detector.

4.2.3.3 Data Collection and Results Presentation

Once the crystal is mounted and centered, a preliminary rotational image is collected to screen the sample quality and to select parameters for later steps. An automatic collection routine can then be used to collect a preliminary set of frames for determination of the unit cell. Reflections from these frames are auto-indexed to select the reduced primitive cell and calculate the orientation matrix which relates the unit cell to the actual crystal position within the beam. The primitive unit cell is refined using least squares and then converted to the appropriate crystal system and Bravais lattice. This new cell is also refined using least squares to determine the final orientation matrix for the sample. After the refined cell and orientation matrix have been determined, intensity data is collected. Generally this is done by collecting a sphere or hemisphere of data using an incremental scan method, collecting frames in 0.1° to 0.3° increments (over certain angles while others are held constant). Data is typically collected between 4° and 60° 2θ for molybdenum radiation. A complete data collection may require anywhere between 6 – 24 hours, depending on the specimen and the diffractometer. Exposure times of 10 – 30 seconds per frame for a hemisphere of data will require total run time of 6 – 13 hours.

After the data have been collected, corrections for instrumental factors, polarization effects, X-ray absorption and (potentially) crystal decomposition must be applied to the entire data set. This integration process also reduces the raw frame data to a smaller set of individual integrated intensities.

When the final data set have been produced, the phase problem must be solved to find the unique set of phases that can be combined with the structure factors to determine the electron density and, therefore, the crystal structure. A number of different procedures exist for solving the phase problem, but the most common method is the least squares.

Solution of the phase problem leads to the initial electron density map. Elements can be assigned to intensity centers, with heavier elements associated with higher intensities. Distances and angles between intensity centers can also be used for atom assignment based on likely coordination. If the sample is of a known material, a template may be used for the initial solution.

Once the initial crystal structure is solved, various steps can be done to attain the best possible fit between the observed and calculated crystal structure. The final structure solution will be presented with an R value, which gives the percent variation between the calculated and observed structures.

4.3 Computations

For the aims of this thesis different computational approaches have been employed. Among them, *ab initio* quantum chemistry methods of DFT (density functional theory), perturbation theory and coupled cluster techniques have been used for describing the molecular systems under investigation as well as for some effects observed in the solid state. In this chapter short notation for each of the employed methods is given.

4.3.1 Density Functional Theory

DFT methods are often considered to be *ab initio* methods for determining the molecular electronic structure, even though many of the most common functionals use parameters derived from empirical data, or from more complex calculations. In DFT, the total energy is expressed in terms of the total one-electron density rather than the wave function. In this type of calculation, there is an approximate Hamiltonian and an approximate expression for the total electron density. DFT methods can be very accurate for little computational cost. Some methods combine the density functional exchange functional with the Hartree-Fock exchange term and are known as hybrid functional methods. DFT is among the most popular and versatile methods available in condensed-matter physics, computational physics, and computational chemistry.

DFT has been very popular for calculations in solid state physics since the 1970s. In many cases the results of DFT calculations for solid-state systems agreed quite satisfactorily with experimental data. Also, the computational costs were relatively low when compared to traditional ways which were based on the complicated many-electron wavefunction, such as Hartree-Fock theory and its descendants. However, DFT was not considered accurate enough for calculations in quantum chemistry until the 1990s, when

the approximations used in the theory were greatly refined to better model the exchange and correlation interactions. DFT is now a leading method for electronic structure calculations in chemistry and solid-state physics.

Despite the improvements in DFT, there are still difficulties in using density functional theory to properly describe intermolecular interactions, especially van der Waals forces (dispersion); charge transfer excitations; transition states, global potential energy surfaces and some other strongly correlated systems. Its poor treatment of dispersion renders DFT unsuitable (at least when used alone) for the treatment of systems which are dominated by dispersion or where dispersion competes significantly with other effects.

4.3.2 Hartree-Fock Method

In computational chemistry, the Hartree-Fock method is an approximate method for the determination of the ground-state wavefunction and ground-state energy of a quantum many-body system.

The Hartree-Fock method assumes that the exact, N-body wavefunction of the system can be approximated by a single Slater determinant (in the case where the particles are fermions) or by a single permanent of N spin-orbitals (in the case of bosons). By invoking the variational principle, one can derive a set of N-coupled equations for the N spin orbitals. Solution of these equations yields the Hartree-Fock wavefunction and energy of the system, which are approximations of the exact ones. The Hartree-Fock method finds its typical application in the solution of the electronic Schrödinger equation of atoms, molecules, and solids.

The Hartree-Fock method is also called the self-consistent field method. The solutions to the resulting non-linear equations behave as if each particle is subjected to the mean field created by all other particles. The equations are almost universally solved by means of an iterative, fixed-point type algorithm. For molecules, Hartree-Fock is the central starting point for most *ab initio* quantum chemistry methods.

4.3.3 Moeller-Plesset Perturbation Theory

Moeller-Plesset perturbation theory (MP) is one of several quantum chemistry post-Hartree-Fock *ab initio* methods in the field of computational chemistry. It improves on the Hartree-Fock method by adding electron correlation effects by means of Rayleigh-Schrödinger perturbation theory, usually to second (MP2), third (MP3) or fourth (MP4) order.

MP2, MP3, and MP4 Moeller-Plesset calculations are standard levels used in calculating small systems and are implemented in many computational chemistry codes. However, various important molecular properties calculated at MP3 and MP4 level are in no way better than their MP2 counterparts, even for small molecules. Higher level MP calculations, generally only MP5, are possible in some codes. They are rarely used because of their costs.

4.3.4 Coupled Cluster Methods

Coupled cluster (CC) is a numerical technique used for describing many-body systems. Its most common use is as one of several quantum chemical post-Hartree-Fock *ab initio* quantum chemistry methods in the field of computational chemistry. It starts from the Hartree-Fock molecular orbital method and adds a correction term to take into account electron correlation. Some of the most accurate calculations for small to medium sized molecules use this method.

The method was initially developed by Fritz Coester and Hermann Kümmel in the 1950s for studying nuclear physics phenomena, but became more frequently used after reformulating the method for electron correlation in atoms and molecules. It is now one of the most prevalent methods in quantum chemistry that includes electronic correlation. The classification of traditional coupled-cluster methods rests on the highest number of excitations allowed in the definition of \check{T} . The abbreviations for coupled-cluster methods usually begin with the letters "CC" (for coupled cluster) followed by **S** - for single excitations (shortened to singles in coupled-cluster terminology), **D** - for double

excitations (doubles), **T** - for triple excitations (triples) and **Q** - for quadruple excitations (quadruples). Thus, the \check{T} operator in CCSDT has the form:

$$T = \check{T}_1 + \check{T}_2 + \check{T}_3$$

Terms in round brackets indicate that these terms are calculated based on perturbation theory. For example, a CCSD(T) approach simply means that the coupled-cluster method includes singles and doubles fully calculated within the method and triples calculated with perturbation theory.

The complexity of equations and the corresponding computer codes, as well as the cost of the computation increases sharply with the highest level of excitation. For many applications the sufficient accuracy may be obtained with CCSD, and the more accurate (and more expensive) CCSD(T) is often called "the gold standard of quantum chemistry" for its excellent compromise between the accuracy and the cost. More complicated coupled-cluster methods such as CCSDT and CCSDTQ are used only for high-accuracy calculations of very small molecules. The inclusion of all n levels of excitation for the n -electron system gives the exact solution of the Schrödinger equation within the given basis set, within the Born-Oppenheimer approximation (although schemes could also be drawn up to work without the Born-Oppenheimer approximation with great cost).

5 Special Part

The objective of this PhD work is to demonstrate means for obtaining isomerically pure bulk amounts of individual higher fullerenes aiming at their further chemical and structural investigation. This part of the thesis is divided into two sections. The first one is devoted to the various chromatographic techniques and different methodologies (chromatographic systems selection) developed and employed throughout, resulting in the bulk isolation of a number of individual fullerene isomers in pure form. The second section is dedicated to the structural investigations, through single crystal X-ray analyses, of a number of crystals containing derivatives of individual higher fullerene isomers. The connectivity patterns of the respective parent fullerenes are crystallographically confirmed for the first time. Special attention is given to some peculiar findings concerning the reactivities of higher fullerenes in general, as well as to the description of a type of intermolecular interaction, which is believed to be the structure formation motive.

5.1 Opening Remarks

The molecular structures of all stable fullerenes up to C_{100} have been predicted by mathematical enumeration.^[12] Combining this geometric contrivance with NMR studies has resulted in the molecular structure confirmation of diverse fullerene species. However, in many cases NMR analyses are restricted to only assigning fullerene isomers to point groups, making the final outcome ambiguous. Therefore, a direct method of structure determination, such as X-ray crystallography, is envisaged to solve the query of single isomer recognition. To prepare high quality mono-constituent fullerene crystals is an unfeasible task. This is due to the virtually spherical shape of all fullerenes, which gives rise to orientational and dynamic disorder even at low temperatures. Two different ways to solve this problem have generally been followed. Along the first approach, cocrystals of fullerenes with many other molecular species have been investigated.^[42] However, from the vast number of fullerene cocrystals, only one structure of a fully

ordered higher fullerene is reported – C₈₄(14) · AgTPP (Ag tetraphenylporphyrin).^[43] The second option has been focused on fullerene derivatives. For the aims of this work, chlorination has been preferred as a method of covalent derivatization. There are two main reasons advocating the choice made. First, the relative stability of the carbon-chlorine bond provides a possibility to separate otherwise scarcely separable isomers through their chlorine derivatives, avoiding the laborious recycling HPLC. The parent fullerene molecules can be regenerated later from their chlorine derivatives under elevated temperatures (soft regeneration). Second, halogenation, and particularly chlorination, represents an efficient approach for obtaining well crystallized fullerene species (see Table 3). Notwithstanding that halogenation partially lifts the conjugation of the π -electrons, the overall carbon connectivities have been found to persist in all halogenated fullerenes known thus far.

Table 3 Different halogenated fullerenes, the molecular structures of which have been confirmed through single crystal X-ray diffraction analyses. Note: depicted in bold are the compounds the structures of which are reported and discussed as a topic of this thesis. All structures reported in this thesis are of isomerically pure fullerenes. The crystals of the compounds denoted with * contain more than one fullerene isomer at the fullerene site (mixture of isomers). The crystals of the compounds denoted with ** contain individual fullerene isomers (only one fullerene isomer occupies the fullerene site in the respective crystal structure)

Halogen	F	Cl	Br
Fullerene			
C₆₀	C₆₀F₁₈ ^[44-47] , C ₆₀ F ₃₆ ^[48] , C ₆₀ F ₄₈ ^[49]	C ₆₀ Cl ₆ ^[50,51] , C ₆₀ Cl ₂₄ ^[52,53] , C ₆₀ Cl ₂₈ ^[54] , C ₆₀ Cl ₃₀ ^[47,53-55]	C₆₀Br₆ ^[56-59] , C ₆₀ Br ₈ ^[57-59] , C₆₀Br₂₄ ^[57-60]
C₇₀	C₇₀F₃₈ ^[61]	C ₇₀ Cl ₁₀ ^[62] , C ₇₀ Cl ₁₆ ^[63] , C ₇₀ Cl ₂₈ ^[64]	C₇₀Br₁₀ ^[62,65]
C₇₆(1)	-	C ₇₆ Cl ₁₈ ^[66]	-

$C_{78}(2)$	-	$C_{78}(2,3)Cl_{18}^{[62]*}$	$C_{78}(2,3)Br_{18}^{[69]*}$
$C_{78}(3)$	-	$C_{78}(2)Cl_{18}, C_{78}(3)Cl_{18},^{[67]**}$	-
$C_{78}(5)$	-	$C_{78}(5)Cl_{18}^{[68]}$	-
$C_{80}(2)$	-	$C_{80}Cl_{12}^{[70]}$	-

5.2 Isolation of Parent Fullerene Species – “Classical” and Alternative Approaches

5.2.1 Introduction

The systematic procedure which renders an enriched solution of higher fullerenes might be presented with the protocol displayed in Figure 26.

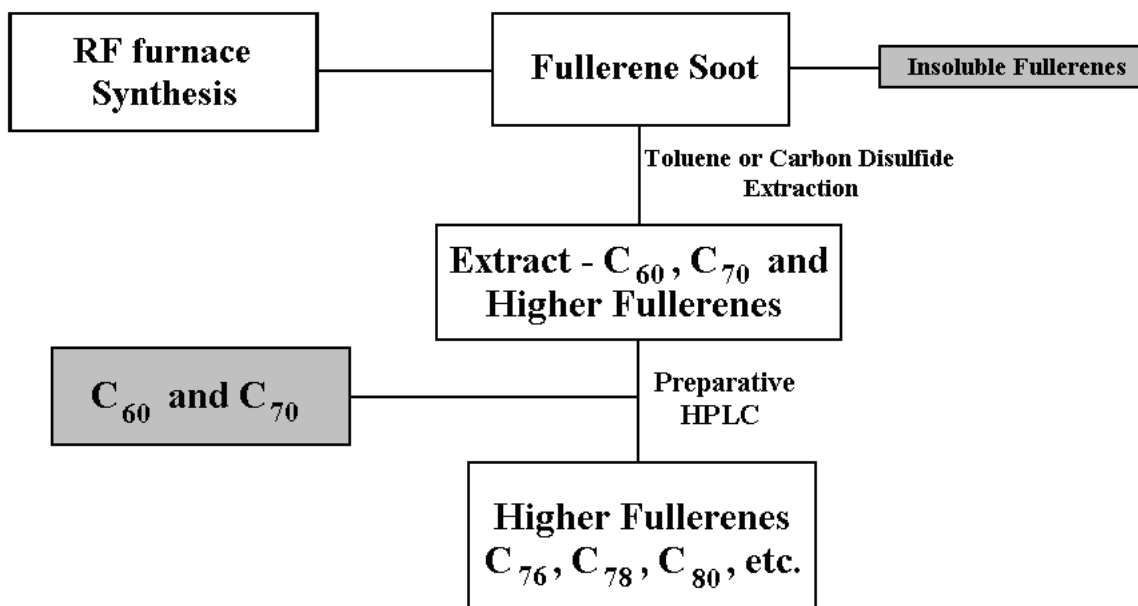


Figure 26 Systematic Procedure for obtaining enriched in higher fullerenes extract

The raw fullerene-containing soot generated along the RF-furnace route,^[28,29] has to be extracted in order to isolate the soluble fraction containing C₆₀, C₇₀ and the soluble isomers of some higher fullerenes from the rest of the solid material which consists mainly of graphitic particles as well as a fraction of insoluble fullerenes. The extraction medium of choice is either toluene (extraction with xylene has been attempted, but it has not shown to be a more effective extraction medium than toluene), or carbon disulfide depending on the extraction method employed. When soxhlet extraction is used, carbon disulfide is usually chosen because it has proven to be more effective than toluene. For comparison, after 48 hours of soxhlet extraction with toluene, the residual soot still contains some amounts of unextracted soluble fullerenes (a second extraction of the residual material with carbon disulfide confirms that). However, only 24 hours of extraction with carbon disulfide are enough to extract the whole fraction of soluble material. The same result is obtained with the accelerated solvent extractor Dionex ASE 100 using toluene as the extraction medium. After 20 – 25 cycles (each cycle lasts for approximately 25 minutes) the same amount of soot as that used for the soxhlet 24-hour-extraction with carbon disulfide is fully extracted.

The next step is the so called crude fraction collection. Before the introduction of the sample (the crude fullerene extract) into the liquid chromatograph becomes possible, it should be filtrated in order to get rid of the small graphitic particles which are usually present in the extract. The filters used for that purpose are with pore size of 0.45 µm (PTFE, Rotilabo®-Spritzenfilter, Carl Roth GmbH, Karlsruhe, Germany). The filtrated extract containing C₆₀, C₇₀ and the fraction of soluble higher fullerenes is introduced into the liquid chromatograph aiming at the separation of individual subfractions, each enriched with a concrete member of the higher fullerenes. The procedures which follow this crude fraction collection are individual for each fullerene, but as a final result render an isomerically pure fullerene species.

Within the scope of this thesis the following higher fullerene species have been isolated in isomerically pure form and in bulk amounts: D₂-C₇₆(1), D₃-C₇₈(1), C_{2v}-C₇₈(2), C_{2v}-C₇₈(3), D_{3h}-C₇₈(5), D₂-C₈₀(2), C₂-C₈₂, C₂-C₈₄, Cs-C₈₄(14), D₂-C₈₄ and D_{2d}-C₈₄ (fullerene nomenclature according to [12]).

5.2.2 Isolation of D₂-C₇₆(1)

The isolation procedure for C₇₆(1) is comparatively simple. This fullerene has first been isolated in pure form by R. Ettl et al. in 1991.^[8] For the needs of this thesis, C₇₆(1) has been separated from the coeluting C₇₈-fraction with the help of the Buckyprep column within two consecutive steps. In the first step (preparative fraction collection) the C₇₆-containing fraction is separated from the rest of the extract using a BP column (20 × 250 mm). A typical chromatogram displaying three consecutive injections in the automated preparative HPLC system is shown in Figure 27.

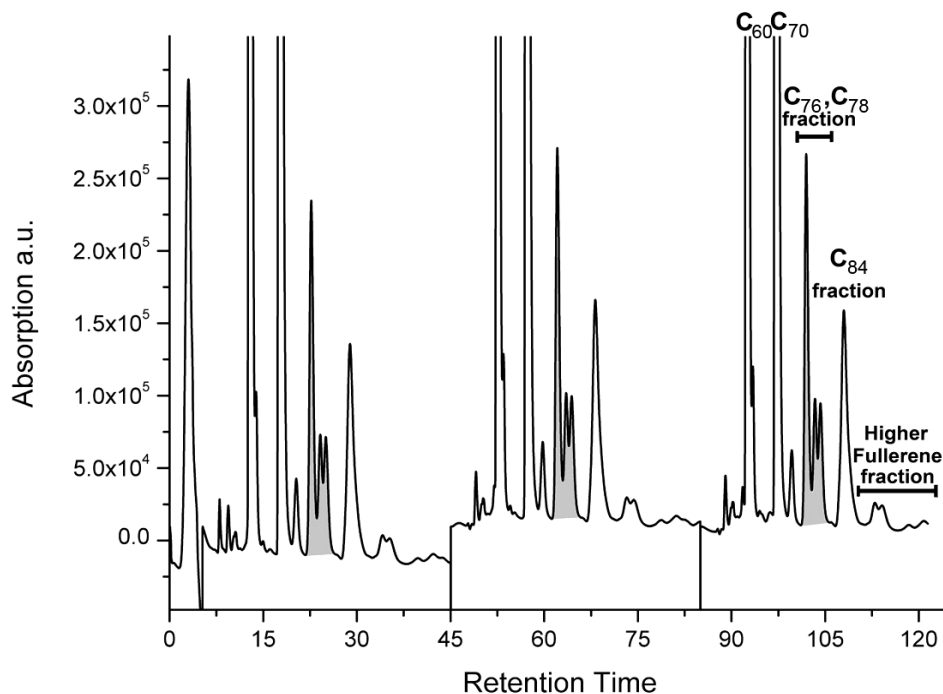


Figure 27 Preparative fraction collections, where the C₇₆-containing fractions are highlighted in gray

Collected C₇₆-containing fractions are concentrated before the second step of separation (semipreparative compound isolation). The second step, recycling HPLC, is executed with another BP column (10 × 250 mm) aiming at the separation of two subfractions: the first containing pure C₇₆(1) and the second a mixture of C₇₈(1), C₇₈(2) and C₇₈(3)

fullerenes, which is later used for the isolation of isomerically pure C_{78} species. The semipreparative run is presented in Figure 28. Toluene – hexane mixture (4:1) is used as a mobile phase for the first and second steps of separation with flow rates of 20 ml/min and 5 ml/min, respectively. The temperature in the column compartment is set to 20°C, although separations under different temperature conditions have been also attempted. The temperature of 20°C has shown to be the most suitable for this chromatographic system.

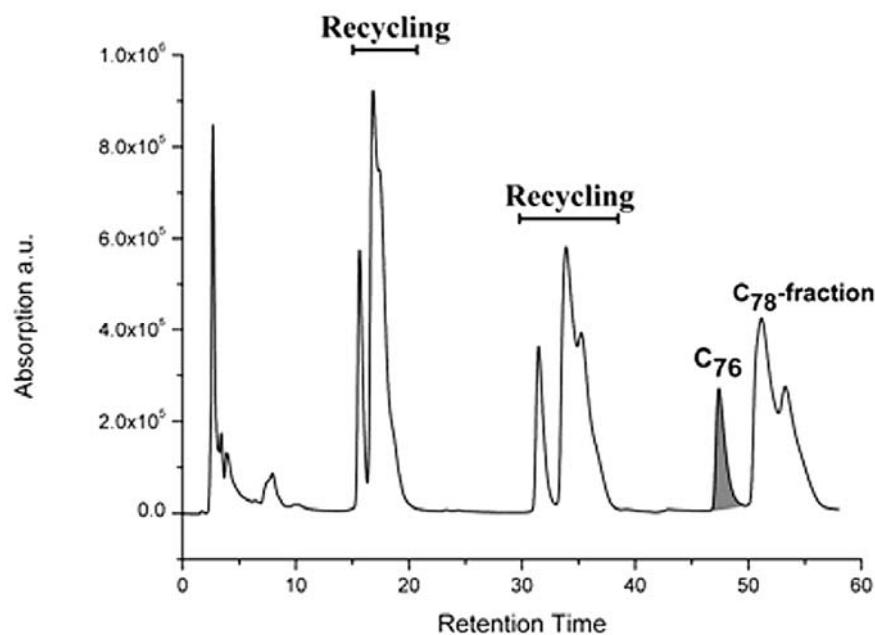


Figure 28 Recycling HPLC (semipreparative run) showing the isolation of a pure C_{76} -fraction (highlighted in grey)

5.2.3 Isolation of D_{3h} - C_{78} (5), D_2 - C_{80} (2), C_2 - C_{84} , C_s - C_{84} (14), D_2 - C_{84} and D_{2d} - C_{84} – Introduction of a New Mobile Phase for the Separation of Fullerene Species

The above mentioned fullerene isomers have been isolated in pure form with the help of an improved mobile phase consisting of 1:1 mixture of HPLC-grade toluene and dichloromethane. This new mobile phase provides conditions for the separation of C_{78} (5)

fullerene, which was mistakenly believed to be insoluble in common HPLC solvents (therefore absent from fullerene extracts) due to its very low HOMO-LUMO gap.^[15,16] However, thanks to the increased separation power of the chromatographic system using the new mobile phase composition, it is possible to show that $C_{78}(5)$ is present in solution.^[68] Most probably because of its very low amount in extracts and the insufficient ability of the conventionally employed in fullerene separation chromatographic systems to demonstrate its presence (it coelutes with the other C_{78} isomers), this isomer of C_{78} was never isolated in pure form before. The section of a chromatogram presented in Figure 29 shows the improved separation capability of the chromatographic system with the new mobile phase:

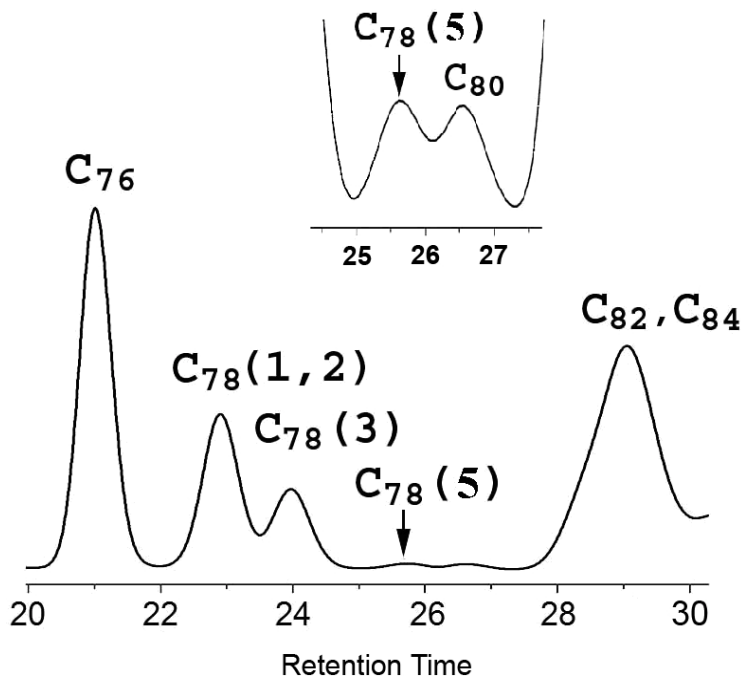


Figure 29 A section of a chromatogram showing the presence of $C_{78}(5)$ in extracts (note the scarce amounts of material). The inset represents a magnified region of the same chromatogram for better visibility

The first step towards the isolation of $C_{78}(5)$ in pure form is the preparative collection of its fraction which coelutes with the fractions of C_{76} , C_{78} (isomers 1,2 and 3), C_{82} and C_{84} (with its array of isomers). Here, again, the preparative BP column (20×250 mm) is used

for the fraction collection step with a mobile phase of toluene-hexane in ratio 4:1, 20 ml/min flow rate, and temperature of 20°C in the column compartment. Technically, a small fraction covering a time window of about two minutes and comprising the “tail” of the main C_{78} -fraction and the front of the next C_{82} – C_{84} -fraction is collected. Therefore, the fraction of $C_{78}(5)$ contains also amounts of C_{76} , all other isomers of C_{78} , $C_{80}(2)$ and C_{82} – C_{84} mixture (Figure 29). The next step is the introduction of the combined $C_{78}(5)$ -fractions (after proper concentration) into the semipreparative HPLC system for further purification. Usually, two cycles are enough to eliminate almost the whole amounts of C_{76} and C_{78} (1 and 2), and to cut off the most of $C_{78}(3)$ and C_{82} – C_{84} fractions. Nevertheless, comparatively high amounts of $C_{78}(3)$ and C_{82} fullerenes are still present (Figure 30).

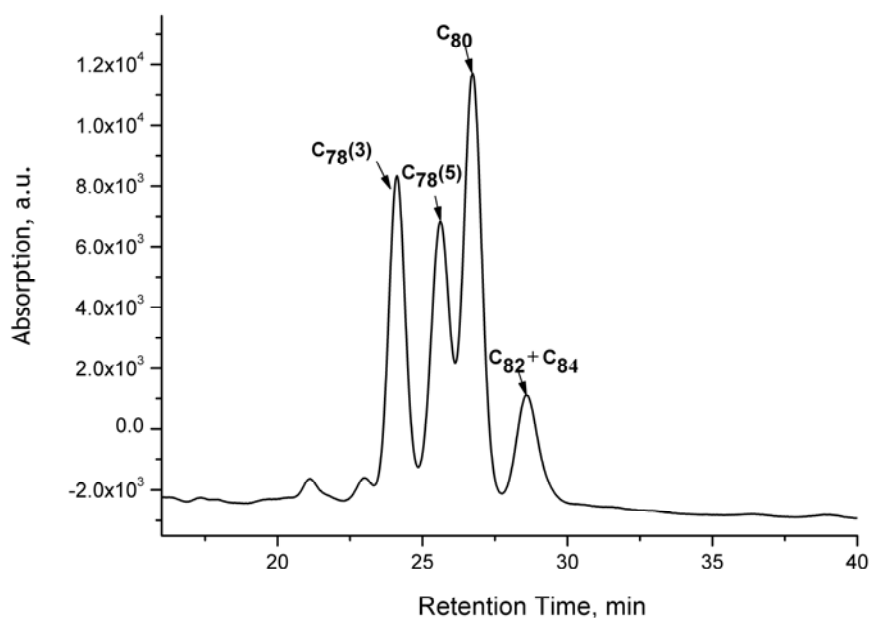


Figure 30 A section of a chromatogram showing the compounds distribution in $C_{78}(5)$ -containing fraction after elimination of the “interfering” C_{76} , $C_{78}(1,2)$ and the most of C_{82} – C_{84} fractions

Therefore, few more cycles in the semipreparative HPLC system are necessary in order to obtain pure $C_{78}(5)$ and $C_{80}(2)$ species. Additional chromatograms showing in detail the recycling stage of the whole isolation procedure for $C_{78}(5)$ and $C_{80}(2)$ are provided in the

Appendix Section of this thesis. The semipreparative BP column (10 × 250 mm) is employed during the compound isolation stage (recycling HPLC), while the mobile phase composition is set to 1:1 mixture of toluene-dichloromethane with flow rate of 5 ml/min and column compartment temperature of 20°C. The UV/VIS spectrum of C₇₈(5) is shown in Figure 31.

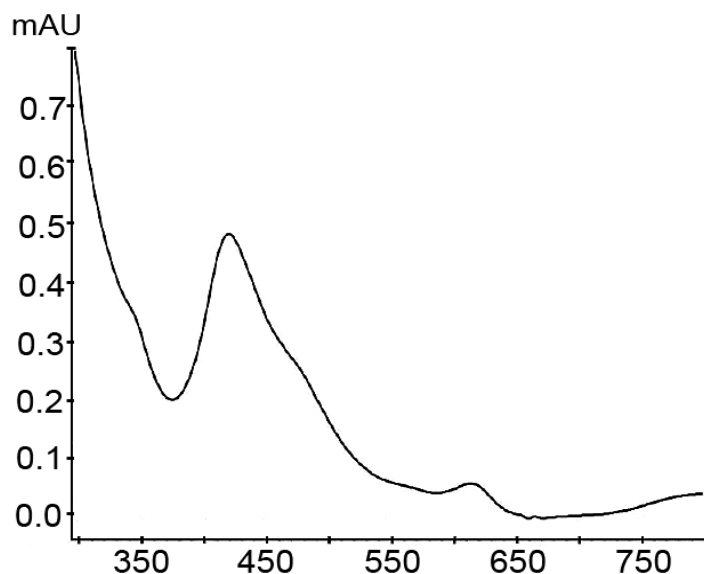


Figure 31 The UV/VIS spectrum of C₇₈(5) fullerene made in a mixture of toluene-dichloromethane (1:1) used as the solvent medium

The same chromatographic systems – preparative BP column as a stationary phase and toluene – hexane (4:1) as a mobile phase (flow rate 20 ml/min and column compartment temperature 20°C) are employed for the preparative fraction collection stage aiming at the isolation of four C₈₄ isomers – C₂-C₈₄, C_s-C₈₄(14), D₂-C₈₄ and D_{2d}-C₈₄. The consecutive isolation procedures are identical to those used for the isolation of C₇₈(5) and C₈₀(2), and the chromatograms showing the recycling HPLC for all four C₈₄ species are given in the Appendix Section. The chromatographic conditions used during this last stage of compound isolation are: semipreparative BP column as a stationary phase, toluene – dichloromethane mixture (1:1) as a mobile phase at 5 ml/min, and temperature in the column compartment set to 20°C.

The identity confirmation for all isolated compounds has been achieved through their TOF mass spectra together with the UV/VIS spectra (details are given in the Appendix Section). The newly developed methodology for the isolation of C₈₀(2) as well as the four C₈₄ isomers is more effective than the systematic procedures suggested in the literature.^[71-73]

5.2.4 An Alternative Route towards the Preparative Isolation of the Fullerene Isomers – D₃-C₇₈(1), C_{2v}-C₇₈(2) and C_{2v}-C₇₈(3)

A new rapid approach towards the preparative isolation of individual C₇₈-fullerene isomers is suggested. The three most abundant representatives of this cage can be obtained in isomerically pure form in three consecutive stages. Chemical modification with ICl provides a reasonable methodology for separation of isomers 1 and 2 through their chlorinated derivatives, the thermal instability of which enables the soft regeneration of the parent fullerenes.

5.2.4.1 Short Introduction to C₇₈-fullerenes – the First Multimembered Fullerene Family

Among the higher fullerenes, C₇₈ is the first representative possessing more than two IPR isomers,^[12] constituting by this the smallest multimembered fullerene family. According to the nomenclature suggested,^[12] the following IPR isomers have been predicted: D₃-C₇₈(1), C_{2v}-C₇₈(2), C_{2v}-C₇₈(3), D_{3h}-C₇₈(4) and D_{3h}-C₇₈(5). The first three have been isolated from fullerene extracts by means of different chromatographic methods.^[9,10] Due to the mistakenly ascribed insolubility in common solvents, a feature associated to some fullerenes' low or zero HOMO-LUMO gaps,^[15,16] C₇₈(5) has been only recently identified in fullerene extracts.^[68] The last member of the C₇₈-fullerene family, C₇₈(4), still remains undiscovered (there is no experimental evidence for its existence). Despite the relatively high abundance of extractable C₇₈ isomers, only a few derivatives of isomerically pure (with respect to the parent cages) fullerenes have been reported.^[62,67-69,74] The major handicap retaining any further investigation of the pristine fullerenes is a consequence of

the difficulties in obtaining preparative amounts of them, a drawback directly resulting from the inefficiency and laboriousness of the available separation techniques. Therefore, a more effective procedure for preparing bulk amounts of pure pristine fullerene isomers is needed.

5.2.4.2 Synthetic Approach towards the Chromatographic Isolation of Bulk Amounts of C₇₈-fullerene Isomers

As a first step, the C₇₈-containing fraction is separated from the rest of the fullerene extract using the preparative BP column as described for the isolation of C₇₆(1). The second step (recycling HPLC) is executed with the semipreparative BP column. Two subfractions are collected; the first one (**I**) containing a mixture of C₇₈(1) and C₇₈(2) isomers, and the second (**II**) pure C₇₈(3). Toluene – hexane mixture (4:1) is used as a mobile phase for both steps of separation with flow rates of 20 ml/min and 5 ml/min, respectively. The temperature in the column compartment is held to 20°C. Consecutively, the solvent from **I** is evaporated to dryness and the dry material redissolved in chlorobenzene. To this solution (50 ml, with approximate concentration of 5 mg/ml) slowly and under constant stirring, a solution of ICl in chlorobenzene in big excess with respect to the fullerene mixture (*ca.* 1:20 mol equivalents) is added. From thus obtained mixture, the solvent is evaporated to dryness (approximate evaporation temperature of 60°C), the residue redissolved in toluene and subsequently subjected to separation. The chlorine derivatives of C₇₈(1) and C₇₈(2) obtained from the reaction of ICl with the respective fullerenes are collected. At this stage the semipreparative BP column equipped with a guard column (Buckyprep Guard – 10 × 20 mm) and pure toluene as a mobile phase at flow rate of 5 ml/min are used. The temperature in the column compartment during this stage is held to 10°C in order to avoid any possible compound thermal destruction. Finally, each fraction is evaporated to dryness and the dry residue (yellowish to orange crystalline powder for the different fractions) heated to 300-350°C under vacuum until the color changes to black. The black material obtained gives in each case either isomerically pure C₇₈(1) or C₇₈(2). Approximately 8-10 mg of C₇₈(1) and 40-50 mg of C₇₈(2) can be isolated per full cycle of the above described procedure. The limit arises

from the specific capacity of the BP column used in the first step. Reversed phase polymeric 5C₁₈-AR column (4.6 × 250 mm) and a mixture of toluene – methanol (3:2) as a mobile phase with flow rate of 1ml/min are used to confirm the individual isomer purity. The UV/VIS spectra for both species obtained using this systematic procedure are compared to those previously published,^[9,10] in order to confirm the method successfulness.

5.2.4.3 The Motivation behind the Newly Developed Alternative Methodology

The chromatographic methods used for the isolation of the three most abundant C₇₈ isomers employ reversed phase octadecylsilyl (ODS) columns.^[9,10] Although the isomer purity achieved is satisfactory, the retention of fullerenes on C₁₈ packings is generally weak resulting in very low loadability (for the possible reasons explaining the weak interaction between the ODS stationary phases and fullerene molecules consult chapter 4.1.3.3 of this thesis). During the course of this work, the capacities of 5C₁₈-AR and BP columns have been investigated and compared (for reference the analytical columns (4.6 × 250 mm) of both stationary phases have been used). The capacity of C₁₈ column is exceeded when an amount of 150 µg sample is injected. At the same time, considerable drop in the separation efficiency is observed for the BP column when amounts higher than 6.75 mg of sample are introduced. Simple calculation shows that the loadability of the BP column exceeds that of C₁₈ about 45 times. Therefore, the use of C₁₈ packings as stationary phases for the preparative isolation of fullerene species is rather limited with respect to the expected yields. Since the BP phase alone is not capable of separating C₇₈(1) and C₇₈(2) (although it gives isomerically pure C₇₈(3)), an alternative technique avoiding the inefficient and laborious use of ODS phases is needed to provide preparative and fast separation of these two isomers.

Chemical modification has proven to be a reasonable approach towards the separation of individual isomers, since the derivatives of higher fullerenes are much easier to separate.^[75,76] In contrast to the methods reported in the literature, functionalization of the parent C₇₈ cages with ICl is chosen in the present case. The choice made is justified considering the following dependences: a) the reaction between the two C₇₈ isomers and

ICl is found to be rather selective, resulting in the generation of a few products for each of the isomers, b) the resolution achieved between the adjacent peaks (Figure 32) is satisfactory, providing a “single-run” isolation procedure (in contrast to the method suggested by Crassous et al.,^[76] c) the C-Cl bonds in the respective chlorine derivatives of both parent species are weak enough to provide soft conditions for nondestructive fullerene regeneration – only the C-Cl bonds are cleaved (the connectivity patterns of the pristine fullerenes are preserved), in contrast to the trifluoromethylation technique,^[74,75,77,78] which provides no means for selective removal of the CF₃ groups, d) the chlorine derivatives are stable enough at least during the separation stage.

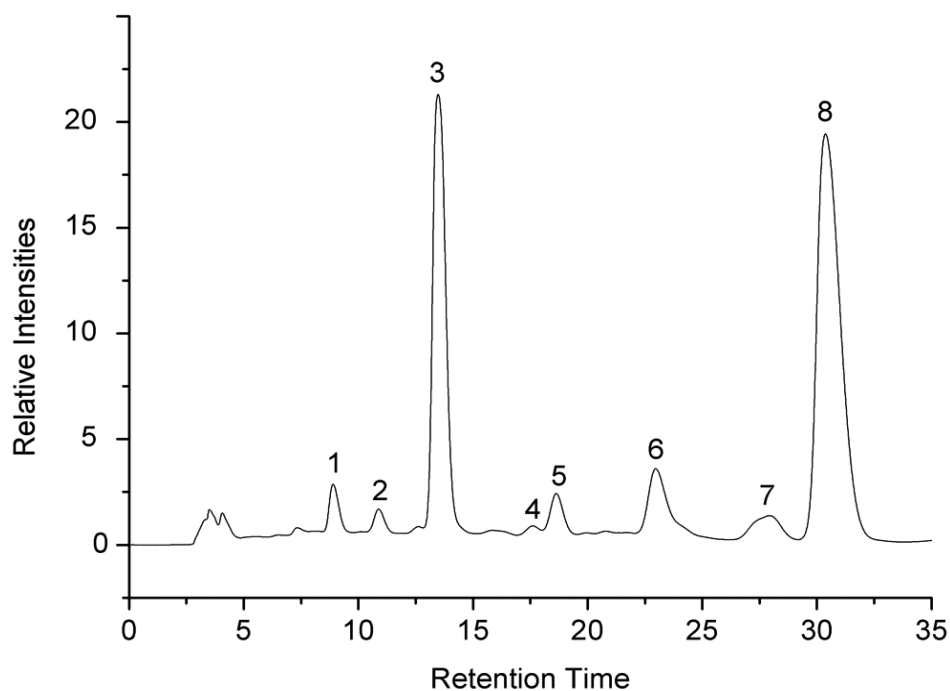


Figure 32 HPLC profile of the products of reaction of C₇₈ (mixture of isomers 1 and 2) with ICl. Eight prominent peaks might be distinguished

As can be seen in Figure 32, eight notable peaks corresponding to the chlorine derivatives of C₇₈(1) and C₇₈(2) can be distinguished. Each of the corresponding compounds (fraction 7 consists of two species) is isolated as a single fraction and subsequently decomposed at 300-350°C. The identity of each of the two fullerene isomers obtained

after decomposing the different derivatives is unambiguously given by their UV/VIS spectra (Figure 33), whereas the individual purity is confirmed by analyzing them on a 5C₁₈-AR column (for reference see Figure 34).

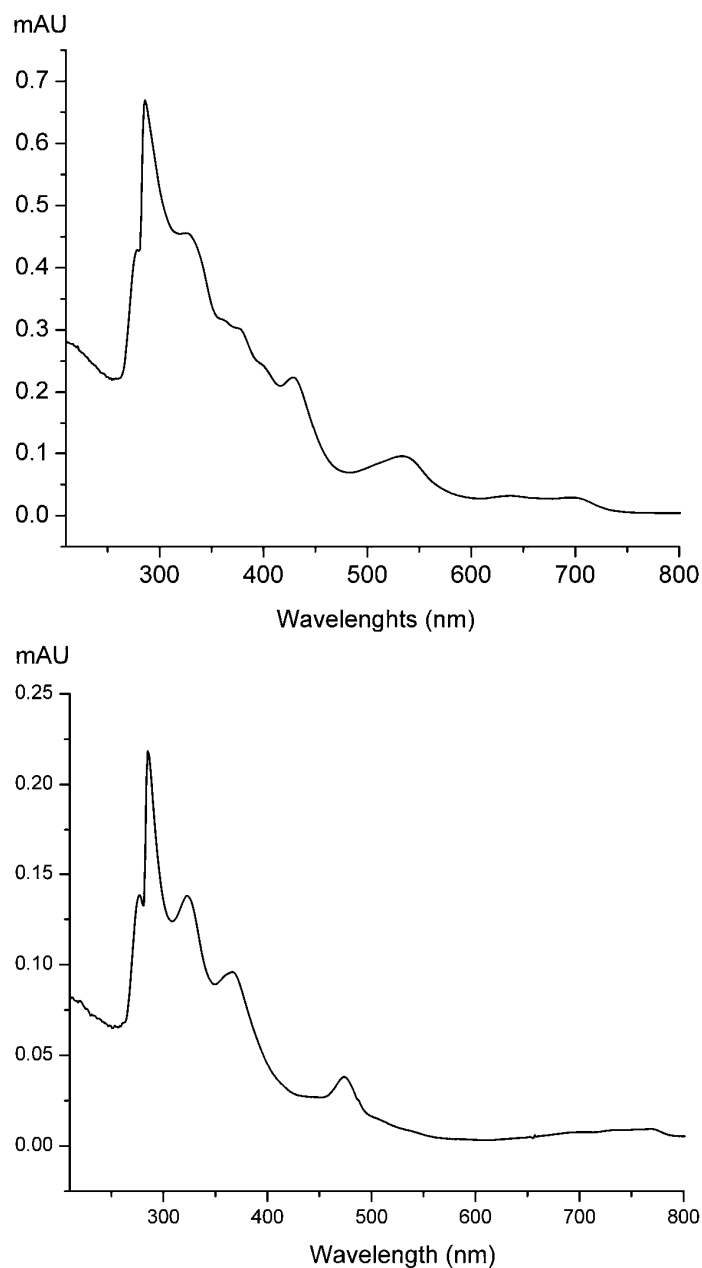


Figure 33 UV/VIS spectra of pure C₇₈ isomers 1 and 2. Top: C₇₈(2). Bottom: C₇₈(1). The spectra of both pristine fullerene isomers are identical to those previously reported.^[9,10]

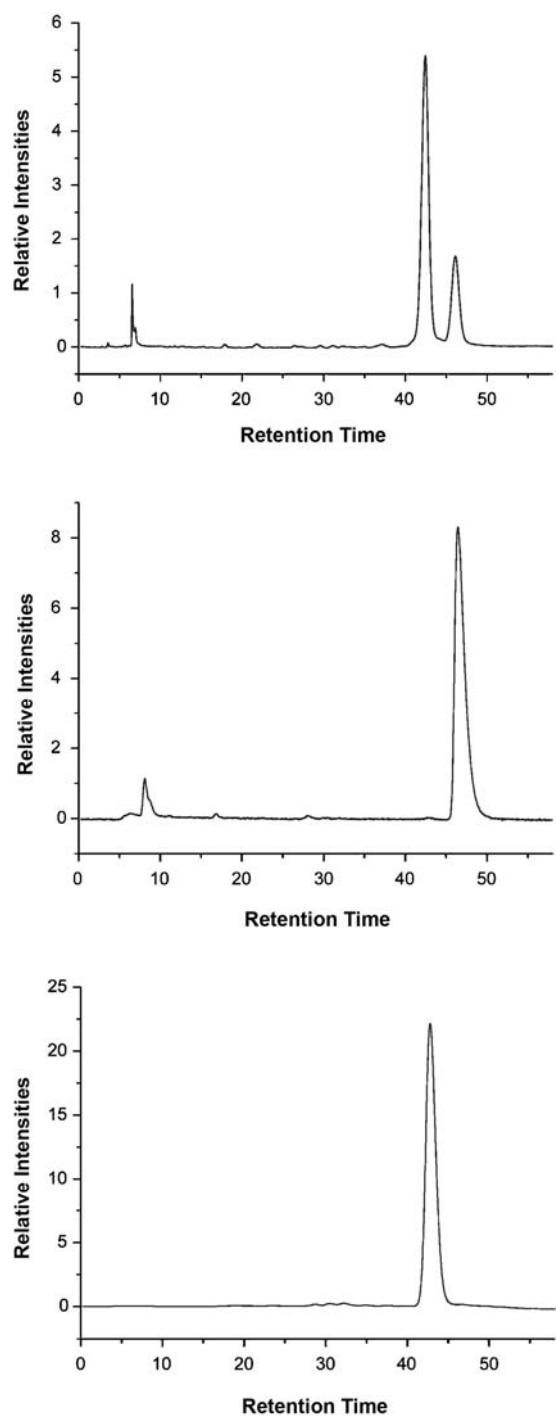


Figure 34 Different HPLC profiles of C₇₈ isomers on reversed phase 5C₁₈-AR (polymeric) column. Top: mixture of C₇₈(2), the first peak on the chromatogram, and C₇₈(1). Middle: Pure C₇₈(1) obtained after the decomposition of different compounds after the reaction of C₇₈ isomeric mixture with ICl. Bottom: Pure C₇₈(2) obtained employing the same procedure as to C₇₈(1)

As a final verification, the isomerically pure $C_{78}(1)$ and $C_{78}(2)$ need anew be subjected to chlorination with ICl, following the described procedure, in order to fully validate the suggested methodology. The distribution of the products obtained in each case substantiates the assignment made by the initial experiment. The three prominent peaks in the chromatogram shown in Figure 35 (left) correspond to the products obtained after chlorinating $C_{78}(1)$, while the other seven visible in the same figure (right) can be assigned to the chlorine derivatives of isomer $C_{78}(2)$.

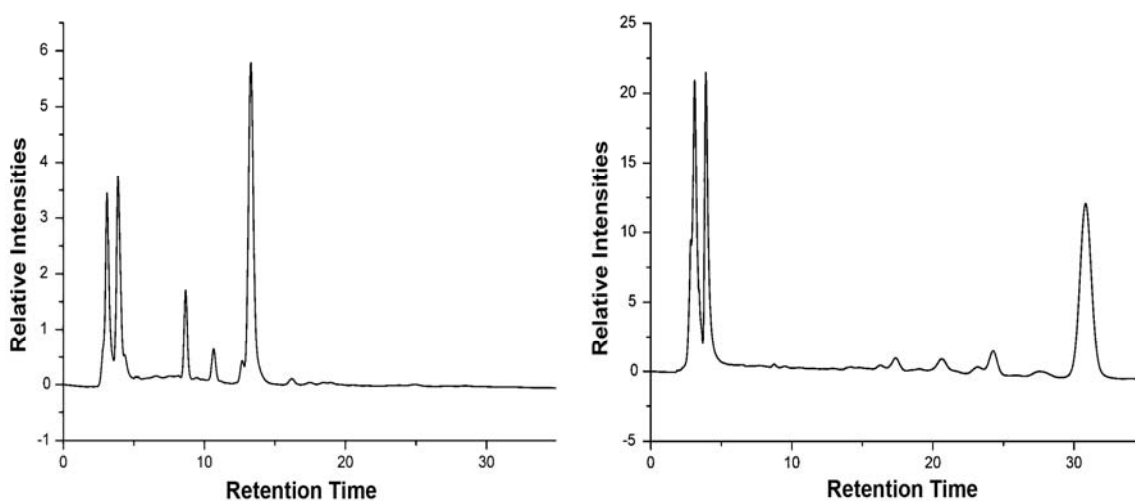


Figure 35 Left: HPLC profile of the three main peaks corresponding to the chlorinated derivatives of $C_{78}(1)$. Right: seven different peaks assigned to $C_{78}(2)$ chlorine-bearing adducts. The two notable peaks observed on both chromatograms with retention times around 3 and 4 min do not correspond to fullerene species.

As one can see, based on this confirmative assignment, the chromatogram shown in Figure 32 can be divided into two parts corresponding to two distinct fractions - from 0 to 15, and from 15 to 35 min - each containing exclusively products of $C_{78}(1)$ and $C_{78}(2)$, respectively.

The attempts to characterize any of the isolated chlorinated products of both isomers have failed. Interestingly, the HPLC analyses executed for each already isolated fraction only a few hours after the reaction and initial separation (before sample heating), have shown

neither the peak of the corresponding species nor that of the parent fullerene. This observation is explained with the high reactivity of the chlorine derivatives which most probably polymerize. On the basis of such high reactivity (instability) no further investigation is possible.

To summarize, a new faster method for the preparative isolation of the three most abundant isomers of C₇₈-fullerene has been developed. The selectivity of reaction of C₇₈ isomers 1 and 2 with ICl resulting in the formation of a few products only, as well as their efficient chromatographic resolution make this technique suitable for isolation of bulk amounts of these two species. Presumably, this method could be applied to other fullerene mixtures, especially to higher than C₈₂ fullerenes, which usually consist of many different isomers that cannot be isolated in pure form by means of common HPLC techniques (without derivatization of the starting material). There is still a great number of fullerene species waiting to be discovered and characterized, the further investigation of which is heavily hampered by the general inability to obtain them in isomerically pure form.

5.2.5 C₂-C₈₂ – a Facile Route for Its Isolation

C₈₂-fullerene has nine isomers obeying the IPR. From these, three possess C₂, three C_s, two C_{3v} and one C_{2v} symmetry. Actually, only one isomer of this family has been found in fullerene extracts, namely an isomer with C₂ symmetry.^[79,80] However it is still an open question which out of the three possible C₂ isomers has been reported to exist in extracts.

Thus far reported chromatographic procedures used for the separation of C₈₂ from the coeluting C₈₄-fraction have proven to be effective but rather extensive and laborious (multistage recycling HPLC).^[72,81] Here, a new single-run method for separation of bulk amounts of this fullerene species is reported.

The first step, fraction collection, is executed in compliance with the already described for the isolation of C₇₆-fullerene procedure. Here, again, the preparative BP column as a stationary phase and a mixture of toluene – hexane (4:1) as a mobile phase are used. The flow rate of the mobile phase is adjusted to 20 ml/min and the temperature in the column

compartment to 20°C. Under these conditions, C₈₂ coelutes with the big fraction containing diverse C₈₄ isomers (Figure 36).

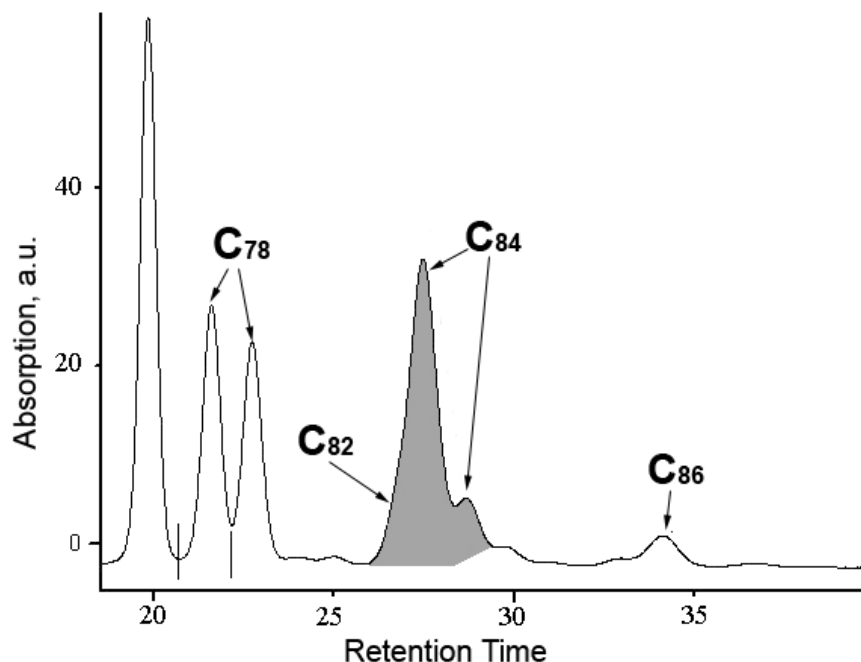


Figure 36 Section of the chromatogram corresponding to the preparative stage of fraction collection. The fraction containing C₈₂ as well as the coeluting C₈₄-fraction are highlighted in grey

In the next step, contrary to the reported in the literature conditions,^[72,81] where recycling HPLC on BP and PYE columns combined with different ratios of toluene – hexane mixtures as mobile phases are utilized for the separation of C₈₂, a single-run separation of the target compound is demonstrated. Here, instead the BP a BP-M column with dimensions 4.6 × 250 mm is used. The mobile phase is adjusted to 4:1 mixture of toluene and methanol and the temperature in the column compartment is set to 15°C. The full C₈₂-peak resolution from the neighboring C₈₄-fraction is demonstrated by the chromatogram in Figure 37.

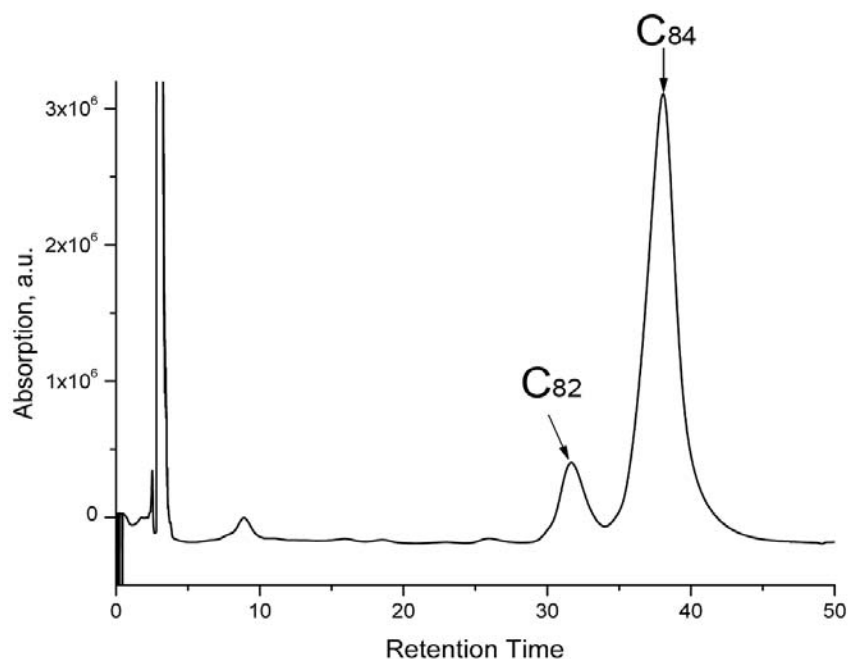


Figure 37 Separation of C_{82} on a Buckyprep-M column with toluene – methanol (4:1) as a mobile phase. The preparatively separated fraction containing the C_{82} -fullerene and the major isomers of C_{84} is presented here

Unfortunately, an attempt to provide single-step isolation for C_{82} has proven ineffective. When the above described chromatographic system is applied to the crude fullerene extracts directly, i.e. during the fraction collection stage, C_{82} fraction coelutes with this of C_{80} making it impossible to collect the pure compound (Figure 38). As an alternative procedure one might consider the reversed application of both steps: as a fraction collection stage, a preparative BP-M column (20 x 250 mm) can be effectively used, while for the second step (compound isolation) either the semipreparative or the analytical BP columns (10 x 250mm or 4.6 x 250 mm) can be employed. Since for the preparative collection of all fractions throughout the course of this work the preparative BP column is used, the “normal” sequence of the two steps for the isolation of the isomerically pure C_2 - C_{82} fullerene has been suggested.

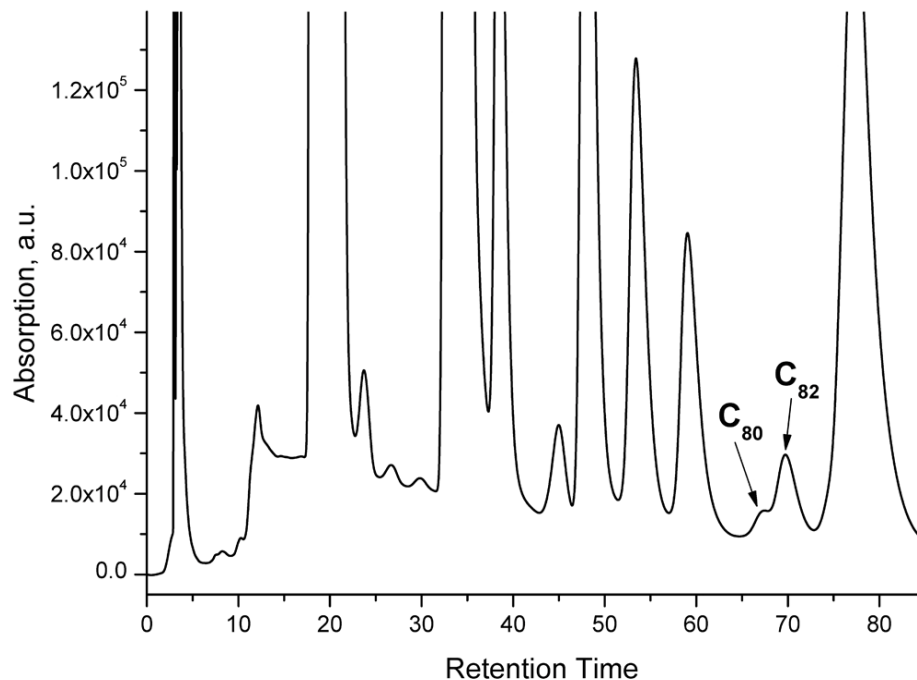


Figure 38 A chromatogram representing the analysis of the crude fullerene extract on a Buckyprep-M column (4.6 x 250mm) with a mixture of toluene – methanol (4:1) used as the mobile phase is presented here

5.2.6 Conclusion

In summary, conditions for the preparative isolation of eleven isomerically pure fullerene species have been demonstrated. These are: C₇₆(1), C₇₈(1), C₇₈(2), C₇₈(3), C₇₈(5), C₈₀(2), C₂-C₈₂, C₈₄(14), C₂-C₈₄, D₂-C₈₄ and D_{2d}-C₈₄. Two new chromatographic systems providing faster and more efficient means for obtaining bulk amount of pure fullerene isomers are discussed. An alternative approach employing a method of covalent derivatization of the three most abundant C₇₈-fullerene isomers is suggested too. This method is based on the reaction of the C₇₈-fullerene mixture with ICl, which has proven to be rather selective resulting in the generation of a few chlorinated products only. The chromatographic separation of these chlorine derivatives is facile and fast (retention time of the most strongly retained compound is only 30 min). This method can be potentially attempted for other fullerene mixtures (higher fullerenes).

5.3 Structural Studies of Highly Chlorinated Fullerene Derivatives

5.3.1 Short Introductory Remarks

In this section of the thesis, the crystal and molecular structures of five chlorine derivatives of the higher fullerenes $C_{76}(1)$, $C_{78}(2,3,5)$ and $C_{80}(2)$ are thoroughly described. These are: $C_{76}Cl_{18} \cdot TiCl_4$, $C_{78}(2)Cl_{18} \cdot Br_2 \cdot TiCl_4$, $C_{78}(3)Cl_{18}$, $C_{78}(5)Cl_{18}$ and $C_{80}Cl_{12}$. Special attention is paid to the changes in bond lengths of the original carbon connectivities after chlorinating the pristine fullerene molecules, as well as to the formation of different isolated aromatic regions in the derivatized fullerenes. This approach has proven to be rather effective because one of the reasons defining the stability of highly halogenated fullerene molecules is the formation of aromatic substructures in them. On the basis of the addition patterns of the chlorine atoms in the investigated structures, a suggestion for a possible reactivity principle characteristic for all higher fullerenes is made. Finally, the discovery of an unusual type of intermolecular interaction between chlorine atoms belonging to neighboring fullerene molecules has initiated an extensive study of the possible nature of this phenomenon. Theoretical calculations aiming at the estimation of the strength of this intermolecular “bonding” are well under way.

Halogenation and especially chlorination have proven to be efficient approaches for obtaining well crystallized fullerene species. Many ordered crystal structures of different halogenated derivatives of C_{60} - and C_{70} -fullerenes have already been reported.^[44-65] Chlorination offers opportunities for selective modifications of the fullerene cages, which otherwise show rather unspecific reactivities. It is demonstrated that a mixture of Br_2 and $TiCl_4$ acts as a selective chlorinating agent for diverse fullerene isomers, resulting in ordered and high quality crystals of the respective chlorine derivatives of these species.

5.3.2 C₇₆(1)Cl₁₈ · TiCl₄ – Structure Determination of the Chlorine Derivative of the Chiral D₂ Isomer of C₇₆

The synthesis of the first halogenated derivative of D₂-C₇₆ fullerene, C₇₆Cl₁₈, and its structure analysis by single-crystal X-ray crystallography is discussed. The emphasis is directed to some structural peculiarities including the molecular packing, the covalent carbon-carbon bonding as well as some extremes in the intermolecular interactions.

5.3.2.1 Synthetic Procedure

The pristine fullerene was produced by evaporation of graphite along the RF-furnace route, details of which have been reported elsewhere.^[28,29] The fullerene soot was Soxhlet extracted and separated by two-step HPLC as described in chapter 5.2.1 of this thesis. The new fullerene halide was obtained through chlorination of C₇₆ (approximately 0.2 mg) in 1 ml mixture of Br₂ : TiCl₄ (1 : 100 v/v) in a closed glass ampoule. The reaction mixture was frozen, evacuated and sealed. Orange crystals formed directly on the glass wall after heating the medley at 150°C for one week. Subsequently, the ampoule was opened and the excess solvent decanted. The product was found to be stable on air for at least one month. During the course of this thesis, all crystal structures were solved using SHELTXL.^[82] Quantum chemical calculations for molecular geometry optimizations were performed using the DFT method of B3LYP/6-31G with Gaussian 03.^[83]

5.3.2.2 Crystallographic Data

X-ray diffraction data were obtained using Bruker APEX II CCD diffractometer (Moka radiation ($\lambda = 0.71073 \text{ \AA}$), graphite monochromator). The crystal structure was solved and all atoms refined in the anisotropic approximation using SHELTXL. Crystals of C₂-C₇₆Cl₁₈ in C₇₆Cl₁₈ · TiCl₄: 0.03 × 0.02 × 0.01 mm; orthorhombic; space group *Pbca*; a = 11.5543(9), b = 21.2875(17), c = 47.168(4) Å; V = 11601.5(16) Å³, Z = 8; 2 θ_{\max} = 47.65°; -13 < h < 13, -24 < k < 24, -53 < l < 53; $\lambda = 0.71073 \text{ \AA}$; T = 100(2) K; reflections = 105007; independent reflections = 8909; data/restraints/parameters = 8909/0/892; full-

matrix least-squares refinement on F^2 ; semiempirical absorption correction from equivalents; $\mu = 1.217 \text{ mm}^{-1}$ (transmission min/max = 0.964/0.988); final R indices ($F_o > 4\sigma(F_o)$) are $R_1 = 0.0478$ and $wR_2 = 0.087$ (R_1 (all data) = 0.0972 and wR_2 (all data) = 0.1036); **CCDC-650718**.

5.3.2.3 Molecular Packing, Bond Distances and Aromatic Structure Formation

Halogenation, as a method of covalent derivatization, has been applied almost exclusively to C_{60} and C_{70} thus far (see Table 3) mainly due to their wide accessibility. The third most abundant in extracts fullerene is the D_2 -symmetric C_{76} , which represents the smallest IPR chiral fullerene. Although C_{76} is of great interest in fullerene chemistry,^[84] no ordered crystal structure of C_{76} has been presented so far.

The first halogenated derivative of C_{76} -fullerene, $C_{76}Cl_{18}$, and the crystal structure of its solvate, $C_{76}Cl_{18} \cdot TiCl_4$, is analyzed by single-crystal X-ray crystallography. The quality of the crystals has allowed a structure determination of high accuracy presenting all atoms in ordered and fixed positions (see Figure 39).

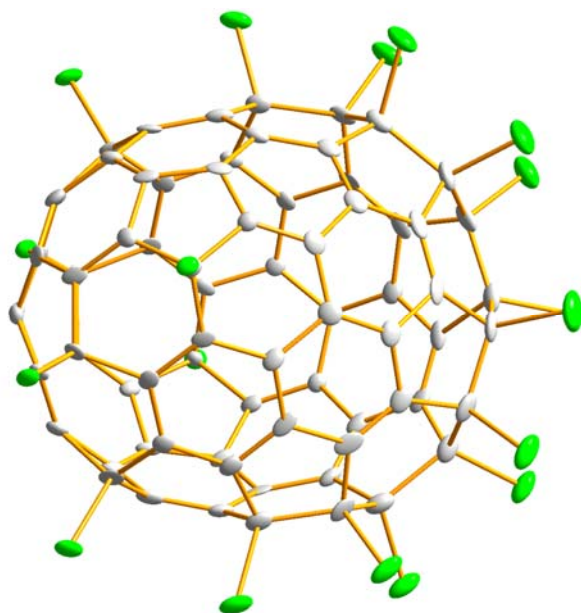


Figure 39 ORTEP projection of the molecular structure of $C_{76}Cl_{18}$ in the crystal at 100 K. Thermal ellipsoids are drawn at 50% probability level

The crystal structure consists of two enantiomers of $C_{76}Cl_{18}$, the carbon skeletons of which have remained as proposed for the pristine D_2-C_{76} enantiomers,^[8,12] and $TiCl_4$. According to the numbering scheme to be used, the descriptors assigned to the fullerene molecules are $^{f,s}C$ (clockwise) and $^{f,s}A$ (anticlockwise).^[85] The crystal packing appears to be dominated by the different polarities as well as by optimization of space filling. The fullerene molecules form 2D arrays extending parallel to (001) in such a way that their more densely chlorinated parts approach $TiCl_4$ moieties, whereas the less halogenated halves of the fullerene cages are coordinated towards one another, as can be seen on Figure 40.

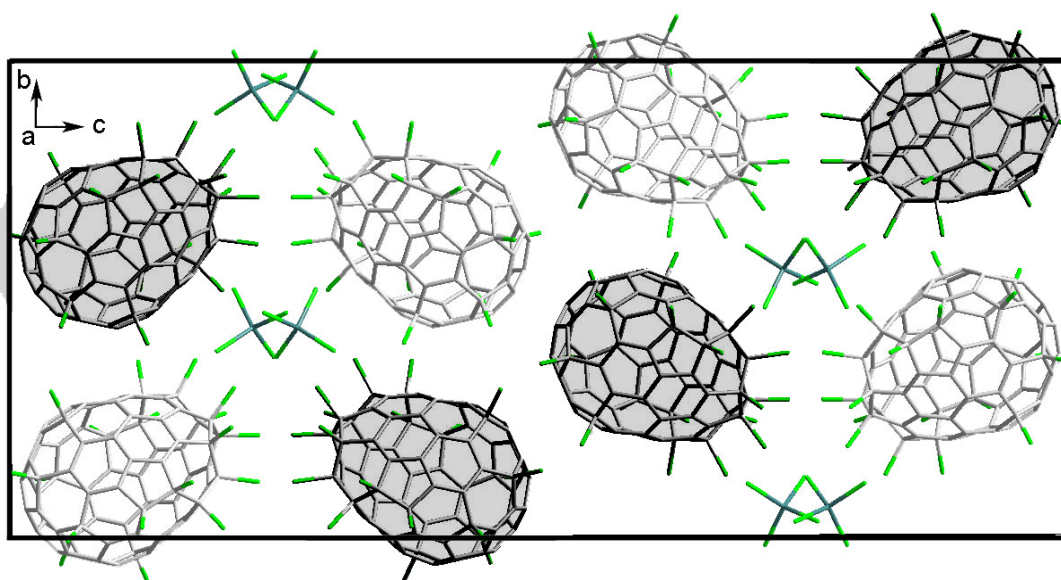


Figure 40 Projection of the structure of $C_{76}Cl_{18} \cdot TiCl_4$ onto the (100) plane. Shaded – $^{f,s}C$ isomer, unshaded – $^{f,s}A$ isomer

$C_{76}Cl_{18}$ possesses C_2 point group symmetry. The chlorine atoms build up two belts around the cage, both of which forming clockwise helices in the case of $^{f,s}C$ -isomer, and anticlockwise helices in the case of $^{f,s}A$ isomer (a schematic representation can be seen in Figure 41).

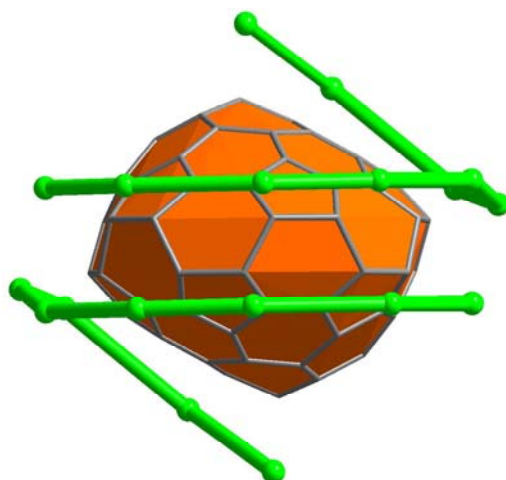


Figure 41 Visualization of the two belts of chlorine atoms in $C_{2-^{fs}}C$ isomer of $C_{76}Cl_{18}$. The chlorine atoms are linked together for clarity

All carbon-carbon and carbon-chlorine bond lengths in $C_{76}Cl_{18}$ are presented in Tables 4 and 5, where the deviation from C_2 point group symmetry for $C_{76}Cl_{18}$ in the crystal as well as the comparison between experimentally obtained and DFT calculated values of the bond lengths are shown too.

Table 4 DFT-calculated and experimentally observed carbon-carbon bond lengths in $C_{76}Cl_{18}$

C-C Bond	X-ray	C-C Bond	X-ray	Average	Deviation from C_2 symmetry	DFT
1-2	1.4190	75-76	1.4330	1.4260	0.014	1.4320
1-6	1.4110	71-76	1.4090	1.4100	0.002	1.4120
1-10	1.4370	67-76	1.4340	1.4355	0.003	1.4470
2-3	1.4020	74-75	1.3910	1.3965	0.011	1.4140
2-13	1.5300	64-75	1.5210	1.5255	0.009	1.5200
3-4	1.4370	73-74	1.4230	1.4300	0.014	1.4430
3-16	1.5270	61-74	1.5370	1.5320	0.010	1.5350
4-5	1.3740	72-73	1.3860	1.3800	0.012	1.3910

4-19	1.5150	58-73	1.5180	1.5165	0.003	1.5220
5-6	1.3830	71-72	1.3870	1.3850	0.004	1.4050
5-22	1.5390	57-72	1.5180	1.5285	0.021	1.5390
6-7	1.4160	70-71	1.4180	1.4170	0.002	1.4220
7-8	1.3390	69-70	1.3340	1.3365	0.005	1.3600
7-23	1.4930	54-70	1.4920	1.4925	0.001	1.4910
8-9	1.4060	68-69	1.4040	1.4050	0.002	1.4160
8-26	1.5020	51-69	1.5100	1.5060	0.008	1.5010
9-10	1.3900	67-68	1.3970	1.3935	0.007	1.4030
9-28	1.4330	49-68	1.4200	1.4265	0.013	1.4310
10-11	1.4320	66-67	1.4240	1.4280	0.008	1.4380
11-12	1.3750	65-66	1.3690	1.3720	0.006	1.3860
11-30	1.4240	47-66	1.4210	1.4225	0.003	1.4270
12-13	1.5130	64-65	1.5190	1.5160	0.006	1.5150
12-33	1.4120	44-65	1.4080	1.4100	0.004	1.4120
13-14	1.5120	63-64	1.5010	1.5065	0.011	1.5090
14-15	1.3410	62-63	1.3490	1.3450	0.008	1.3640
14-34	1.4420	43-63	1.4420	1.4420	0	1.4430
15-16	1.5230	61-62	1.5110	1.5170	0.012	1.5220
15-37	1.4360	40-62	1.4400	1.4380	0.004	1.4430
16-17	1.5150	60-61	1.5200	1.5175	0.005	1.5210
17-18	1.3580	59-60	1.3570	1.3575	0.001	1.3670
17-38	1.4270	39-60	1.4260	1.4265	0.001	1.4440
18-19	1.5160	58-59	1.5130	1.5145	0.003	1.5160
18-41	1.4230	36-59	1.4280	1.4255	0.005	1.4380
19-20	1.5420	57-58	1.5310	1.5365	0.011	1.5430
20-21	1.3870	56-57	1.3730	1.3800	0.014	1.3860

20-42	1.4380	35-57	1.4410	1.4395	0.003	1.4420
21-22	1.5160	55-56	1.5180	1.5170	0.002	1.5260
21-45	1.4360	32-56	1.4320	1.4340	0.004	1.4470
22-23	1.6190	54-55	1.6370	1.6280	0.018	1.6350
23-24	1.5640	53-54	1.5730	1.5685	0.009	1.5690
24-25	1.7090	52-53	1.7040	1.7065	0.005	1.6920
25-26	1.5630	51-52	1.5810	1.5720	0.018	1.5760
25-48	1.5000	29-52	1.5020	1.5010	0.002	1.5000
26-27	1.6980	50-51	1.6720	1.6850	0.026	1.6930
27-28	1.5000	49-50	1.5050	1.5025	0.005	1.5050
27-50	1.5790	-	-	1.5790	-	1.5750
28-29	1.3460	48-49	1.3460	1.3460	0	1.3620
29-30	1.4140	47-48	1.4180	1.4160	0.004	1.4260
30-31	1.3510	46-47	1.3770	1.3640	0.026	1.3980
31-32	1.4070	45-46	1.4010	1.4040	0.006	1.4110
31-53	1.5060	24-46	1.5090	1.5075	0.003	1.5100
32-33	1.4290	44-45	1.4300	1.4295	0.001	1.4330
33-34	1.4160	43-44	1.4260	1.4210	0.010	1.4340
34-35	1.3790	42-43	1.3830	1.3810	0.004	1.3920
35-36	1.4220	41-42	1.4240	1.4230	0.002	1.4360
36-37	1.4030	40-41	1.3980	1.4005	0.005	1.4040
37-38	1.4130	39-40	1.4250	1.4190	0.012	1.4330
38-39	1.4090	-	-	1.4090	-	1.4040

Table 5 DFT-calculated and experimentally observed carbon-chlorine bond lengths in C₇₆Cl₁₈

C-Cl Bond	X-ray	C-Cl Bond	X-ray	Average	Deviation from C₂ symmetry	DFT
C64-Cl1	1.824	C13-Cl18	1.846	1.835	0.022	1.939
C61-Cl2	1.839	C16-Cl17	1.817	1.828	0.022	1.924
C58-Cl3	1.823	C19-Cl16	1.815	1.819	0.008	1.920
C55-Cl4	1.804	C22-Cl15	1.812	1.808	0.008	1.895
C54-Cl5	1.794	C23-Cl14	1.796	1.795	0.002	1.899
C53-Cl6	1.787	C24-Cl13	1.794	1.791	0.007	1.895
C52-Cl7	1.775	C25-Cl12	1.773	1.774	0.002	1.894
C51-Cl8	1.790	C26-Cl11	1.784	1.787	0.006	1.882
C50-Cl9	1.784	C27-Cl10	1.780	1.782	0.004	1.888

Adding halogen atoms to the fullerene cage leads to change of some carbon atoms' hybridization from sp² to sp³. This alteration significantly modifies the π-system of the fullerene molecule. The main factor generally contributing to the stability of highly halogenated fullerenes is the formation of a number of isolated aromatic systems in the respective molecules. As can be seen from the Schlegel diagram (Figure 42), the sp² hybridized carbon atoms in C₇₆Cl₁₈ form a rather extended “aromatic” system.

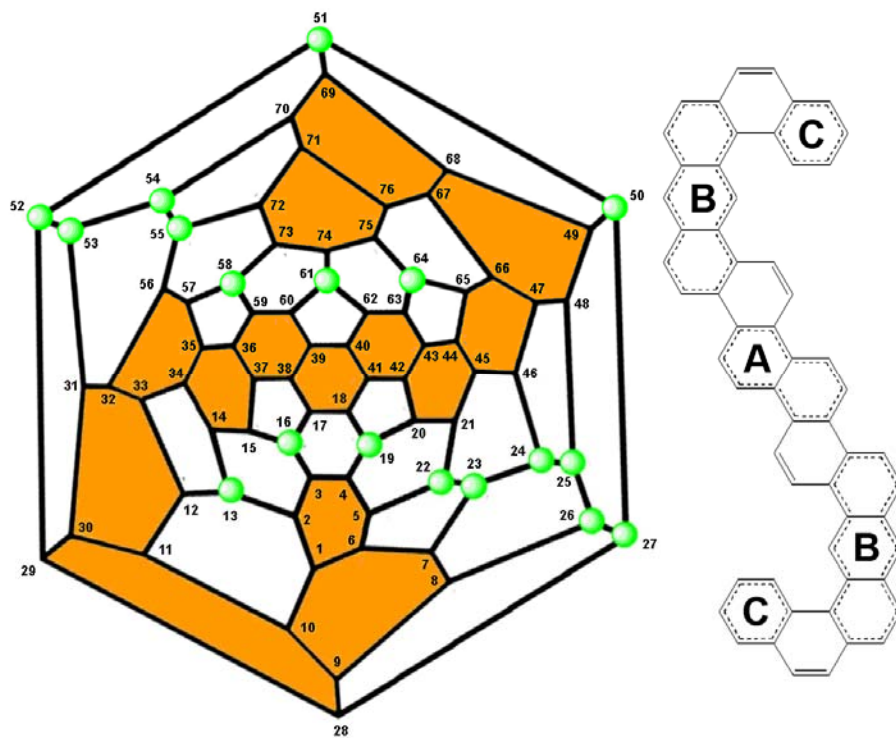


Figure 42 Left: Schlegel diagram of the experimentally observed C_2 -^{f,s}C isomer of $C_{76}Cl_{18}$ with the corresponding numbering scheme for carbon atoms. Right: a schematic presentation of the newly formed π -system

In contrast to all known π -systems of halogenated fullerenes, the one reported here is not comprised of isolated fragments but expands over the whole molecule. The “aromatic girdle” which consists of 14 six-membered cycles forms a helix in the same direction as the chlorine atoms (clockwise helix in the case of ^{f,s}C-isomer, and anticlockwise helix in the case of ^{f,s}A isomer). A comparison between the theoretically calculated carbon-carbon bond lengths in the pristine C_{76} molecule and those in $C_{76}Cl_{18}$ demonstrates the tendency of decreasing alternation in the π -system of the aromatic girdle (see Figure 43).

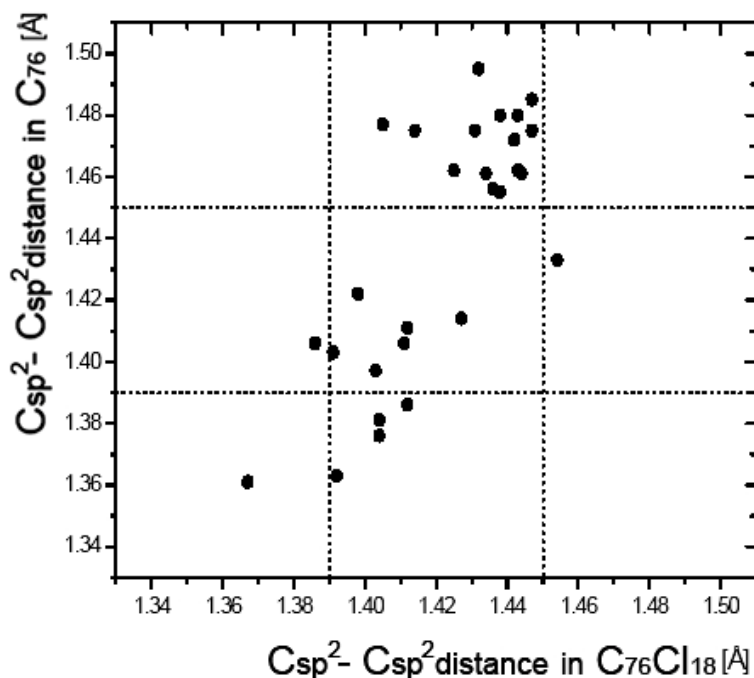


Figure 43 Decreasing of bond lengths alternation in the aromatic girdle in $C_{76}Cl_{18}$ in comparison to the same fragment in the pristine C_{76} -fullerene. Bond lengths are calculated using the DFT level of theory

Despite the apparent conjugation, the non-planar character of this helix leads to partial localization of the electron density. Formation of two 14-electron anthracene fragments (B), two 6-electron benzene rings (C) and one 10-electron naphthalene ring (A) can be distinguished (consult Figure 42, right). The presence of 4 double bonds (1.33–1.35 Å) is obvious, too. Nevertheless, the bonds between the aromatic moieties are relatively short (1.42–1.43 Å), which substantiates the comparatively strong interaction between them, and despite their non-planar character, all of these moieties are conjugated.

The trend towards “planarity”, which the π -system exerts on one hand, and the strong repulsion of vicinal chlorine atoms on the other hand lead to a considerable distortion of the fullerene cage. These facts explain the formation of extremely long $Csp^3 - Csp^3$ bonds which reach values up to 1.71 Å. Quantum chemical calculations are in good agreement with the presence of such long bonds, as can be concluded from Figure 44. A carbon-carbon single bond of similar magnitude is known only for extremely strained cyclobutenes substituted with bulky additives. The world record for the longest $Csp^3 -$

Csp^3 bond of 1.721 – 1.733 Å is held by naphthocyclobutene derivatives.^[86] In the case of highly deformed fullerenes, a comparable elongation of a $\text{Csp}^3 - \text{Csp}^3$ bond was observed in $\text{C}_{60}\text{F}_{18}$ – 1.68 Å,^[44-47] and $\text{C}_{60}\text{Cl}_{30}$ – 1.70 Å.^[47,53-55]

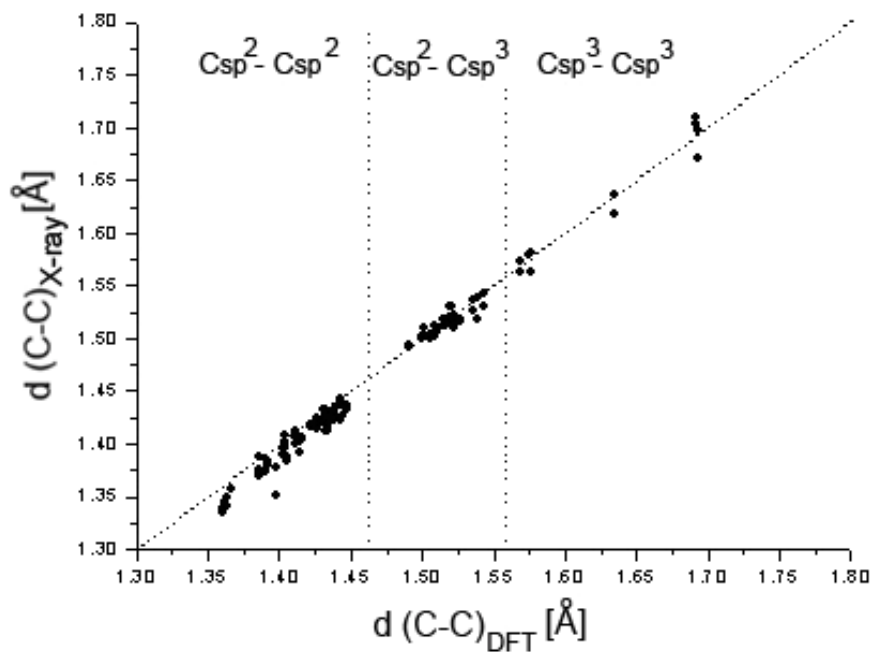


Figure 44 Correlation between the experimentally obtained and the DFT calculated C–C distances in $\text{C}_{76}\text{Cl}_{18}$. The extreme spread of C–C bond lengths is clearly visible

Analysis of the C–Cl bond lengths reveals some unexpected trends: vicinal chlorine atoms, which endure strong mutual repulsion, are characterized by insignificant elongation of the C–Cl bond lengths, while those in which chlorine atoms are not strained by repulsion are substantially elongated. The same bond-lengths distribution was predicted by DFT calculation and can be explained by the interaction between the corresponding carbon atoms and the aromatic system. The longest C–Cl distances (1.815 – 1.846 Å) are encountered where chlorine-bearing carbon atoms connect directly to three sp^2 -hybridized carbons, whereas the intermediate (1.804 – 1.812 Å) and shortest (1.773 – 1.796 Å) bonds are present where sp^3 -carbon atoms bind with two and one sp^2 partners, respectively.

To summarize, the carbon connectivity pattern of the chiral D_2 - C_{76} isomer has been confirmed by single crystal X-ray analysis of $C_{76}Cl_{18} \cdot TiCl_4$. The tendency of halogen-free carbon atoms to develop conjugated subunits is defined as the structure-determining factor. The long C–C bonds, the distance of 1.71 Å marking the highest value thus far reported for fullerene derivatives, might serve as hyphenation points when trying to break down the cage in a controlled manner. Thus, halogenation offers opportunities for selective modifications of fullerenes, which otherwise show rather unspecific reactivities.

5.3.3 Crystal Structures of $C_{78}(2)Cl_{18} \cdot Br_2 \cdot TiCl_4$, $C_{78}(3)Cl_{18}$, $C_{78}(5)Cl_{18}$

The existence of several structural isomers drastically complicates the investigation, as well as the structure determination of higher fullerenes. After C_{76} , the next recoverable from soot fullerene, C_{78} , has five IPR isomers.^[12] Although separation techniques applicable to the soluble C_{78} isomers are available (see sections 5.2.2 and 5.2.3), only few crystal structures including soluble C_{78} isomers as halogenated derivatives were reported thus far.^[62,69] However, in these cases different structural isomers occupy the fullerene sites, which are presumably $C_{78}(2)$ and $C_{78}(3)$. The carbon connectivities of $C_{78}(5)$ were crystallographically confirmed through analysis of $C_{78}(5)(CF_3)_{12}$.^[74] Herein, the single-crystal X-ray determinations of fullerene derivatives of individual C_{78} fullerene cages in their crystal structures – $C_{78}(3)Cl_{18}$ (structure **I**) $C_{78}(2)Cl_{18} \cdot Br_2 \cdot TiCl_4$ (structure **II**), and $C_{78}(5)Cl_{18}$ (structure **III**) are discussed.

5.3.3.1 Synthesis of the Fullerene Halides

The parent fullerenes were produced and isolated in isomerically pure form as described previously in sections 4.1.1, 5.2.3 and 5.2.4 of this thesis. The new fullerene halides were obtained through chlorination of the pristine species (0.5 mg each) in 2 ml mixture of Br_2 : $TiCl_4$ (1 : 100 v/v) in glass ampoules. The reaction mixtures were frozen with liquid nitrogen, evacuated and sealed. Yellow crystals in the case of $C_{78}(3)$ and $C_{78}(5)$, and red crystals in the case of $C_{78}(2)$ formed directly on the glass wall after keeping the mixtures

at 90°C for ten days. Subsequently, the ampoules were cut open and the excess solvent decanted. The products were found to be stable on air for at least one month.

5.3.3.2 Crystallographic Data

X-ray diffraction data were obtained using Bruker APEX II CCD diffractometer (MoK α radiation ($\lambda = 0.71073\text{\AA}$), graphite monochromator). The crystal structures were solved and all atoms refined in the anisotropic approximation using SHELTLX. Crystal data for Structure **I** - C₇₈(3)Cl₁₈: yellow crystal 0.04 × 0.02 × 0.01 mm; hexagonal; space group *P6₃/m*; $a = 13.0202(16)$, $c = 18.726(5)$ Å; $V = 2749.3(8)$ Å³; $Z = 2$; $2\theta_{\max} = 42.0^\circ$; $-13 < h < 13$, $-13 < k < 13$, $-18 < l < 18$; $T = 100(2)$ K; reflections = 15118; independent reflections = 1025; Data/restraints/parameters = 1025/0/147; $\mu = 0.953$ mm⁻¹ (transmission min/max = 0.977/0.991); final R indices ($F_o > 4\sigma(F_o)$) are $R_1 = 0.0434$ and $wR_2 = 0.1241$ (R_1 (all data) = 0.0532 and wR_2 (all data) = 0.1316); **CCDC 662360**. Crystal data for Structure **II** - C₇₈(2)Cl₁₈ · Br₂ · TiCl₄: red crystal 0.02 × 0.01 × 0.01 mm; hexagonal; space group *P6₃/mmc*; $a = 14.6910(13)$ Å, $c = 17.045(2)$ Å; $V = 3186.0(6)$ Å³; $Z = 2$; $2\theta_{\max} = 45.0^\circ$; $-15 < h < 15$, $-15 < k < 15$, $-18 < l < 18$; $T = 100(2)$ K; reflections = 19471; independent reflections = 826; Data/restraints/parameters = 826/7/114; $\mu = 2.365$ mm⁻¹ (transmission min/max = 0.954/0.977); final R indices are $R_1 = 0.0711$ and $wR_2 = 0.2024$ (R_1 (all data) = 0.0916 and wR_2 (all data) = 0.2234); **CCDC 653031**. Crystal data for Structure **III** - C₇₈(4)Cl₁₈: yellow crystal 0.02 × 0.02 × 0.01 mm; hexagonal; space group *P6₃/m*; $a = 13.055(5)$ Å, $c = 18.762(14)$ Å; $V = 2769(2)$ Å³, $Z = 2$; $2\theta_{\max} = 41.74^\circ$; $-13 < h < 13$, $-13 < k < 13$, $-18 < l < 18$; $T = 100(2)$ K; reflections = 13445; independent reflections = 1018; Data/restraints/parameters = 1018/0/118; $\mu = 0.946$ mm⁻¹ (transmission min/max = 0.964/0.988); final R indices are $R_1 = 0.0601$ and $wR_2 = 0.1401$ (R_1 (all data) = 0.1201 and wR_2 (all data) = 0.1629); **CCDC 686048**.

5.3.3.3 Structural Features, Constitution Patterns and Extended Channels Formation

$C_{78}(5)Cl_{18}$ forms solvent free crystals in the hexagonal space group $P 6_3/m$. The quality of the crystals obtained has granted an accurate structure determination presenting all atoms in ordered and fixed positions (see Figure 45). The $C_{78}(5)Cl_{18}$ molecule exhibits D_{3h} point group symmetry – preserved from the parent $D_{3h}-C_{78}(5)$.

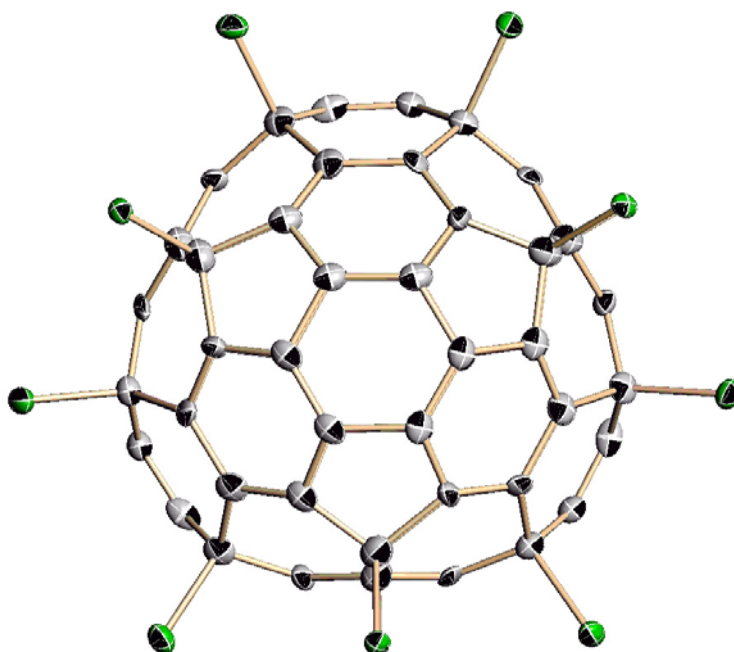


Figure 45 ORTEP projection of the molecular structure of $C_{78}(5)Cl_{18}$ in the crystal at 100 K. Thermal ellipsoids are drawn at 50% probability level

The carbon-carbon bond lengths in $C_{78}(5)Cl_{18}$ are presented in Table 6, where the deviation from D_{3h} point group symmetry in the crystal and that between experimentally obtained and DFT calculated values of the corresponding bond lengths are shown too. The numbering of the carbon atoms is according to Ref. [87], and is shown in Figure 46.

Table 6 DFT-calculated and experimentally observed carbon-carbon bond lengths in $C_{78}(5)Cl_{18}$. Deviation from D_{3h} point group symmetry and that between calculated and observed values is shown too

C-C bond	X-Ray, Å		X-Ray Average	DFT, Å	Deviation X-Ray/DFT	Deviation from D_{3h} symmetry
1-1	1.317	--	1.317	1.33240	-0.015	--
1-2	1.495	1.536	1.516	1.50978	0.0057	-0.041
2-3	1.484	1.521	1.503	1.51399	-0.0115	-0.037
3-3	1.400	1.407	1.404	1.40027	0.0032	-0.007
2-4	1.513	1.565	1.539	1.51028	0.0287	-0.052
3-5	1.386	1.394	1.390	1.39709	-0.0071	-0.008
4-4	1.425	--	1.425	1.43791	-0.0130	--
4-6	1.382	1.397	1.390	1.39220	-0.0027	-0.015
5-7	1.514	--	1.514	1.49228	0.0217	--
6-7	1.529	1.537	1.533	1.53057	0.0024	-0.008
6-19	1.412	1.421	1.417	1.41332	0.0032	-0.009
18-19	1.460	--	1.460	1.45770	0.0023	--
19-19	1.390	--	1.390	1.38818	0.0018	--

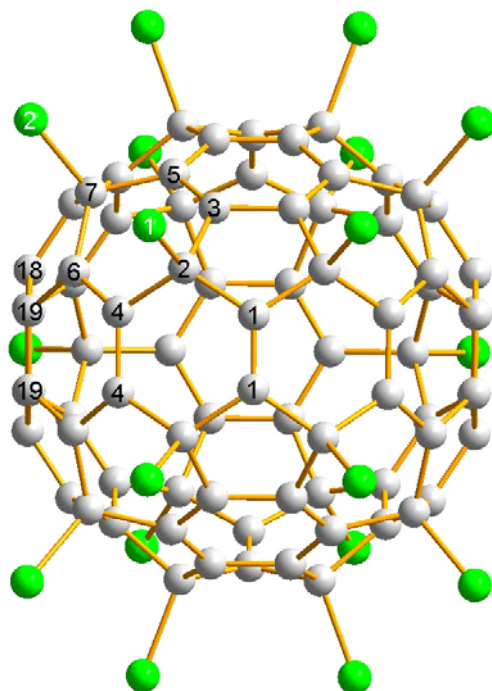


Figure 46 Numbering of carbon atoms in $C_{78}(5)$, taken from Ref. [87]. Numbering of chlorine atoms is symmetry dependent (only two different types of C–Cl bonds are present)

The carbon-chlorine bond lengths in $C_{78}(5)Cl_{18}$ are presented in Table 7, where the deviation from D_{3h} point group symmetry in the crystal and that between experimentally obtained and DFT calculated values of the corresponding bond lengths are shown too.

Table 7 DFT-calculated and experimentally observed carbon-chlorine bond lengths in $C_{78}(5)Cl_{18}$

C-Cl bond	X-Ray, Å		X-Ray Average	DFT, Å	Deviation X-Ray/DFT	Deviation from D_{3h} symmetry
C2-Cl1	1.823	1.862	1.843	1.929	-0.086	0.039
C7-Cl2	1.833	--	1.833	1.921	-0.088	--

Experimentally derived and DFT-calculated C–C bond distances are in a good accordance. The stabilizing factor in $C_{78}(5)Cl_{18}$ is the formation of nine “aromatic” rings

– a trend typical for halogenated fullerenes (see Figure 47, left). Three of these rings are characterized by a high degree of equivalence in the bond lengths – ranging from 1.386 to 1.407 Å, very close to those in benzene (1.395 Å). According to the structural criterion of aromaticity,^[88,89] these fragments possess high π -electron delocalization and are fully aromatic. Such high level of equivalence in C–C bonds in fullerene cages has never been observed before. The degree of alternation in bond lengths in the other six six-membered rings is more pronounced (1.382 – 1.425 Å), therefore they have been considered to be only “partly aromatic” (Figure 47, right).

Interestingly, all 18 chlorine atoms can virtually be divided into three groups – each consisting of six chlorine atoms lying in one plane. This arrangement leads to the formation of three almost equilateral “chlorine hexagons” which are parallel to the plains of the “aromatic rings” (Figure 48).

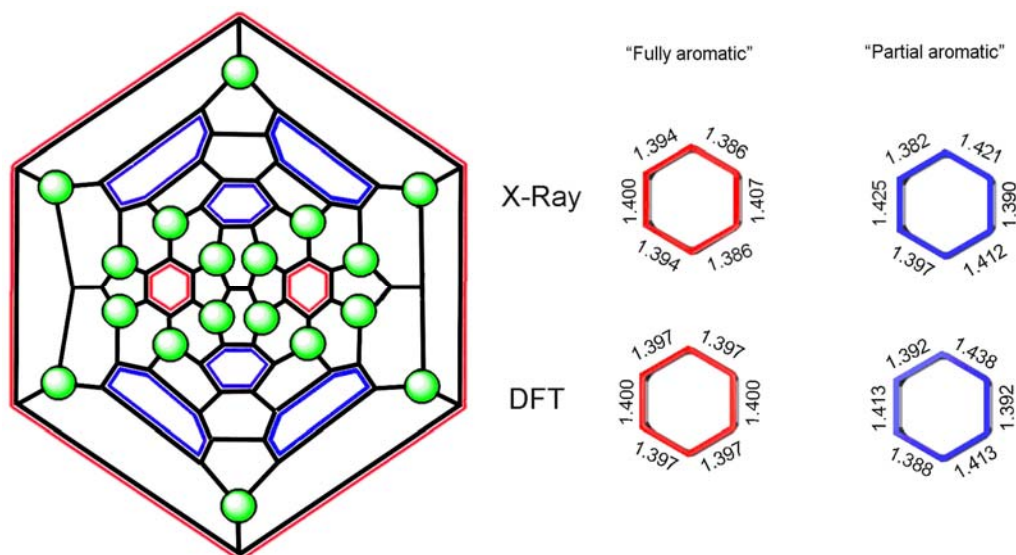


Figure 47 Left: Schlegel diagram of C₇₈(5)Cl₁₈ presenting the chlorination pattern (chlorine atoms are visualized as green circles), as well as the aromatic substructures, differently colored on the basis of their relative degree of aromaticity (red – fully aromatic, blue – partially aromatic). Right: X-ray derived and DFT calculated C–C bond distances in both – fully and partially aromatic subunits

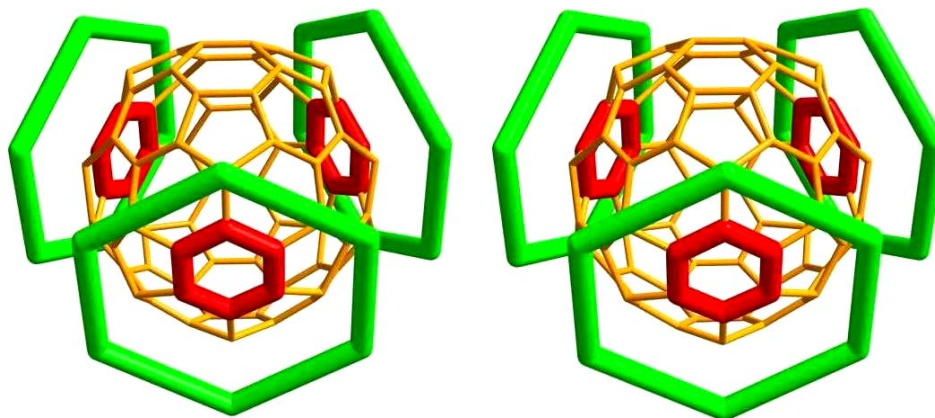


Figure 48 Stereo view of $C_{78}(5)Cl_{18}$ molecule. Three groups of chlorine atoms form three equilateral hexagons (green) each in a plane parallel to the aromatic subunits (represented in red)

The hcp-like (hexagonal close packing) arrangement of the fullerene molecules in structure **III** leads to the development of large tunnels extending along [001] of the hexagonal lattice, creating by this tunnel-like voids. The inner “surface” of these tunnels is formed only by chlorine atoms. The green circles in Figure 49 (top) represent the van-der-Waals radii of chlorine atoms. The “empty” space is clearly visible in the center. The diameter of the tunnels is Approximately 2.4 \AA , big enough to accommodate small molecules such as hydrogen.

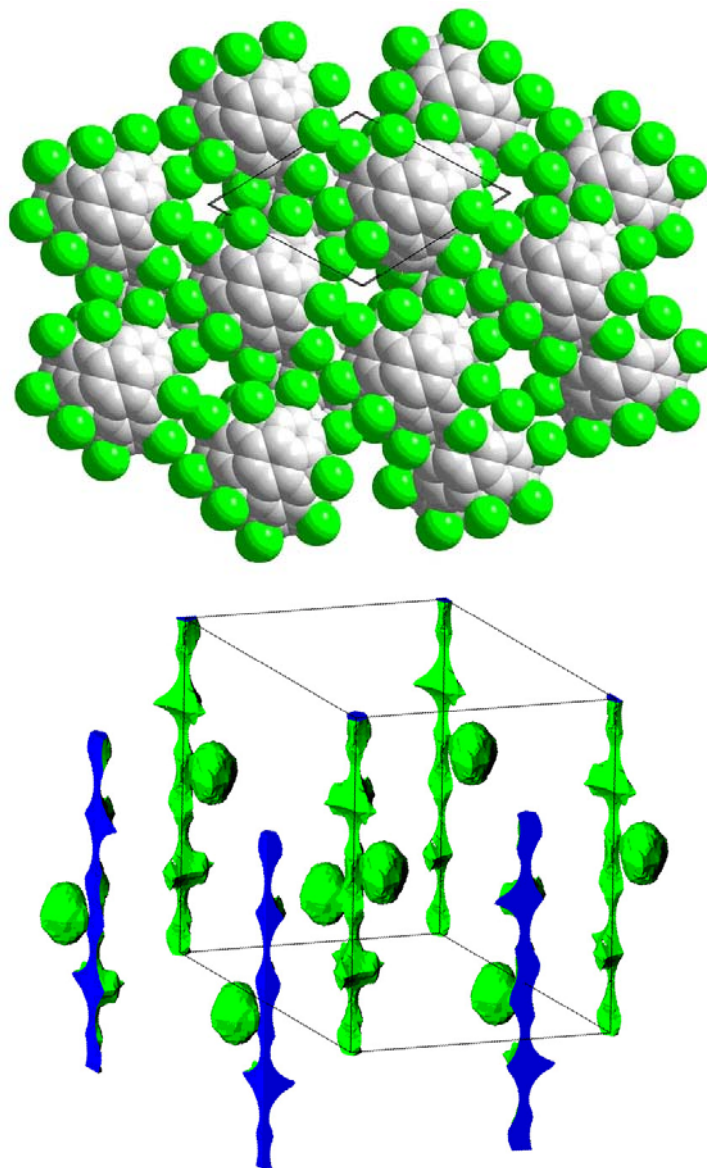


Figure 49 Top: Space filling representation of the crystal structure of $C_{78}(5)Cl_{18}$. Bottom: The 3D view of interstices accessible for molecules with diameters smaller than 2.4 Å. The unit cell is shown for guidance in both pictures

$C_{78}(3)Cl_{18}$ is displaying the same overall packing as $C_{78}(5)Cl_{18}$ (space group $P 6_3/m$) but the fullerene molecules are disordered between three orientations. $C_{78}(2)Cl_{18}$ crystallizes in the hexagonal space group $P 6_3/mmc$ and is as well characterized by fullerene disorder around the threefold crystallographic axis. Despite this disorder in structures **I** and **II** the connectivities of both isomers can be reliably derived from X-ray data. Both isomers

$C_{78}(2)Cl_{18}$ and $C_{78}(3)Cl_{18}$, as well as the pristine $C_{78}(2)$ and $C_{78}(3)$, possess C_{2v} point group symmetry and differ formally in the orientation of only one C–C bond. Virtually, both fullerene molecules can be represented as a combination of two trimethyltrindane fragments, capping the cage from the top and bottom, and three pyracylene fragments encircling it (Figure 50). In the case of $C_{78}(2)$, two of the three pyracylene fragments are disposed in such a manner that the central C–C bond in them is perpendicular to the equatorial mirror plane, while in the third fragment this bond is parallel to the same plane. For $C_{78}(3)$ the situation is reversed. In both crystal structures (**I** and **II**), the fullerene molecules are orientationally disordered around the threefold axis. Since the symmetry of both fullerene derivatives approaches D_{3h} , the position of all carbon atoms except those constituting the central bond in the pyracylene unit virtually superimpose under 120° rotation. As a consequence, the obtained disorder does not obstruct the reliable structure determination because the isomer's identity is unambiguously given by the relative site occupancies of the carbon atoms constituting the central bond in the pyracylene subunits.

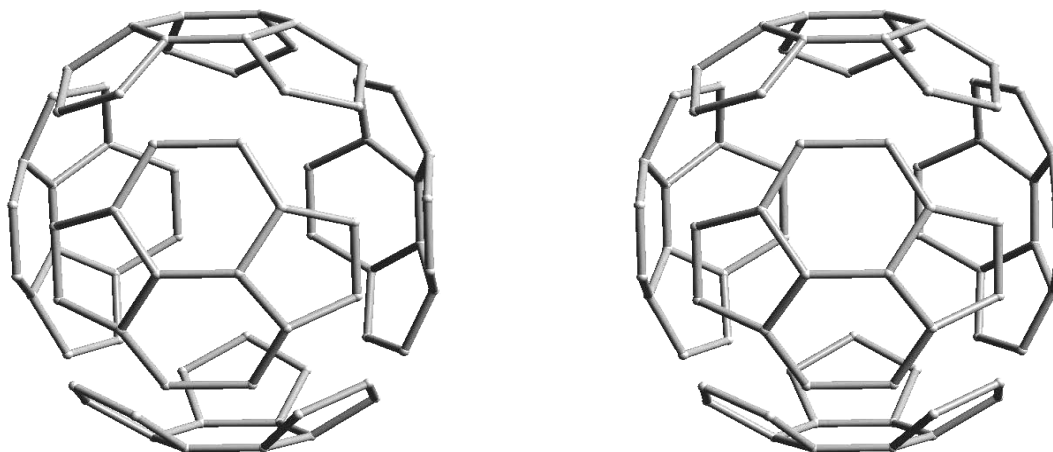


Figure 50 Stereo view of $C_{78}(2)$ showing the partitioning of the fullerene cage into two trimethyltrindane (methyl groups are omitted for clarity) and three pyracylene fragments

Analysis of crystal structure **I** gives the site occupancies of the carbon atoms constituting the parallel and perpendicular – relative to the equatorial mirror plane – central bonds in

the pyracylene subunits of 0.65 : 0.35, respectively, which assigns the structure to $C_{78}(3)$ isomer (expected site occupancies of 0.67 : 0.33). The experimental site occupancies of 0.36 : 0.64 in crystal structure **II** attribute it to $C_{78}(2)$ isomer (theoretically 0.33 : 0.67). By superimposing DFT-optimized $C_{78}Cl_{18}$ structure motifs, disorder around the threefold axis has been simulated. As can be seen from Figure 51, remarkable deviation from D_{3h} symmetry is observed only for the equatorial pyracylene fragments. Comparing the superposition of the calculated structure motifs with the results of X-ray data refinement for $C_{78}(3)Cl_{18}$ reveals that only the carbon atoms constituting the pyracylene fragments display some prolongation of the experimentally obtained thermal ellipsoids (see Figure 51, right), while the rest of the carbon as well as all chlorine atoms (chlorine atoms are not presented in Figure 51) are more symmetrical with respect to the shape of their displacement ellipsoids, an observation which is in a good agreement with the presented model. It is worth mentioning that chlorine atoms follow the partitioning of the C-cage into chlorine substituted trimethyltrindane and pyracylene fragments resulting in a tiny enlargement of the displacement ellipsoids of the chlorine atoms attached to the pyracylene entities (ORTEP representations of $C_{78}(2)Cl_{18}$ and $C_{78}(3)Cl_{18}$ are given in the Appendix section of this work). Thus, in the case of $C_{78}(2)Cl_{18}$ and $C_{78}(3)Cl_{18}$ not only the molecular structure can be reliably determined, but also some bond distances can be assessed with satisfying accuracy.

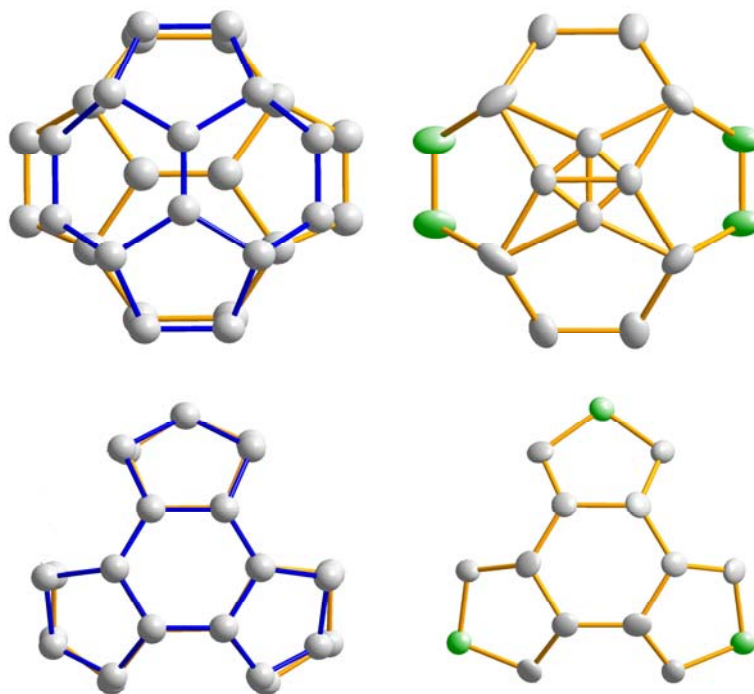


Figure 51 Left: superposition of all three orientations of the pyracylene (top) and trindane (bottom) fragments from the DFT-optimized model of $C_{78}(3)Cl_{18}$. The bonding pattern in blue represents the two coinciding fragments, while the orange one depicts the third. Right: ORTEP plots of the corresponding fragments in the crystal structure of $C_{78}(3)Cl_{18}$. Chlorine-bearing carbon atoms are presented in green

The chlorination patterns of $C_{78}(2)Cl_{18}$, $C_{78}(3)Cl_{18}$ and $C_{78}(5)Cl_{18}$ are shown in Figure 52. The difference between these structures is formally in the position of the equatorial double bonds (the central bonds in the pyracylene subunits). The stabilizing factor for the localization of the chlorine atoms is the formation of nine close to planar aromatic C-C rings (in all three structures) and the absence of double bonds in the pentagons, a feature typical for halogenated fullerene derivatives.

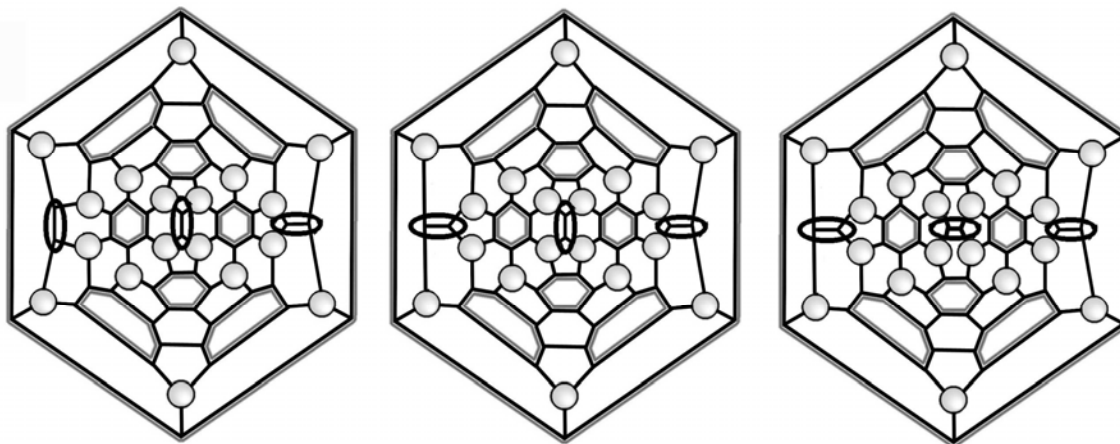


Figure 52 Schlegel diagram of $C_{78}(2)Cl_{18}$ (left), $C_{78}(3)Cl_{18}$ (center) and $C_{78}(5)Cl_{18}$ (right). The aromatic zones are double-marked and the chlorine atoms are depicted by spheres. The difference between the structures lies in the orientation of the equatorial C–C bonds (selected)

5.3.4 Crystal Structure of $C_{80}(2)Cl_{12}$

The carbon cages constituted of 80 atoms have recently been in focus mainly because of the big number of metalo- and cluster endohedral fullerenes which became available, leaving behind the investigation of the hollow isomers of this fullerene. C_{80} has seven structural isomers obeying the IPR.^[12] Two of them, $D_{5d}-C_{80}(1)$ and $D_2-C_{80}(2)$, have been found in fullerene extracts and isolated by means of HPLC techniques.^[71,90,91] Recently, a third representative of the family, $C_{2v}-C_{80}(5)$, was identified and its constitution pattern confirmed by ^{19}F -NMR measurement of its exohedral derivative $C_{80}(5)(CF_3)_{12}$.^[74] Although the relative abundance of $C_{80}(2)$ to $C_{80}(1)$ of *ca.* 30 : 1,^[90] as well as the simple isolation procedure for $C_{80}(2)$ provide ground for investigating the chemical reactivity of this species, no exohedral derivative of it has ever been synthesized. Probing the reactivity of this isomer appears particularly worthwhile when taking into consideration that it represents another chiral fullerene after $D_2-C_{76}(1)$.

5.3.4.1 Synthetic Procedure

The parent fullerene was synthesized and isolated in pure form as described previously in sections 4.1.1 and 5.2.2. The new fullerene halide was obtained through chlorinating the pristine species (0.3 mg) in 1.5 ml mixture of Br₂ : TiCl₄ (1 : 100 v/v) in a glass ampoule. The reaction mixture was frozen with liquid nitrogen, evacuated and sealed. Orange crystals of C₈₀(2)Cl₁₂ formed directly on the glass wall after keeping the mixture at 120°C for ten days. Subsequently, the ampoule was cut open and the excess solvent decanted. The product was found to be stable on air for at least one month.

5.3.4.2 Crystallographic Data

X-ray diffraction data were obtained using Bruker APEX II CCD diffractometer (Moka radiation ($\lambda = 0.71073\text{\AA}$), graphite monochromator). The crystal structure was solved and all atoms refined in the anisotropic approximation using SHELXTL. Crystals of D₂-C₈₀Cl₁₂: 0.04 × 0.02 × 0.02 mm; monoclinic; space group C2/c; a = 21.043(3), b = 11.1665(14), c = 21.510(3) Å; $\alpha = \gamma = 90^\circ$, $\beta = 106.235(2)^\circ$; V = 4852.8(11) Å³; Z = 4; $2\theta_{\text{max}} = 55.56^\circ$; $-27 < h < 27$, $-14 < k < 14$, $-28 < l < 28$; $\lambda = 0.71073\text{\AA}$; T = 100(2) K; reflections/parameters = 13.7325; full-matrix least-squares refinement on F²; $\mu = 0.746\text{ mm}^{-1}$ (exp. absorpt. min/max = 0.9708/0.9852); final R indices are R₁ = 0.0422 and $wR_2 = 0.0769$; **CCDC- 706381**.

5.3.4.3 C₈₀Cl₁₂ – Structure Description

The quality of C₈₀(2)Cl₁₂ crystals has allowed structure determination of high accuracy, presenting all atoms in ordered and fixed positions (Figure 53). The solvent free crystals consist of the two enantiomers of C₈₀Cl₁₂, as a racemic mixture, with the connectivity patterns of the carbon atoms preserved as suggested for the pristine C₈₀(2) enantiomorphs.^[12] The molecules exhibit D₂ point group symmetry, unchanged from the parent species (D₂-C₈₀(2)).

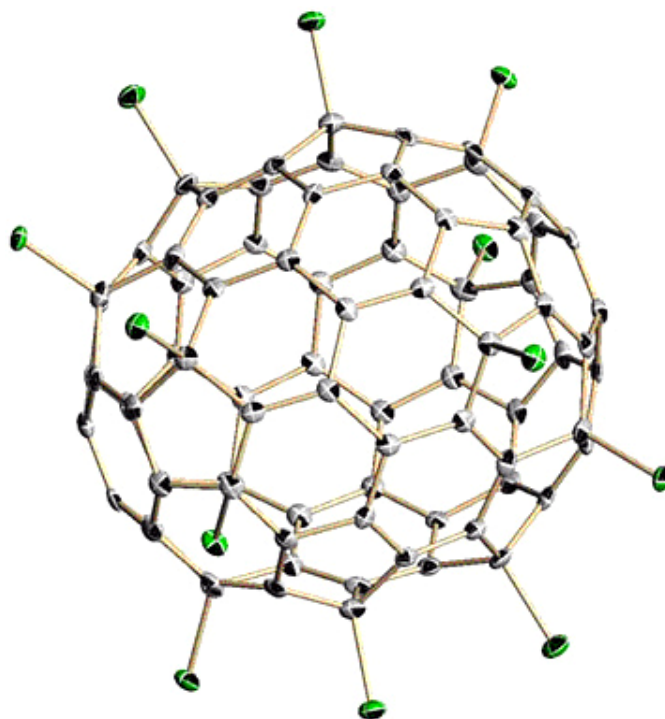


Figure 53 ORTEP plot of $C_{80}Cl_{12}$ molecule in the crystal. Displacement ellipsoids are drawn at 50% probability level

In Table 8 and Figure 54 the correlation between the experimentally obtained and DFT-calculated carbon-carbon bond lengths for $C_{80}Cl_{12}$, as well as the corresponding bond lengths in the DFT-optimized $C_{80}(2)$ model are presented (the numbering of the carbon atoms is given for reference in Figure 55).

Table 8 Bond distances in DFT-optimized $C_{80}(2)$, DFT-optimized $C_{80}Cl_{12}$ and X-Ray data for $C_{80}Cl_{12}$. X-Ray average data as well as DFT/X-Ray deviation for $C_{80}Cl_{12}$ is given too

C-C Bond	DFT C_{80}	DFT $C_{80}Cl_{12}$	X-Ray $C_{80}Cl_{12}$		X-Ray Average $C_{80}Cl_{12}$	DFT/X-Ray Deviation
1-1	1.396	1.402	1.397	1.397	1.397	0.005
1-2	1.453	1.436	1.424	1.424	1.424	0.012
1-3	1.461	1.446	1.438	1.442	1.440	0.006
2-4	1.398	1.405	1.400	1.398	1.399	0.006

2-6	1.460	1.442	1.438	1.435	1.437	0.005
3-5	1.394	1.367	1.359	1.362	1.361	0.006
3-7	1.440	1.517	1.518	1.517	1.518	0.001
4-5	1.456	1.440	1.435	1.423	1.429	0.011
4-8	1.453	1.436	1.425	1.424	1.425	0.011
5-9	1.440	1.517	1.512	1.513	1.513	0.004
6-7	1.465	1.524	1.528	1.533	1.531	0.007
6-11	1.381	1.368	1.355	1.354	1.355	0.013
7-12	1.418	1.530	1.529	1.536	1.533	0.003
8-10	1.435	1.435	1.431	1.429	1.430	0.005
8-13	1.395	1.388	1.380	1.385	1.383	0.005
9-10	1.471	1.528	1.529	1.535	1.532	0.004
9-14	1.406	1.510	1.512	1.504	1.508	0.002
10-15	1.407	1.385	1.377	1.376	1.377	0.008
11-13	1.456	1.436	1.431	1.425	1.428	0.008
11-16	1.445	1.505	1.501	1.515	1.508	0.003
12-14	1.474	1.414	1.399	1.397	1.398	0.016
12-17	1.466	1.438	1.431	1.423	1.427	0.011
13-18	1.431	1.435	1.429	1.436	1.433	0.002
14-19	1.466	1.436	1.426	1.431	1.429	0.007
15-15	1.460	1.468	1.458	1.470	1.464	0.004
15-19	1.472	1.474	1.469	1.468	1.469	0.005
16-17	1.429	1.518	1.513	1.522	1.518	0.000
16-20	1.433	1.538	1.537	1.539	1.538	0.000
17-20	1.406	1.381	1.375	1.372	1.374	0.007
18-19	1.410	1.413	1.404	1.402	1.403	0.010
18-20	1.465	1.417	1.404	1.404	1.404	0.013

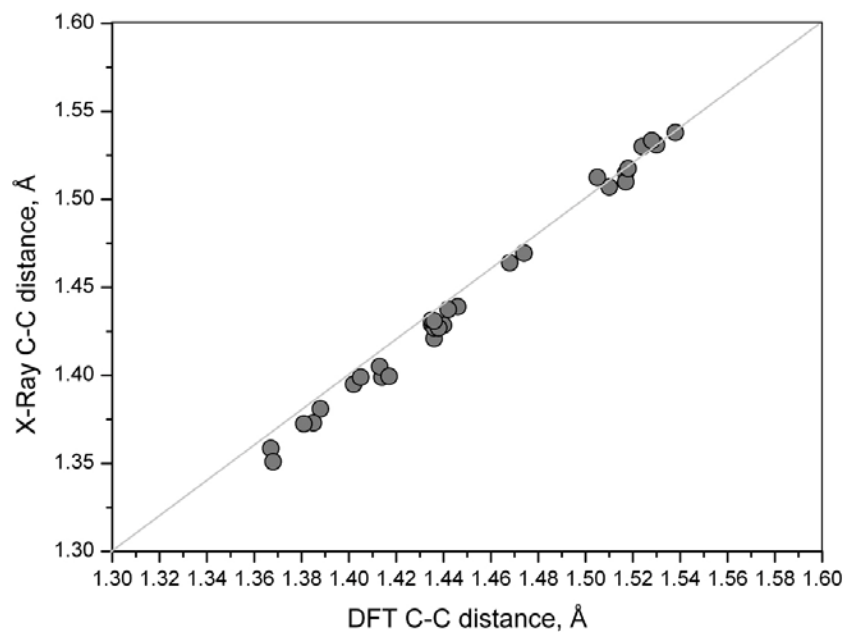


Figure 54 Correlation between the experimentally obtained C–C distances and the DFT-calculated ones in $C_{80}Cl_{12}$

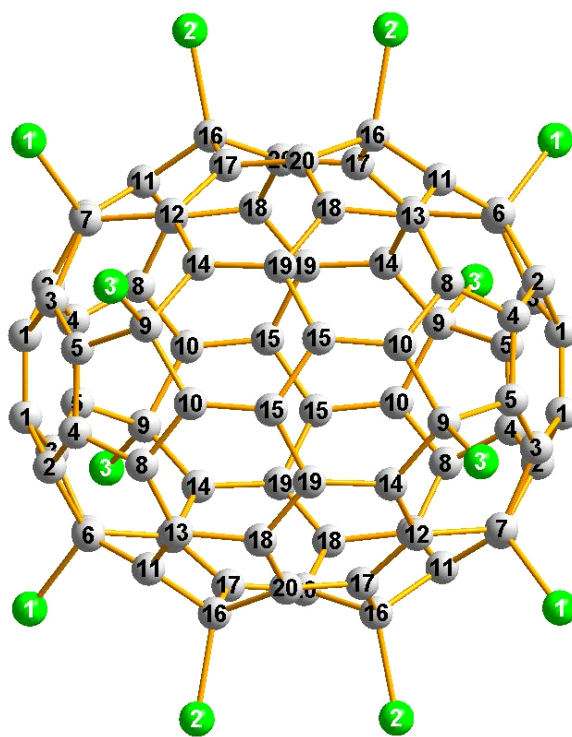


Figure 55 Numbering of carbon and chlorine atoms in $C_{80(2)}Cl_{12}$

In Table 9 the experimentally obtained and DFT-calculated carbon-chlorine bond lengths in $C_{80}Cl_{12}$, as well as the corresponding X-Ray/DFT deviation are presented.

Table 9 DFT-calculated and experimentally observed carbon-chlorine bond lengths in $C_{80(2)}Cl_{12}$

C-Cl bond	X-Ray	X-Ray Average	DFT, Å	Deviation X-Ray/DFT, Å	
C7-Cl1	1.835	1.839	1.837	1.929	-0.092
C9-Cl3	1.835	1.839	1.837	1.944	-0.107
C16-Cl2	1.820	1.821	1.821	1.917	-0.096

The poor correlation between DFT-calculated and experimentally obtained C-Cl bond lengths shows the insufficient accuracy of the hybrid B3LYP method of DFT when it comes to the computation of this type of bond in chlorinated fullerenes. Nevertheless, B3LYP offers the best compromise between accuracy and computational cost for sophisticated cases such as all presented thus far chlorinated fullerene species.

5.3.5 An Empirical Rationale of Halogen Atoms Addition Pattern in Higher Fullerenes

The molecular structures of the chlorinated fullerenes discussed thus far or more precisely the addition patterns of chlorine atoms in them, has prompted an extensive analysis of the crystal structures of all known higher fullerene derivatives (together with some C_{60} and C_{70} halogenated species) with the intention to develop a general principle of higher fullerene reactivity.

5.3.5.1 Steric Strain in Fullerenes

A characteristic feature of fullerenes which makes them interesting and defines their unique chemical and physical properties is the steric strain induced by the geometric peculiarities of the fullerene molecule. The Hückel molecular orbital model, which gives reliable predictions about the relative stabilities of planar aromatic hydrocarbons when combined with standard C–C and C–H σ -bond energies, is not that suitable when applied to isolated fullerene molecules. One reason for that is that the curvature of the fullerene surface destroys the separability of σ - and π -orbitals upon which the Hückel theory is based. Although this separation may be approximately maintained in C₆₀, it can be entirely lost in less symmetrical fullerene molecules. Therefore, the stability of fullerenes cannot be predicted using the Hückel theory alone, but is estimated as a balance between π -electronic stability and steric strain (π -electronic stability and steric strain are generally in opposition), with the latter encompassing all the effects in the electronic structures of fullerenes that are neglected at the Hückel level. In order to discuss all the effects in the electronic structures qualitatively, it is convenient to assume that the valence orbitals of each carbon atom in a fullerene molecule are hybridized in such a manner that the resulting three σ -orbitals point directly along the bonds with neighboring atoms. This approach has first been suggested by Haddon et al., with developing the so called π -orbital axis vector (POAV) scheme.^[92] The direction of the remaining π -orbital, and the s- and p-components of all four hybrid orbitals, are then uniquely determined by orthogonality constraints, which ensure that local σ - π orthogonality is maintained within each atomic valence shell.^[92] In the case of an ideal “planar” carbon atom with 120° σ -orbitals bond angles, perfect sp² hybridization is present and no rehybridization occurs. However, since 60 of all bond angles in a fullerene molecule are approximately 108° (five such bond angles in each of the twelve pentagons), the degree of rehybridization in fullerenes is rather substantial. A closer look at Figure 56 reveals that the rehybridization from the ideal sp² is smallest when only one pentagon is involved and biggest in the case when three pentagons are fused. The degree of rehybridization accounts for the different strain energy in fullerene molecules. Several possible sources of strain energy can be

identified involving both the σ - and π -electrons. The most prominent is the reduced π -orbital overlap and therefore weaker π -bonding.^[13,93]

The qualitative features of π -orbital misalignment might be well illustrated by two limiting examples – a graphene sheet and a C_{20} fullerene molecule.^[12] In graphene the p_π orbitals of neighboring atoms are perfectly aligned, while in the case of C_{20} the respective orbitals (here with certain s-orbital character) are almost sp^3 -hybridized and point outwards from the vertices of a dodecahedron, as presented in Figure 57.

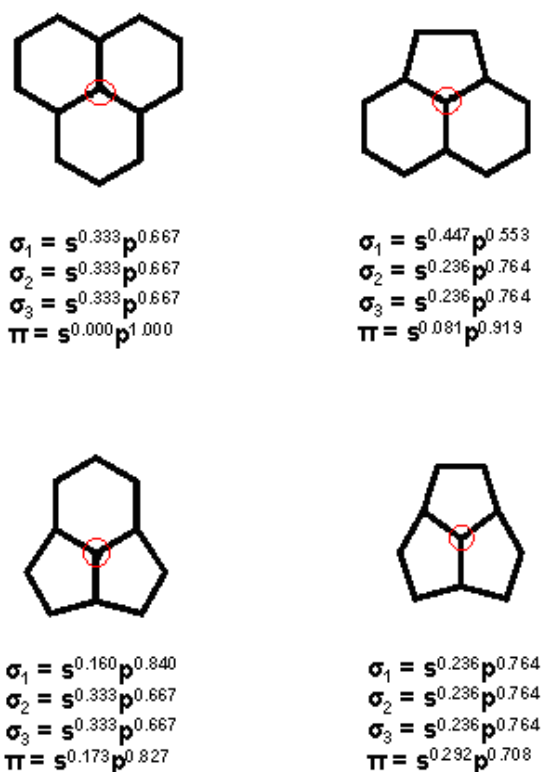


Figure 56 Fractional hybridization of carbon atoms (highlighted in red). The s and p components of the σ - and π - hybrid orbitals have been calculated assuming bond-directed σ -orbitals and idealized polygonal bond angles

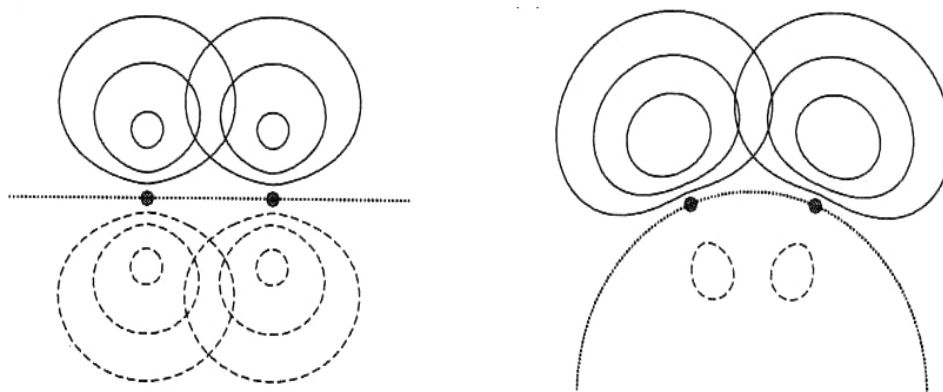


Figure 57 Hybrid orbitals overlapping in graphene (left), and C_{20} (right). The orbitals are constructed from 2s and 2p orbitals with the same exponent, where the positive (solid lines) and the negative (dashed lines) contours correspond to the same numerical values in both cases.^[12]

These hybrid orbitals overlap less than p_{π} orbitals in graphene, resulting weaker π -bonding and concomitant steric strain. Therefore, the carbon atoms in C_{20} , the fullerene species characterized with the highest strain energy, are considered to be the most pyramidal carbon atoms, i.e. with the highest θ_p angles ($\theta_{\sigma\pi} = \theta_p + 90^\circ$ is the POAV-angle^[92]). Other fullerenes have more diverse carbon atom environments with varying degrees of rehybridization, and thus exhibit intermediate degrees of π -orbital misalignment between graphene and C_{20} .

Aside from the rehybridization itself, another reason for inducing steric strain in fullerene molecules is the different degree of rehybridization between neighboring atoms. It is well known from the principles of molecular orbital theory that any difference in the energy of the two orbitals that combine to form a bond reduces the overall strength of this bond. In graphene all σ -bonds are formed from equal in energy “pure” sp^2 orbitals, while the π -bonding is a result of p-orbital overlap. In fullerenes, energetic mismatch occurs in both σ - and π -systems, since different in energy orbitals overlap to form the respective bonds. Therefore, the more curved the fullerene surface and the more diverse the chemical environment of each carbon atom, the higher the steric strain.

5.3.5.2 Addition Pattern of Chlorine Atoms in Higher Fullerenes

A notable feature in higher fullerenes is the addition pattern of the chlorine atoms. In $C_{80}Cl_{12}$, the most pyramidal carbon atoms, those connecting two pentagons (through inter pentagon carbon-carbon bonds - ICCB), are not attacked during chlorine addition to $C_{80}(2)$, although in other cases they have been found to be the most reactive ones.^[94-96] The “most inert” carbon atoms, the atoms constituting the junction of three hexagons – THJ (the yellow circles in Figure 58, top), are not preferred for chlorine addition too. The θ_p angles for the THJ-carbon atoms are with the lowest values, making any addition to them unfavorable (Figure 58, bottom). Therefore, the reaction favored sites are at these carbon atoms which fuse a pentagon with two hexagons (pentagon-hexagon junction - PHJ) but do not bridge two pentagons (to be distinguished from ICCB).

In most of the reported halogenated higher fullerenes the halogen atoms bind to carbon atoms at 1,4 positions in the hexagons (i.e. to PHJ carbon atoms) in such a way that contiguous ribbons of halogen atoms form. This can be seen in Figure 58, where the chlorine atoms are connected to carbon atoms at 1,4 positions in the hexagons (carbon atoms to which chlorine attach are depicted in green in Figure 58). The rest of PHJ-carbon atoms (blue-colored in Figure 58) remain intact simply because further chlorine addition would create 1,2 pattern, which is unfavorable. Due to the local geometry peculiarities, a 1,2 addition pattern would imply short intramolecular distances between vicinal chlorine atoms creating by this strong repulsive forces. The tendency of generating ribbons of 1,4 addition exclusively has first been reported by Kareev et al.,^[75] proposing by this a principle of higher fullerene reactivity. However, the violation of this principle in the case of $C_{76}Cl_{18}$ where ten out of eighteen chlorine atoms bind to ICCB carbon atoms, thus at 1,2 positions in hexagons (see Figure 42 left), needs further discussion.

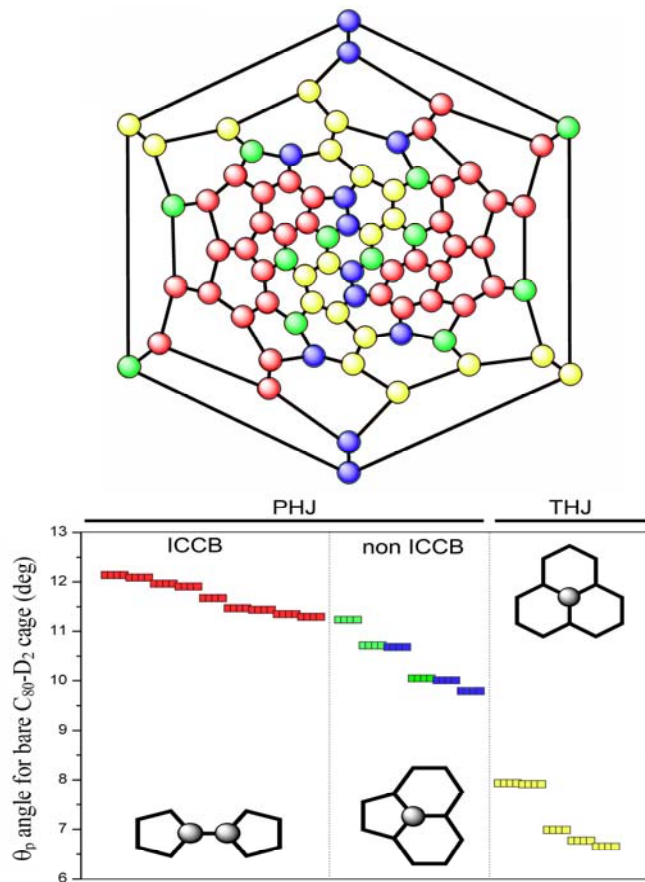


Figure 58 Bottom: A chart showing the θ_p angle distribution for bare-cage DFT-optimized D_2 - C_{80} . ICCB carbon atoms are highlighted in red, PHJ in blue (and green, where chlorine binds) and THJ in yellow. Top: Schlegel diagram of D_2 - $C_{80}(2)$ presenting the same color code for the carbon atoms as in the θ_p -chart

Based on Euler's theorems for systematically addressing topologies of convex polyhedra, the molecular structures of all higher than C_{60} IPR-satisfying fullerenes contain THJ fragments. In higher fullerenes, the central C–C bonds in the pyrene fragments are the longest ones,^[43] although the geometry of these fragments is suitable for effective conjugation and shortening of the respective bonds. The C–C bond lengths in $C_{84}(14)$ depend on the type of fragment in which they are incorporated. In first approximation, four different fragments can be recognized as presented in Figure 59. The shortest lengths (1.34 – 1.38 Å) correspond to the bonds between two pentagons in the pyracylene fragments, while the longest ones (1.46 – 1.48 Å) are involved in pyrene fragments (the

central bond in the pyrene fragment, the one bridging two hexagons). Interestingly, decreasing the number of pentagons in the fragments leads to significant elongation of the corresponding bond in comparison to the aromatic bond length (1.40 Å), despite that the geometry in these fragments is more suitable for effective conjugation. For comparison, in the isolated pyrene molecule the length of the corresponding bond is 1.422 Å.^[97]

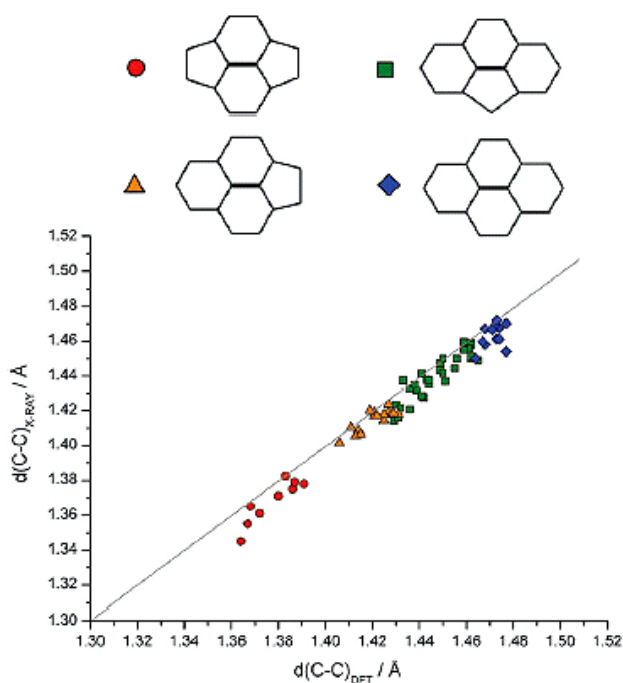


Figure 59 Correlation between the experimentally obtained and the DFT calculated C–C bond distances in C₈₄(14). Correlation between the C–C bond length and the type of fragment in which the corresponding bonds are involved (the bonds under consideration are shown in bold)

Such elongation of these bonds is a direct consequence of the curvature introduced to the “inherently planar” pyrene fragments. Since a direct addition to THJ carbon atoms is unfavorable, the system endeavors to release strain in these extended areas by modifying them through introducing sp³ hybridized carbon atom(s) at least in one of the member-hexagons. On that account, the only possible sites for chlorine attack are the PHJs. As a parallel directing force one has to consider the formation of quasi-aromatic systems (the two phenomena should not be regarded separately). Figure 60 provides an insight into the

changes occurring to the π -system of the parent $C_{80}(2)$ fullerene cage upon chlorination. The carbon atoms to which chlorine atoms connect in $C_{80}Cl_{12}$ have changed their hybridization to sp^3 (class α), destroying by this all THJ in the sense described above. The sp^2 hybridized carbon atoms connected to C_{sp^3} neighbors (class β) have decreased significantly their θ_p angles, while the rest remained more or less the same (class γ - C_{sp^2} connected to C_{sp^2} only). The trend of decreasing pyramidalization after chlorine addition observed for the sp^2 hybridized carbon atoms obviously stabilizes the molecule by creating rather extended quasi-aromatic systems (two belts comprising eight hexagons each are depicted in gray in Figure 60).

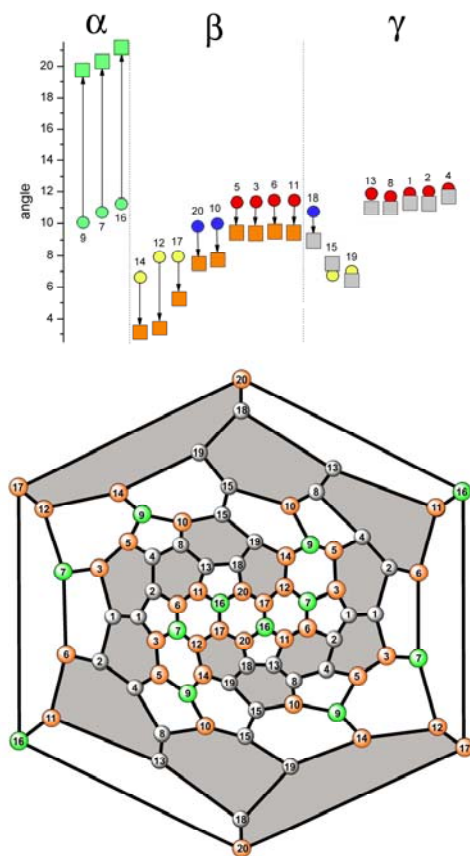


Figure 60 Top: Schematic representation of θ_p angle change after chlorine addition to bare-cage $C_{80}(2)$ - circles depict the carbon atoms in the pristine fullerene (the color codes bear the same meaning as in Figure 58) whereas squares correspond to those in $C_{80}Cl_{12}$. Bottom: Schlegel diagram of $C_{80}Cl_{12}$ showing two extended “aromatic” systems (in gray)

Now, if we go back to the proposed principle of higher fullerene reactivity,^[75] the formation and orientation of 1,4 addition ribbons are conditioned by the contiguous arrangement of THJ carbon atoms (see Figure 58 top, where the yellow circles form string-like array), as well as by the generation of stable conjugated systems. Reacting further the fullerene molecule is possible if additional energy is gained by introducing another π -system. A good example here is provided by the structures of $C_{70}X_{10}$ ($X = Cl, Br$),^[62,65] and $C_{70}Cl_{16}$.^[63] In $C_{70}X_{10}$ the halogen atoms build up a loop of 1,4 addition around the equatorial mirror plane of C_{70} , releasing by this the strain in THJ fragments and leaving behind essentially the same alternant bond pattern characteristic for C_{60} . Halogenating $C_{70}X_{10}$ further results in the product $C_{70}Cl_{16}$, in which the additional six chlorine atoms replicate the addition pattern in $C_{60}X_6$ ($X = Cl, Br$).^[50,51;56-59] Since in I_h - C_{60} there are no THJ fragments and only two types of bonding exist (one of them ICCB), the existence of a whole homologous series of halogen derivatives (Table 3), demonstrates the “availability” of the ICCB carbon atoms for chlorine addition. Therefore, the presence of a string of contiguous 1,2 addition in $C_{76}Cl_{18}$ where 10 chlorine atoms are attached to ICCB carbon atoms is not unusual (as suggested in reference [75]), as far as all “obstructive” THJ are eliminated and an extended “aromatic” system is created. Moreover, the ICCB carbon atoms have higher values of their θ_p angles compared to THJ carbon atoms, providing by this appropriate local geometry for 1,2 addition scenario – higher degree of separation between vicinal chlorine atoms, hence weaker repulsive interactions. A closer look at Figures 60 and 61 reveals that after the first prerequisite, the “termination” of THJ areas, is satisfied, the chlorine atoms are arranged so that they isolate the π -system of the molecule. This is well in accordance to the conception of steric strain, where one of its components is the stability of the π -system. From the criteria of aromaticity and antiaromaticity,^[88,89] it is clear that the pentagons are antiaromatic. Therefore, the participation of their π -electrons in the common π -system of the parent fullerene molecule is destabilizing. Actually, what is observed (well visible for $C_{76}Cl_{18}$ and $C_{80}Cl_{12}$ in Figures 61 and 60, respectively) is the stabilization of the π -system by getting rid of the antiaromatic regions. On the other hand, the most pyramidal carbon atoms in C_{76} (the ICCB carbon atoms depicted in red in Figure 61), significantly decrease their θ_p angles in $C_{76}Cl_{18}$, additionally releasing steric

strain – all 26 chlorine-free ICCB carbon atoms are part of the extended aromatic system (the orange girdle).

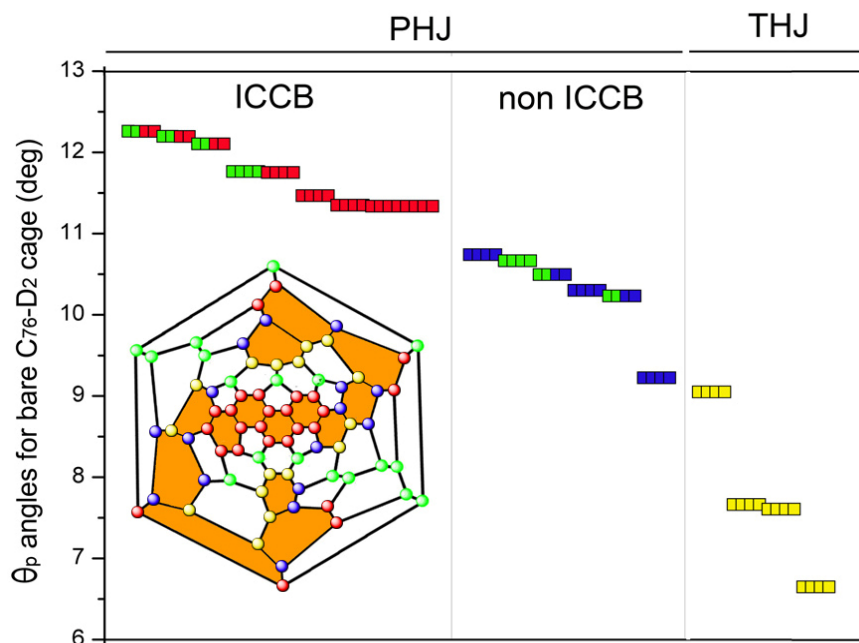


Figure 61 Schematic representation of θ_p angle distribution in the parent C_{76} cage. The color codes bear the same meaning as in Figure 58. The Schlegel diagram of $C_{76}Cl_{18}$ shows the distribution of the different classes of atoms as well as the extended aromatic systems (in orange)

The same observation holds true for the three isomers of $C_{78}Cl_{18}$ reported earlier. Since the chlorine atoms addition pattern is basically the same for the three molecules, only $C_{78}(5)Cl_{18}$ will be discussed here. A look at Figure 62 confirms the concluded thus far: the chlorine atoms build ribbons of 1,4 addition in such a manner that at each end of the fully aromatic planar “benzene rings” (see Figure 62) one sp^3 carbon atom is introduced. The remaining π -system of the fullerene cage might well be described as composed of nine independent benzene fragments isolated by chlorine atoms at 1,4 positions in the surrounding hexagons. Here, too, all conditions introduced by the principle of reactivity are fulfilled – the strain in THJ is eliminated, while stable isolated π -systems are created. The antiaromatic fragments from the common π -system are eliminated, while the steric strain is significantly released through change in the values of the θ_p angles of the ICCB carbon atoms. Twelve ICCB carbon atoms have decreased their θ_p angles with 0.7° (the

two groups of six atoms connecting the three closely disposed aromatic fragments in Figure 62) upon chlorinating the parent C_{78} -cage, while the other six (constituting the newly formed double bonds between pentagons) has dramatically changed their θ_p angles from 11.2 to 6.2°. All other carbon atoms which remain intact upon chlorination have decreased the values of their θ_p angles too (not shown in Figure 62).

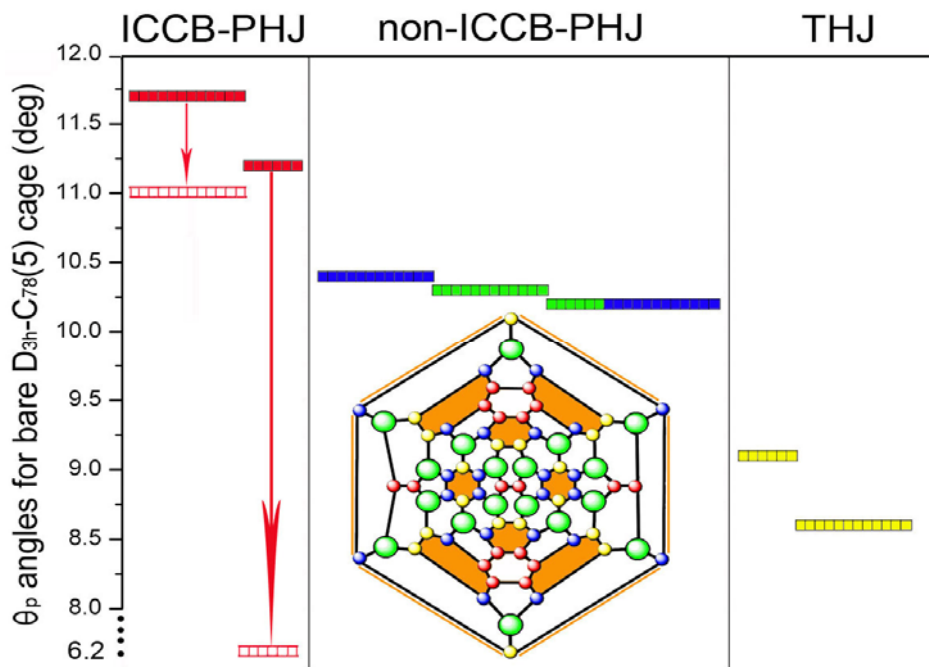


Figure 62 Schematic representation of θ_p angle distribution in the parent $C_{78}(5)$ cage. The Schlegel diagram of $C_{78}Cl_{18}$ shows the distribution of the different classes of atoms as well as the isolated aromatic systems (in orange)

To conclude, stabilizing of the newly-formed chlorine-containing fullerene derivatives is achieved through two parallel interconnected driving mechanisms. The first one is defined as strain-releasing geometry optimization. Formally this stage might be divided into two parts. The curvature of the fullerene molecule leads to a decrease in values of the p_π -overlapping integrals. This is energetically unfavorable and results in a less stable π -system. Locally, it has a strong impact on the “inherently planar” fragments constituted of three or more hexagons. The result is a pronounced elongation of bonds, which otherwise are supposed to be, due to an efficient conjugation, more or less close to the

“aromatic” bond length of 1.4 Å. This trend is obvious for higher fullerenes and has been demonstrated by the X-ray single crystal analysis of C₈₄(14) . AgTPP.^[43] The additional weakening of the common π -electron system of the parent fullerene molecule comes from the high level of pyramidalization encountered for the ICCB carbon atoms (θ_p angles $> 11^\circ$). The resultant rehybridization away from sp^2 for these atoms, similarly to the effect felt on the extended regions of hexagon junctions, leads to minimized values of the respective p_π -overlapping integrals. Adding chlorine atoms to specific sites at the fullerene surface, i.e. introducing sp^3 hybridized carbon atoms, minimizes the values of ICCB-carbon-atoms θ_p angles which tend to approach 90° . The cut-off sizes of the extensive joint-hexagon fragments leave the strained THJ carbon atoms “relaxed” through flattening the local geometry. In effect, all intact carbon atoms decrease their θ_p angles value, which consequently unifies them in a chlorine-free “flat” fragment(s). Actually, one might regard the addition pattern scenario as fencing off the “survived” areas (the islands of aromaticity). Hence, the second component of steric strain as defined in 5.3.5.1 receives its tribute too: the destabilizing antiaromatic fragments are weeded off and the energy of the remaining (or better newly formed) π -electron system is significantly minimized. This result is, of course, expected since the flattened θ_p angles of the unreacted carbon atoms assume more effective conjugation.

5.3.6 Unusual Short Intermolecular Halogen – Halogen Contacts in Chlorinated Derivatives of Fullerenes

Detailed analyses of the crystal structures of all reported in the scope of this thesis halogenated fullerene derivatives have clearly demonstrated the presence of numerous short Cl...Cl intermolecular contacts, the nature of which has long been a matter of interest and debate.^[98-109] In this chapter special attention is paid to the existing hypotheses of short halogen contact formation in different systems, as well as to the specificity of the respective contacts encountered in the crystal structures of all higher fullerene halides reported thus far in the frames of the present work.

5.3.6.1 Introduction to the Phenomenon of Intermolecular Halogen Interactions

The assumption that attractive interactions between halogen atoms should be considered was based on thorough analyses of crystal structures of chlorinated hydrocarbons.^[99-101] In this context, the halogen...halogen contacts in the crystal structures occurred preferably in two definite geometries, type **I** ($\theta_1 = \theta_2$) and type **II** ($\theta_1 = 180^\circ$, $\theta_2 = 90^\circ$), where θ_1 and θ_2 are the two carbon-halogen...halogen angles.^[99-101] Type **I** contacts can be explained by the nonspherical shape of covalently bonded halogen atoms, which occupy rather ellipsoidal volume in space.^[102] As a consequence, the effective atomic radius of halogen atoms along the extended carbon-halogen bond axis is smaller than the radius perpendicular to this axis. Previous analyses of high-quality crystal structures (excluding structures containing further heteroatoms, which can independently play a major role in determining the packing) have shown that short Cl...Cl distances of about 3.5 Å or even less in the case of head to head contacts ($\theta_1 = \theta_2 = 180^\circ$) can be explained by close packing of anisotropic atoms.^[103] In type **II** contacts, one halogen atom acts as a donor while the other as an acceptor. Such kind of interaction between electronegative atoms (N, O and S), which act as Lewis bases, and halogen atoms is well known as halogen bonding, by analogy with hydrogen bonding.^[104-108] However, it was noted that “preferred orientations” are more typical for iodine atoms and not obviously present in order to establish specific Cl...Cl interactions.^[103] Moreover, quantum chemical calculations have shown that Cl...Cl interactions can be classified as “nonbonding”.^[103] The formation of short Cl...Cl contacts is regarded typical for chlorinated aromatic hydrocarbons which are characterized by low carbon-chlorine bond polarity (C-Cl distance of about 1.70 – 1.73 Å) and rather rare in the case of highly polar C-Cl bonds with C-Cl bond lengths of 1.79 – 1.81 Å. Taking into account the large extension of C-Cl bond lengths in the presented fullerene molecules (ranging from approximately 1.84 to 1.88 Å), which should lead to localization of significant negative charge on the chlorine atoms, the participation of these atoms in short Cl...Cl contacts is largely unexpected. However, analyses of the crystal structures of halogenated C_{76} , $C_{78}(2,3,5)$ and C_{80} fullerenes, clearly point out to the presence of attractive intermolecular Cl...Cl

interactions, the nature of which is presumably different from that of the halogen bonding described previously.

5.3.6.2 Short Halogen – Halogen Contacts in $C_{76}Cl_{18}$, $C_{78}Cl_{18}$ and $C_{80}Cl_{12}$

Within the crystal of $C_{76}Cl_{18}$, the chlorine atoms form a 2D $Cl\cdots Cl$ network with considerably short intermolecular $Cl\cdots Cl$ distances (3.148, 3.170, 3.213 Å) which are about 0.45 Å shorter (the most extreme ones) than the sum of the van der Waals radii of two chlorine atoms (see Figure 63). Taking into account that long C–Cl bonds are characterized by high polarity and localization of negative charge on the Cl atom, the short distances between the corresponding Cl atoms are unexpected. Two of these short separations (3.148, and 3.213 Å) might be described by the halogen bonding theory (quasi-type II contacts). The contacts of 3.17 Å might be explained by the ellipsoid theory – close packing of anisotropic chlorine atoms.

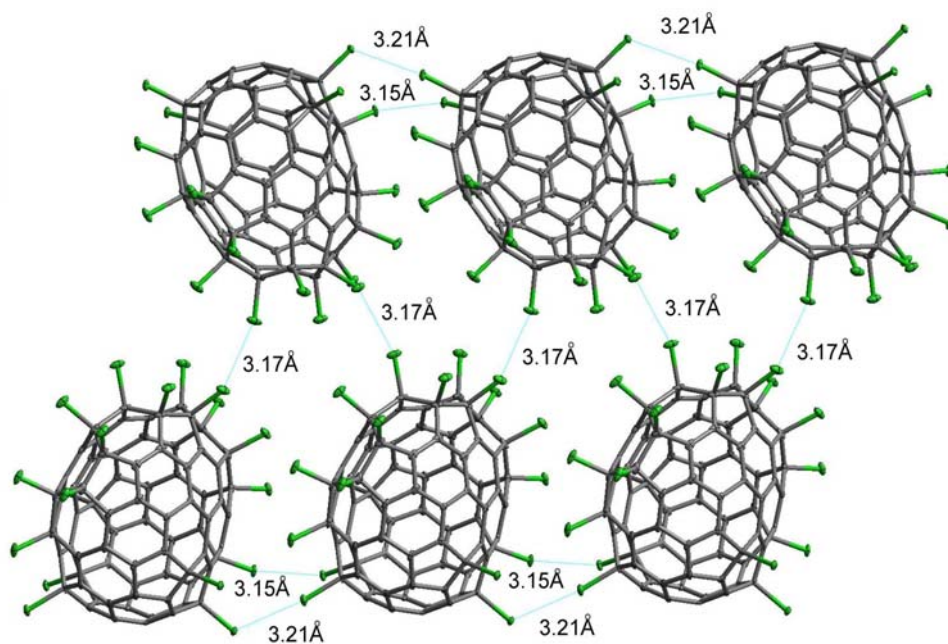


Figure 63 2D-framework of short intermolecular $Cl\cdots Cl$ contacts in the crystal of $C_{76}Cl_{18}$

It has generally been assumed that the elongation of a C–Cl covalent bond leads to localization of negative charge on the Cl atom. The C–Cl bonds in all $C_{78}Cl_{18}$ molecules are strongly elongated (1.84 – 1.87 Å). According to an empirical approach to the estimation of the bond order,^[110-112] this of C–Cl bonds with lengths of about 1.87 Å is only 0.65, which should lead to a very high degree of polarity of these bonds and consequently to localization of significant negative charge on the Cl atom. On the other hand, within the crystal packing of $C_{78}(3)Cl_{18}$ and $C_{78}(5)Cl_{18}$, the chlorine atoms form an extensive 3D Cl··Cl network with short intermolecular Cl··Cl distances of about 3.34 – 3.45 Å, which challenge the concept of “high polarity” of C–Cl bonds. Since within the crystal of $C_{78}(3)Cl_{18}$ and $C_{78}(5)Cl_{18}$ all 18 chlorine atoms are engaged in the formation of Cl··Cl contacts, and all of these are short, the responsible forces have to be inevitably attributed to some attractive interactions between chlorine atoms. It is important to mention that there are no other intermolecular contacts besides Cl··Cl, which could “squeeze” the atoms together, influencing by this the molecular packing. Thus, both crystal structures appear to provide unambiguous evidence for the attractive nature of these intermolecular interactions, and challenge at the same time all explanations discussing this kind of “bonding” provided thus far.

A closer look at the structure in Figure 64, where the molecular packing of the fullerene molecules in the solvent free crystal of $C_{78}(3)Cl_{18}$ is shown, reveals the presence of two- as well as three-centered contacts between the chlorine atoms. The existence of such three-centered contacts prompts each $C_{78}Cl_{18}$ molecule to form 24 short Cl··Cl separations, all of about 3.34 – 3.38 Å.

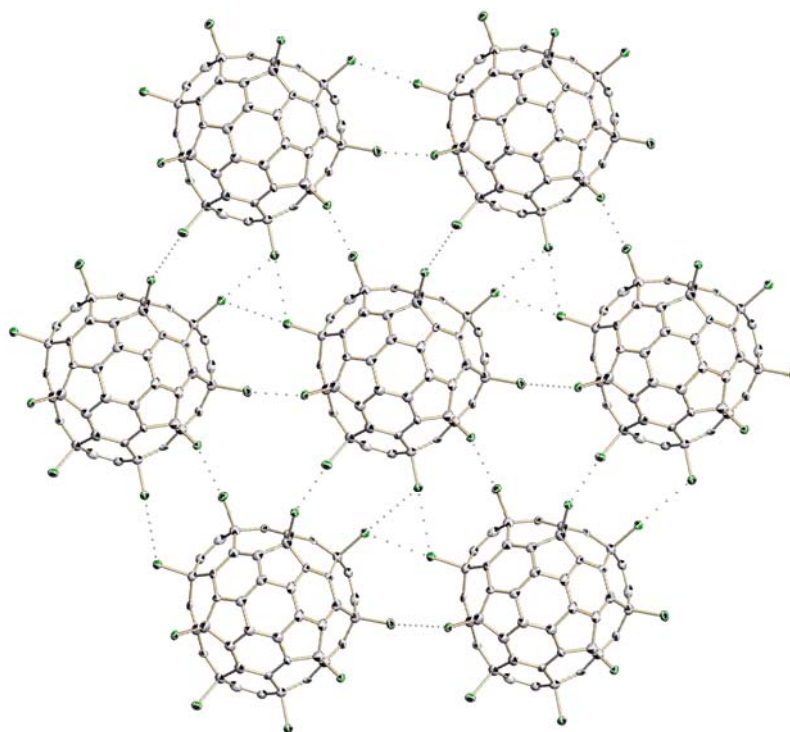


Figure 64 ORTEP projection of $C_{78}(3)Cl_{18}$ showing short two- and three-centered $Cl\cdots Cl$ contacts (represented by dotted lines)

The fully ordered crystals of $C_{78}(5)Cl_{18}$ (which is isostructural to $C_{78}(3)Cl_{18}$) provide the possibility to precisely determine not only all bond lengths but also the intermolecular distances. A closer look at the crystal structure reveals some unexpected phenomena. Firstly, here as in the structure of $C_{78}(3)Cl_{18}$, all chlorine atoms are involved in short intermolecular $Cl\cdots Cl$ contacts, and all of these are shorter than the sum of the van der Waals radii of two chlorine atoms. At the same time, all C–Cl bonds are enormously elongated, reaching the values of 1.87 Å. According to the classical concept of the covalent C–Cl bond, elongation of the interatomic distance must lead to localization of strong negative charge on the Cl atom. However, the short intermolecular distances between chlorine atoms are in discrepancy with this general postulate. Since there are no other intermolecular contacts besides $Cl\cdots Cl$, which we regard significant in influencing the molecular packing, the short $Cl\cdots Cl$ separations are presumably a result of attractive interactions between Cl atoms. Stronger evidence of the attractive nature can be obtained considering two- and three-centered $Cl\cdots Cl$ contacts (Figure 65) in which the chlorine

atoms constituting structurally equal (according to the D_{3h} point group symmetry of $C_{78}(5)Cl_{18}$) C–Cl bonds are involved.

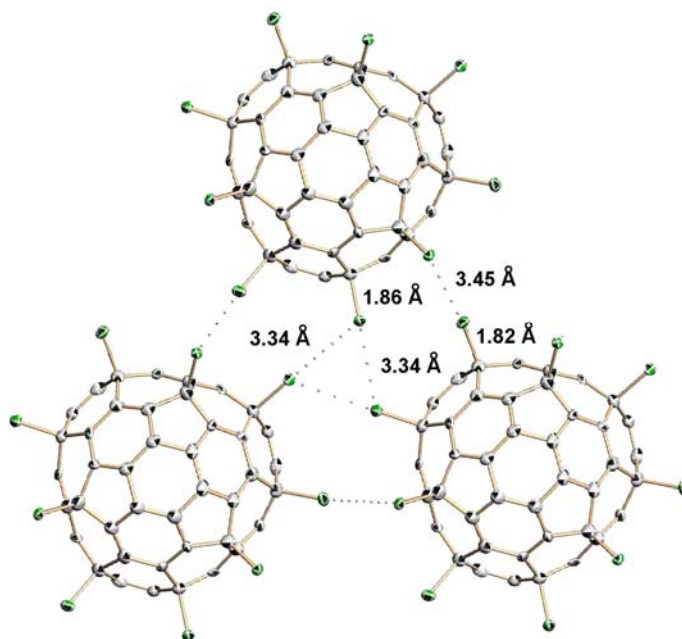


Figure 65 ORTEP plot of $C_{78}(5)Cl_{18}$ molecules in the crystal showing short two- and three-centered Cl...Cl contacts (represented by dotted lines). Identical C–Cl bonds have different lengths due to the magnitude of intermolecular interaction they are involved into. Thermal ellipsoids are drawn at 50% probability level

In the three-centered Cl...Cl contacts, the respective C–Cl bonds are elongated (1.87Å) in comparison to those where two-centered contacts are formed (1.82Å) as presented in Figure 65. In the case of the three-centered contacts the accumulation of a “heavy” negative charge (three chlorine neighbors) within the limited space of contact formation should generate strong repulsive forces. However, exactly the opposite tendency is to be observed – the intermolecular Cl...Cl distances are shorter in the three- compared to the two-centered contacts, 3.34Å and 3.45Å , respectively. The unique structure of $C_{78}(5)Cl_{18}$ provides the possibility to analyze the influence of intermolecular interaction on the C–Cl bond distances and to conclude that the elongation of the C–Cl bonds involved in the shorter Cl...Cl contacts is a result of attractive interactions between the chlorine atoms.

The first example of an unusually short intermolecular Cl...Cl contact (3.21 Å) between two “highly polar” Cl atoms was reported more than 20 years ago in the crystal structure of triphenylmethane chloride.^[113] To our knowledge, no other crystal structure of chlorinated hydrocarbons with such short Cl...Cl separations between chlorine atoms involved in highly elongated C–Cl bonds (1.87 Å) have ever been reported. In the structure of C₇₆Cl₁₈, however, the chlorine atoms form a number of extremely short Cl...Cl contacts (as described above) of about 3.14 Å – 3.21 Å, which are about 0.45 Å shorter than the sum of the van der Waals radii. As a very interesting and important fact, the eight elongated C–Cl bonds (1.821 Å – 1.85 Å) are involved in such contacts, whereas the rest “usual” C–Cl bonds with lengths of 1.777 Å – 1.797 Å do not form any short Cl...Cl contacts. Some chlorinated C₆₀ fullerenes – C₆₀Cl₂₈, C₆₀Cl₃₀ (for references see Table 3), – also form short Cl...Cl contacts, although the C–Cl bonds in these structures are not strongly elongated (1.78 Å – 1.80 Å). The structural similarity of the chlorine-bearing fragments in triphenylmethane chloride,^[113] C₇₆Cl₁₈ and the two C₇₈Cl₁₈ (C₇₈(3)Cl₁₈ and C₇₈(5)Cl₁₈) molecules leads toward the assumption that the tendency of forming short Cl...Cl contacts is due to the unique bonding characteristics of carbon rather than the nature of the chlorine atom itself. In all mentioned cases, the corresponding chlorine atoms are connected to sp³-hybridized carbon atoms, which in turn are directly connected to three phenyl rings. The angular symmetry at the sp³ carbon atom is considerably distorted from tetrahedral. Obviously, such geometry results in a partial rehybridization of the corresponding carbon atom which assumes additional sp² character. The three neighboring aromatic rings additionally stabilize this configuration since the molecule adopts a more extended aromatic state. As a result of the reduced overlap efficiency between the chlorine and carbon atomic orbitals, the corresponding C–Cl bonds are significantly elongated. Consequently, the short intermolecular distances between these chlorine atoms indicate that C–Cl bonds cannot be regarded as highly polar, and significant localization of negative charge on the chlorine atom is less probable. Thus, the elongation of the C–Cl bonds and the absence of strong negative charges on the Cl atoms lead to the assumption that the corresponding bonds are partially homolytically dissociated. This model would consistently explain all the features discussed. The partial homolytic cleavage of C–Cl bonds will impart a partial radical

character to the chlorine atoms, which breaks up the closed-shell character of chlorine and enables it to undergo some weak intermolecular bonding.

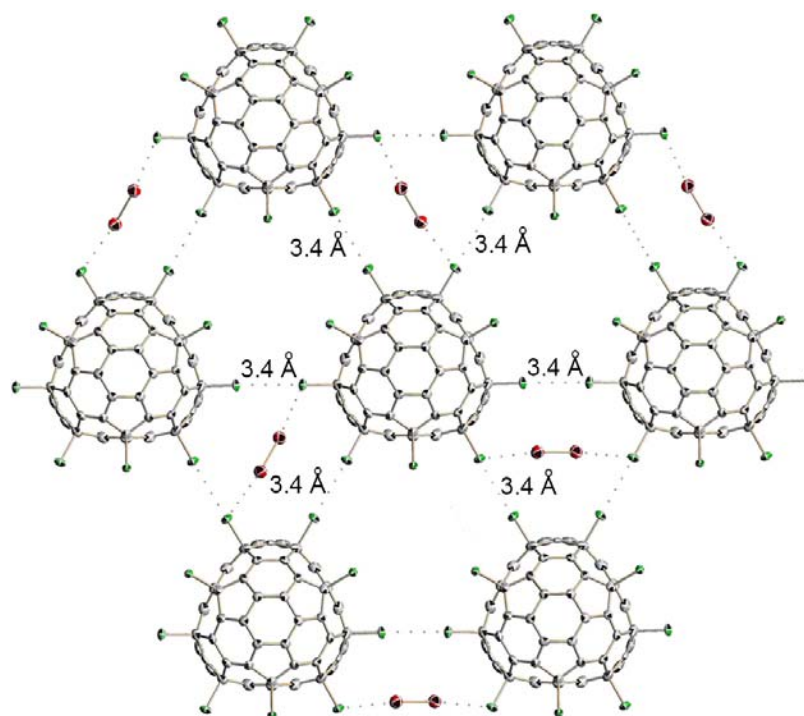


Figure 66 ORTEP projection of $C_{78}(2)Cl_{18} \cdot Br_2 \cdot TiCl_4$ in the crystal. $TiCl_4$ is omitted for clarity. Only one orientation of Br_2 molecule is presented. Short contacts are depicted by dotted lines

Within the crystal packing of $C_{78}(2)Cl_{18}$ each molecule forms 12 $Cl \cdots Cl$ contacts with distances of about 3.4 Å (Figure 66). Such an orientation in the crystal leads to the formation of two dissimilarly sized voids: the larger ones contain disordered $TiCl_4$ molecules while the smaller are occupied by Br_2 molecules. The bromine molecule is disordered between 6 equivalent positions, each oriented along the axis connecting two chlorine atoms as shown in Figure 67 top. As it can be concluded from the electron density map (Figure 67 bottom) the bromine molecule is fixed between two chlorine atoms. The $Cl \cdots Br$ distance of 3.2 Å is enormously short (the sum of the van der Waals radii is of the two atoms is 3.6 – 3.7 Å).

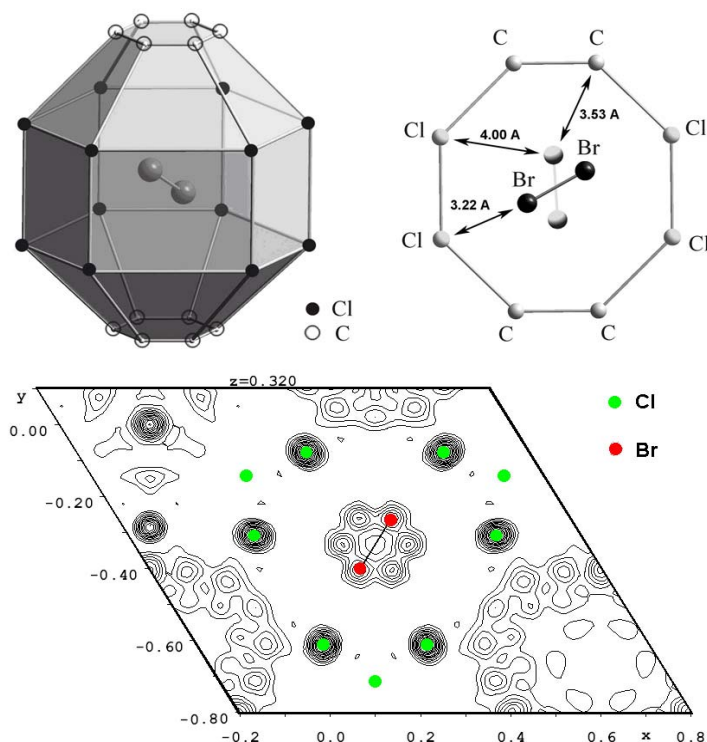


Figure 67 Top: Br₂ in the “molecular box”. The orientation and relative distances between chlorine atoms and the bromine molecule according to X-ray experimental data (depicted black) and the hypothetically possible orientation of Br₂ representing minimized interhalogen repulsions (depicted gray) are shown too. Bottom: Electron density map calculated from observed structure factor (F(obs)). Only one orientation of Br₂ molecule is presented for clarity

The fact that the Br₂ molecule is oriented between two chlorine atoms rather than avoiding any short interhalogen contacts, regardless of the abundant space available (see Figure 67, top, right), as well as the rigidity of the “molecular box” in which it is imprisoned, thus diminishing the influence of crystal packing forces, confirms the attractive nature of halogen-halogen interaction in the given system. The angle C–Cl···Br is close to 120°, which represents an energetically unfavorable geometry for a close contact formation according to quantum chemical calculations.^[103] In the case of Cl···Cl contacts such an orientation results in an exchange-repulsion energy of about 5 kcal . mol⁻¹,^[103] and is expected to be even higher in the case of Cl···Br contacts. It is easy to assume that the attractive forces should be higher than 5 kcal . mol⁻¹, and notwithstanding that such halogen–halogen “bonding” can be classified as weak, the cumulative effect can

constitute significant values of energy. For example, in the cases of $C_{78}(3)Cl_{18}$ and $C_{78}(5)Cl_{18}$ the formation of 24 such “bonds” can provide an amount of energy equal to or greater than $120 \text{ kcal} \cdot \text{mol}^{-1}$, which is higher than the energy of a single C–C bond.

The crystal structure of $C_{80}Cl_{12}$ displays also the presence of short intermolecular chlorine contacts: ten out of twelve chlorine atoms from each fullerene molecule are involved in short intermolecular $Cl \cdots Cl$ contacts ($3.3 - 3.5 \text{ \AA}$) with their neighboring molecules. The other two chlorine atoms also form short intermolecular contacts but with carbon atoms (3.230 \AA). While six of the $Cl \cdots Cl$ separations can be explained by the available theories for short halogen contact formation, four display energetically unfavorable geometry with respect to the angles between the two C–Cl covalent bond axes and the one separating the chlorine atoms (Figure 68).^[103] To my knowledge, such type of contacts has not been previously observed and can be explained neither by close packing of anisotropic van der Waals bodies (Figure 68, the top representation on the right),^[103] nor by the so called halogen bonding (Figure 68, the central representation on the right),^[104-108]

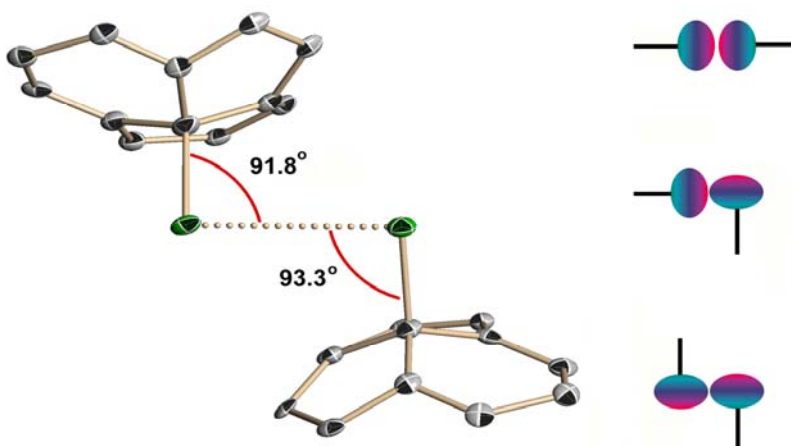


Figure 68 Left: A close contact formation between two chlorine atoms from neighboring fullerene molecules in the crystal structure of $C_{80}Cl_{12}$ (for clarity, only fragments of the two molecules are shown). Right: Possible mutual orientations of chlorine atoms in close contact formation – the top representation shows an example of close packing of anisotropic atoms, the central visualizes the so called halogen bonding, whereas the bottom presents the case in $C_{80}Cl_{12}$ crystal

In summary, the detailed analyses of the crystal structures of $C_{76}Cl_{18}$, $C_{78(2)}Cl_{18}$, $C_{78(3)}Cl_{18}$, $C_{78(5)}Cl_{18}$ and $C_{80}Cl_{12}$ have displayed a conclusive evidence of attractive $Cl\cdots Cl$ interactions in the given systems. We assume that the attractive forces between chlorine atoms are caused by their chemical environment rather than their specific properties, and the nature of such interactions is probably defined by the partial radical character residing on the chlorine atoms, which is a consequence of the significant distortion of the angular symmetry at the sp^3 -hybridized carbon atoms from tetrahedral. Exactly as the non-planar character of sp^2 -hybridized carbon atoms is responsible for the unusual properties of fullerenes, the sp^3 -hybridized carbon not being able to achieve tetrahedral configuration in the exohedral fullerene derivatives defines the unique behavior of these compounds. We are optimistic that further theoretical investigations, which are under progress, as well as the investigation of the chemical behavior of chlorinated fullerenes will confirm our assumptions and verify the radical nature of the partial cleavage of C–Cl bonds in these systems.

5.3.6.3 Quantum Chemical Calculations and Binding Energies in Model Dimers

In order to get an insight into the intermolecular attraction between two halogen atoms from neighboring molecules in the crystals of halogenated fullerenes, quantum chemical calculations were performed, focusing on four aspects: 1) computational method, 2) quality of the basis set, 3) chemical environment of the chlorinated carbon atom, and 4) geometrical constraints being enforced by the cage structure of the fullerene molecule. Dimers of two model compounds, chloromethane and trivinyl-chloromethane, the latter mimicking the sp^2 carbon atoms surrounding the chlorinated carbon atom in the fullerenes, were used for the evaluation (see Figure 69).

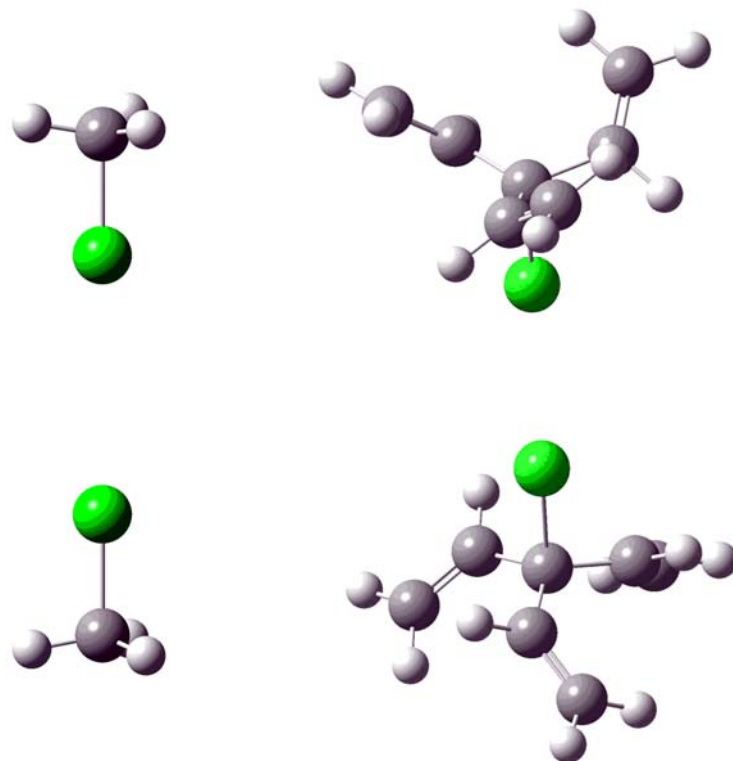


Figure 69 Visual representation of the linear arrangements for the dimers of chloromethane (left) and trivinyl-chloromethane (right)

Table 10 Dimerization energies DE (kJ/mole), Cl...Cl and C-Cl distances (Å) of R₃CCl (R = -H, -CH=CH₂), computed with various methods and basis sets.

method	R = H; aug-cc-pVTZ basis set ¹⁾			R = vinyl; aug-cc-pVDZ basis set ¹⁾		
	DE	R _{Cl...Cl}	R _{C-Cl}	DE	R _{Cl...Cl}	R _{C-Cl}
DFT (PBE)	(0)	-	1.80	(0)	-	1.90
hybrid (B3LYP)	(0)	-	1.80	(0)	-	1.90
MP2	-2.4	3.49	1.78	-5.6	3.39	1.85
CCSD	-0.9	3.72	1.79	-2.7	3.56	1.87
CCSD(T)	-1.7	3.59	1.79			

1)) basis set for the hydrogen atoms

With the DFT methods applied here no binding is obtained for the dimers, neither with the gradient-corrected functional PBE, nor with the hybrid functional B3LYP. With coupled cluster methods, the chloromethane dimer is computed to be stable only with a basis set of at least valence triple zeta quality with additional diffuse functions (aug-cc-pVTZ). Applying perturbation theory of second order (MP2) leads to an overestimation of the dimerization energy.

The different chemical environment in trivinyl-chloromethane leads to an enhancement of the binding energy, to an elongation of the Cl–C bond and to a shortening of the Cl...Cl contact. The values given in Table 6 are for a linear arrangement of the dimers. A slightly larger binding energy is obtained for a bent configuration. This is also the case if the Cl–C–R angle is enlarged to a value similar to the one observed in the fullerenes.

The calculations on the model compounds show, that a proper quantum chemical description of the attractive intermolecular interactions in the chlorinated fullerenes is very demanding, both concerning the method and the quality of the basis set. Moreover, the specific chemical and geometrical environment as it is found in the chlorinated fullerenes has to be considered as well. None of the models used so far for the description of halogen bonding is adequate to describe the particular packing of chlorinated fullerenes in crystals. The present investigations will provide new insight on the role of halogen bonding in the field of crystal engineering.

This part of the work is not finished yet, but some important conclusions might be given at the present stage:

1. The Cl...Cl interaction strongly depends on the chemical surrounding of the chlorine-bearing carbon atom; by introducing sp^2 carbon atoms directly connected to the chlorine-bearing sp^3 carbon atom, the magnitude of Cl...Cl attraction increases.
2. The mutual orientation of the individual units does not influence significantly the magnitude of intermolecular interaction (the dimerization energy).
3. The degree of pyramidalization of the chlorine-bearing carbon atom plays an important role. Strongly pyramidalized carbon atoms (those with high values of the θ_p angle) are more “susceptible” for close contact formation.

5.4 Closing Remarks

The presented work might formally be divided into two general sections. Within the first one, chromatographic purification and isolation of individual fullerene isomers, the following achievements should be highlighted:

1. One more representative of the C_{78} -fullerene family, $C_{78}(5)$, has been isolated from the crude fullerene mixture (the raw extract) and its existence in fullerene-graphitic soots confirmed for the first time. This achievement has proven possible thanks to the newly developed chromatographic system containing a mobile phase with composition ratio toluene/dichloromethane of 1:1. The optimized chromatographic system has been found efficient in obtaining isomerically pure preparative amounts of five other higher fullerene species – $C_{80}(2)$, a C_2 - C_{84} isomer, $C_{84}(14)$, a D_2 - C_{84} and a D_{2d} - C_{84} isomer. The isolation of these fullerenes using the improved chromatographic conditions is time-saving, and therefore more efficient than the respective separation procedures suggested previously.^[71-73]
2. A new preparative methodology for isolation of bulk amounts of the three most abundant C_{78} isomers, $C_{78}(1)$, $C_{78}(2)$ and $C_{78}(3)$, has been suggested. The initial step is based on the “standard” partition of the main C_{78} fraction into two subfractions – the first one containing a mixture of isomers 1 and 2, while the second the pure isomer 3. A selective derivatization of the parent $C_{78}(1)$ and $C_{78}(2)$ with ICl , resulting in the generation of a few products only, is identified as the second step. The consequent single-stage baseline chromatographic separation of the chlorine derivatives of both fullerenes has shown highly efficient, providing bulk amounts of the respective compounds. The final step, thermal dissociation of the carbon-chlorine bonds in each isolated compound, leads to retrieval of the parent fullerenes in isomerically pure form.

3. A newly developed chromatographic system consisting of toluene/methanol in ratio 4:1 as a mobile phase, and the Buckyprep-M column packing as a stationary phase has been successfully employed for the isolation of isomerically pure bulk amounts of a C₂-C₈₂ isomer. The application of this system in obtaining pure preparative amounts of C₂-C₈₂ makes the suggested systematic procedure the most efficient one for this fullerene isomer.

Within the second section, structural studies of individual fullerene derivatives, the following breakthroughs deserve attention.

1. The constitution patterns of the individual fullerene isomers C₇₆(1), C₇₈(2), C₇₈(3), C₇₈(5) and C₈₀(2) have been confirmed for the first time through the single-crystal X-ray analyses of the following fullerene derivatives: C₇₆(1)Cl₁₈, C₇₈(2)Cl₁₈, C₇₈(3)Cl₁₈, C₇₈(5)Cl₁₈ and C₈₀(2)Cl₁₂.
2. Detailed analyses of the molecular structures or more precisely the addition patterns of chlorine atoms in the presented within the frames of this work fullerene derivatives (C₇₆Cl₁₈, C₇₈(2)Cl₁₈, C₇₈(3)Cl₁₈, C₇₈(5)Cl₁₈ and C₈₀Cl₁₂) have suggested a general principle of higher fullerene reactivity. The striving of the new-forming chlorine-fullerene system to minimize as much as possible the “inherited” from the parent fullerene cage steric strain, upon chlorination, has been identified as the reaction main driving force. Two parallel mechanisms work together to release the steric strain. The first one might formally be defined as geometric optimization: the most pyramidalized carbon atoms, which remain intact (unreacted) upon chlorinating the parent fullerene, decrease significantly their pyramidalization level. In other words, the system tries to isolate “pure” (as far as possible and as many as possible) sp²-hybridized carbon atoms introducing sp³ carbon atoms at specific positions. This formal isolation partitions the fullerene surface and designates the appearance of quasi-flat fragments (resembling the natural landscape with its plains surrounded by mountains). Logically, as closer to planar the intact carbon atoms get, as stronger the

conjugation between them. Therefore, the second mechanism in stabilizing the modified fullerene cage is the formation of isolated aromatic system(s) with considerably enhanced conjugation efficiency.

3. Detailed analyses of the crystal structures of all reported within the scope of this thesis chlorinated fullerenes have clearly shown the presence of numerous unusually short intermolecular halogen contacts. Based on thorough investigation of this phenomenon, confirmative suggestions pointing at the attractive nature of the interactions between the interplaying halogen atoms have been proposed. A mechanism involving a partial homolytic cleavage of the covalent C–Cl bonds, breaking by this the closed-shell character of chlorine, is presumably responsible for the attraction between chlorine atoms belonging to neighboring molecules. In support for this hypothesis comes the observation of enormously elongated C–Cl bonds, excluding the possibility of electrostatic interaction (the accumulation of negative charge on chlorine would create repulsive instead of attractive forces). In order to confirm the empirically derived conclusions, quantum chemical calculations exploiting the binding energy in model chlorine-containing dimers have been undertaken, and although this work is still in progress, the initial results are rather confirmative.

6 Literature

1. Jones, D. E. H., Atomization of Chemistry. *New Scientist* **1966**, 31, (511), 493-496.
2. Osawa, E., Superaromaticity. *Kogyo* **1970**, 25, (9), 854-863.
3. Bochvar, D. A.; Gal'pern, E. G., Carbododecahedron, s-Icosahedron, and Carbo-s-Icosahedron Hypothetical Systems. *Doklady Akademii Nauk SSSR* **1973**, 209, (3), 610-612.
4. Davidson, R. A., Spectral Analysis of Graphs by Cyclic Automorphism Subgroups. *Theoretica Chimica Acta* **1981**, 58, (3), 193-231.
5. Kroto, H. W.; Heath, J. R.; O'Brien, S. C.; Curl, R. F.; Smalley, R. E., C-60 - Buckminsterfullerene. *Nature* **1985**, 318, (6042), 162-163.
6. Krätschmer, W.; Lamb, L. D.; Fostiropoulos, K.; Huffman, D. R., Solid C-60 - A New Form of Carbon. *Nature* **1990**, 347, (6291), 354-358.
7. Taylor, R.; Hare, J. P.; Abdulsada, A. K.; Kroto, H. W., Isolation, Separation and Characterization of the Fullerenes C-60 And C-70 - The 3rd Form of Carbon. *Journal of the Chemical Society - Chemical Communications* **1990**, (20), 1423-1424.
8. Ettl, R.; Chao, I.; Diederich, F.; Whetten, R. L., Isolation of C76, A Chiral (D2) Allotrope of Carbon. *Nature* **1991**, 353, (6340), 149-153.
9. Diederich, F.; Whetten, R. L.; Thilgen, C.; Ettl, R.; Chao, I.; Alvarez, M. M., Fullerene Isomerism - Isolation Of C2-Nu-C78 and D3-C78. *Science* **1991**, 254, (5039), 1768-1770.
10. Kikuchi, K.; Nakahara, N.; Wakabayashi, T.; Suzuki, S.; Shiromaru, H.; Miyake, Y.; Saito, K.; Ikemoto, I.; Kainosho, M.; Achiba, Y., NMR Characterization of Isomers of C-78, C-82 and C-84 Fullerenes. *Nature* **1992**, 357, (6374), 142-145.
11. Manolopoulos, D. E.; Fowler, P. W.; Taylor, R.; Kroto, H. W.; Walton, D. R. M., An End to the Search for the Ground-State of C84. *Journal of the Chemical Society - Faraday Transactions* **1992**, 88, (20), 3117-3118.
12. Fowler, P. W.; Manolopoulos, D. E.; An Atlas of Fullerenes, *Clarendon, Oxford*, **1995**.

13. Schmalz, T. G.; Seitz, W. A.; Klein, D. J.; Hite, G. E., Elemental Carbon Cages. *Journal of the American Chemical Society* **1988**, *110*, (4), 1113-1127.
14. Kroto, H. W., The Stability of the Fullerenes C-24, C-28, C-32, C-36, C-50, C-60 and C-70. *Nature* **1987**, *329*, (6139), 529-531.
15. Saito, S.; Okada, S.; Sawada, S.; Hamada, N., Common Electronic-Structure and Pentagon Pairing in Extractable Fullerenes. *Physical Review Letters* **1995**, *75*, (4), 685-688.
16. Diener, M. D.; Alford, J. M., Isolation and Properties of Small-Bandgap Fullerenes. *Nature* **1998**, *393*, (6686), 668-671.
17. Dietz, T. G.; Duncan, M. A.; Powers, D. E.; Smalley, R. E., Laser Production of Supersonic Metal Cluster Beams. *Journal of Chemical Physics* **1981**, *74*, (11), 6511-6512.
18. Powers, D. E.; Hansen, S. G.; Geusic, M. E.; Puiu, A. C.; Hopkins, J. B.; Dietz, T. G.; Duncan, M. A.; Langridgesmith, P. R. R.; Smalley, R. E., Supersonic Metal Cluster Beams - Laser Photo-Ionization Studies of Cu₂. *Journal of Physical Chemistry* **1982**, *86*, (14), 2556-2560.
19. Hopkins, J. B.; Langridgesmith, P. R. R.; Morse, M. D.; Smalley, R. E., Supersonic Metal Cluster Beams of Refractory-Metals - Spectral Investigations of Ultracold Mo₂. *Journal of Chemical Physics* **1983**, *78*, (4), 1627-1637.
20. Curl, R. F., Dawn of the fullerenes: Conjecture and experiment (Nobel lecture). *Angewandte Chemie - International Edition in English* **1997**, *36*, (15), 1567-1576.
21. Haufler, R. E.; Conceicao, J.; Chibante, L. P. F.; Chai, Y.; Byrne, N. E.; Flanagan, S.; Haley, M. M.; O'Brien, S. C.; Pan, C.; Xiao, Z.; Billups, W. E.; Ciufolini, M. A.; Hauge, R. H.; Margrave, J. L.; Wilson, L. J.; Curl, R. F.; Smalley, R. E., Efficient Production of C₆₀ (Buckminsterfullerene), C₆₀H₃₆, and the Solvated Buckide Ion. *Journal Of Physical Chemistry* **1990**, *94*, (24), 8634-8636.
22. Haufler, R. E.; Chai, Y.; Chibante, L. P. F.; Conceicao, J.; Jin, C.; Wang, L. S.; Maruyama, S.; Smalley, R. E., Carbon-Arc Generation of Carbon Sixty-Atom Molecules, *Material Research Society Symposium Proceedings*, Rice University, Houston, **1991**, 627 - 637.

23. Scrivens, W. A.; Tour, J. M., Synthesis of Gram Quantities of C-60 by Plasma Discharge in a Modified Round-Bottomed Flask - Key Parameters for Yield Optimization and Purification. *Journal of Organic Chemistry* **1992**, *57*, (25), 6932-6936.
24. Kikuchi, K.; Nakahara, N.; Honda, M.; Suzuki, S.; Saito, K.; Shiromaru, H.; Yamauchi, K.; Ikemoto, I.; Kuramochi, T.; Hino, S.; Achiba, Y., Separation, Detection, and UV/Visible Absorption-Spectra of Fullerenes - C-76, C-78, C-84. *Chemistry Letters* **1991**, (9), 1607-1610.
25. Haufler, R. E., Techniques of Fullerene Production, *Proceedings - Electrochemical Society*, University California-Davis, Davis, CA, USA, **1994**, 50-67.
26. Anderson, P. E.; Anderson, T. T.; Dyer, P. L.; Dykes, J. W.; Irons, S. H.; Smith, C. A.; Kylin, R. D.; Klavins, P.; Liu, J. Z.; et al., Optimization of Fullerene Yields in a Plasma Arc Reactor, *Proceedings - Electrochemical Society*, University California-Davis, Davis, CA, USA, **1994**, 40-49.
27. Markovic, Z. M.; Jokic, T. L.; TodorovicMarkovic, B. M.; Blanusa, J. L.; Nenadovic, T. M., Model of Improved Arc Generator for Fullerene Production. *Fullerene Science and Technology* **1997**, *5*, (5), 903-918.
28. Jansen, M.; Peters, G.; Wagner, N., Formation Of Fullerenes And Endohedral Metallofullerenes - Preparation in a Radiofrequency Furnace. *Zeitschrift fur Anorganische und Allgemeine Chemie* **1995**, *621*, (4), 689-693.
29. Peters, G.; Jansen, M., A New Fullerene Synthesis. *Angewandte Chemie - International Edition in English* **1992**, *31*, (2), 223-224.
30. Snyder, L. R.; Kirkland, J. J.; Introduction to Modern Liquid Chromatography, *John Wiley & Sons*, New York, **1979**.
31. Gehrke, C. W.; Wixom, R. L.; Bayer, E.; Chromatography – A Century of Discovery 1900 – 2000, *Elsevier*, Amsterdam, **2001**.
32. Kazakevich, Y.; LoBrutto, R.; HPLC for Pharmaceutical Scientists, *John Wiley & Sons*, New York, **2007**.
33. Fetzer, J. C.; Gallegos, E.; The Separation and Identification of Higher Molecular Weight Fullerenes. *Polycyclic Aromatic Compounds* **1992**, *2*, (4), 245-251.
34. Saito, Y.; Ohta, H.; Jinno, K.; Peer Reviewed: Chromatographic Separation of Fullerenes. *Analytical Chemistry* **2004**, *76*, (15), 267A-272A.

35. Gügel, A.; Müllen, K.; Separation of C₆₀ and C₇₀ on Polystyrene Gel with Toluene as Mobile Phase. *Journal of Chromatography A* **1993**, *628*, (1), 23-29.
36. Zarzycki, P. K.; Ohta, H.; Saito, Y.; Jinno, K.; Chromatographic Behavior of C₆₀ and C₇₀ Fullerenes at Subambient Temperature with n-Alkanes Mobile Phases. *Chromatographia* **2006**, *64*, 79-82.
37. Saito, Y.; Ohta, H.; Jinno, K.; Design and Characterization of Novel Stationary Phases Based on Retention Behavior Studies with Various Aromatic Compounds. *Journal of Separation Science* **2003**, *26*, 225-241.
38. Skoog, D. A.; Crouch, S. R.; Holler, F. J.; Principles of Instrumental Analysis, *Cengage Learning*, USA, **2006**.
39. Ajie, H.; Alvarez, M. M.; Anz, S. J.; Beck, R. D.; Diederich, F.; Fostiropoulos, K.; Huffman, D. R.; Kratschmer, W.; Rubin, Y.; Schriver, K. E.; Sensharma, D.; Whetten, R. L., Characterization of the Soluble All-Carbon Molecules C₆₀ And C₇₀. *Journal of Physical Chemistry* **1990**, *94*, (24), 8630-8633.
40. Gasyna, Z.; Schatz, P. N.; Hare, J. P.; Dennis, T. J.; Kroto, H. W.; Taylor, R.; Walton, D. R. M., The Magnetic Circular-Dichroism and Absorption-Spectra of C₆₀ Isolated in Ar Matrices. *Chemical Physics Letters* **1991**, *183*, (3-4), 283-291.
41. Leach, S.; Vervloet, M.; Despres, A.; Breheret, E.; Hare, J. P.; Dennis, T. J.; Kroto, H. W.; Taylor, R.; Walton, D. R. M., Electronic-Spectra and Transitions of the Fullerene C-60. *Chemical Physics* **1992**, *160*, (3), 451-466.
42. Neretin, I. S.; Slovokhotov, Yu. L.; Chemical Crystallography of Fullerenes. *Russ. Chem. Rev.* **2004**, *73*, 455 – 486.
43. Epple, L.; Amsharov, K.; Simeonov, K.; Dix, I.; Jansen, M., Crystallographic Characterization and Identification of a Minor Isomer of C-84 Fullerene. *Chemical Communications* **2008**, (43), 5610-5612.
44. Neretin, I. S.; Lyssenko, K. A.; Antipin, M. Y.; Slovokhotov, Y. L.; Boltalina, O. V.; Troshin, P. A.; Lukonin, A. Y.; Sidorov, L. N.; Taylor, R., C₆₀F₁₈, a Flattened Fullerene: Alias a Hexa-Substituted Benzene. *Angewandte Chemie-International Edition* **2000**, *39*, (18), 3273.
45. Troyanov, S. I.; Boltalina, O. V.; Kouvytchko, I. V.; Troshin, P. A.; Kemnitz, E.; Hitchcock, P. B.; Taylor, R., Molecular and Crystal Structure of the Adducts of C₆₀F₁₈

with Aromatic Hydrocarbons. *Fullerenes Nanotubes and Carbon Nanostructures* **2002**, *10*, (3), 243-259.

46. Goldt, I. V.; Boltalina, O. V.; Sidorov, L. N.; Kemnitz, E.; Troyanov, S. I., Preparation and Crystal Structure of Solvent Free C₆₀F₁₈. *Solid State Sciences* **2002**, *4*, (11-12), 1395-1401.

47. Hubschle, C. B.; Scheins, S.; Weber, M.; Luger, P.; Wagner, A.; Koritsanszky, T.; Troyanov, S. I.; Boltalina, O. V.; Goldt, I. V., Bond Orders and Atomic Properties of the Highly Deformed Halogenated Fullerenes C₆₀F₁₈ and C₆₀Cl₃₀ Derived from Their Charge Densities. *Chemistry-A European Journal* **2007**, *13*, (7), 1910-1920.

48. Hitchcock, P. B.; Taylor, R., Single Crystal X-ray Structure of Tetrahedral C₆₀F₃₆: the Most Aromatic and Distorted Fullerene. *Chemical Communications* **2002**, (18), 2078-2079.

49. Troyanov, S. I.; Troshin, P. A.; Boltalina, O. V.; Ioffe, I. N.; Sidorov, L. N.; Kemnitz, E., Two isomers of C₆₀F₄₈: An Indented Fullerene. *Angewandte Chemie-International Edition* **2001**, *40*, (12), 2285.

50. Shustova, N. B.; Chernyshev, D. Y.; Troyanov, S. I., Crystal Structure of C₆₀C₁₆ Prepared by a Reaction of C-60 with POCl₃. *Mendeleev Communications* **2006**, (4), 209-210.

51. Birkett, P. R.; Avent, A. G.; Darwish, A. D.; Kroto, H. W.; Taylor, R.; Walton, D. R. M., Preparation and C-13 NMR Spectroscopic Characterization of C₆₀Cl₆. *Journal of the Chemical Society-Chemical Communications* **1993**, (15), 1230-1232.

52. Shustova, N. B.; Popov, A. A.; Sidorov, L. N.; Turnbull, A. P.; Kemnitz, E.; Troyanov, S. I., Preparation and Crystallographic Characterization of C₆₀Cl₂₄. *Chemical Communications* **2005**, (11), 1411-1413.

53. Troyanov, S. I.; Shustova, N. B.; Popov, A. A.; Sidorov, L. N., Synthesis and Structures of C-60 Fullerene Chlorides. *Russian Chemical Bulletin* **2005**, *54*, (7), 1656-1666.

54. Troyanov, S. I.; Shustova, N. B.; Popov, A. A.; Sidorov, L. N.; Kemnitz, E., Preparation and Structural Characterization of Two Kinetically Stable Chlorofullerenes, C₆₀Cl₂₈ and C₆₀Cl₃₀. *Angewandte Chemie-International Edition* **2005**, *44*, (3), 432-435.

55. Troshin, P. A.; Lyubovskaya, R. N.; Ioffe, I. N.; Shustova, N. B.; Kemnitz, E.; Troyanov, S. Z., Synthesis and Structure of the Highly Chlorinated [60] Fullerene $C_{60}Cl_{30}$ with a Drum-Shaped Carbon Cage. *Angewandte Chemie-International Edition* **2005**, *44*, (2), 234-237.
56. Birkett, P. R.; Hitchcock, P. B.; Kroto, H. W.; Taylor, R.; Walton, D. R. M., Preparation and Characterization of $C_{60}Br_6$ and $C_{60}Br_8$. *Nature* **1992**, *357*, (6378), 479-481.
57. Troyanov, S. I.; Troshin, P. A.; Boltalina, O. V.; Kemnitz, E., Bromination of [60] Fullerene. II. Crystal and Molecular Structure of [60] Fullerene Bromides, $C_{60}Br_6$, $C_{60}Br_8$, and $C_{60}Br_{24}$. *Fullerenes Nanotubes and Carbon Nanostructures* **2003**, *11*, (1), 61-77.
58. Troshin, P. A.; Kemnitz, E.; Troyanov, S. I., Characterization of Reactions of Fullerene C-60 with Bromine. Crystal Structures of Bromofullerenes $C_{60}Br_6$, $C_{60}Br_6$ Center Dot CS_2 , $C_{60}Br_8$ Center Dot $CHBr_3$ Center Dot $2Br(2)$ and $C_{60}Br_{24}$ Center Dot $C_6H_4Cl_2$ Center Dot Br_2 . *Russian Chemical Bulletin* **2004**, *53*, (12), 2787-2792.
59. Troyanov, S. I., Investigation of the Structure of C-60 Fullerene Halides by the Neutron and Synchrotron Diffraction Methods. *Crystallography Reports* **2006**, *51*, (5), 761-766.
60. Tebbe, F. N.; Harlow, R. L.; Chase, D. B.; Thorn, D. L.; Campbell, G. C.; Calabrese, J. C.; Herron, N.; Young, R. J.; Wasserman, E., Synthesis and Single-Crystal X-Ray Structure of a Highly Symmetrical C-60 Derivative, $C_{60}Br_{24}$. *Science* **1992**, *256*, (5058), 822-825.
61. Hitchcock, P. B.; Avent, A. G.; Martsinovich, N.; Troshin, P. A.; Taylor, R., C-2 $C_{70}F_{38}$ is Aromatic, Contains Three Planar Hexagons, and has Equatorial Addends. *Chemical Communications* **2005**, (1), 75-77.
62. Burtsev, A. V.; Kemnitz, E.; Troyanov, S. I., Synthesis and Structure of Fullerene Halides $C_{70}X_{10}$ (X = Br, Cl) and $C_{78}Cl_{18}$. *Crystallography Reports* **2008**, *53*, (4), 639-644.
63. Troyanov, S. I.; Popov, A. A., A [70] Fullerene Chloride, $C_{70}Cl_{16}$, Obtained by the Attempted Bromination of C-70 in $TiCl_4$. *Angewandte Chemie-International Edition* **2005**, *44*, (27), 4215-4218.

64. Troyanov, S. I.; Shustova, N. B.; Ioffe, I. N.; Turnbull, A. P.; Kemnitz, E., Synthesis and Structural Characterization of Highly Chlorinated C-70, $C_{70}Cl_{28}$. *Chemical Communications* **2005**, (1), 72-74.
65. Troyanov, S. I.; Popov, A. A.; Denisenko, N. I.; Boltalina, O. V.; Sidorov, L. N.; Kemnitz, E., The First X-ray Crystal Structures of Halogenated [70]Fullerene: $C_{70}Br_{10}$ and $C_{70}Br_{10}.3Br(2)$. *Angewandte Chemie-International Edition* **2003**, *42*, (21), 2395-2398.
66. Simeonov, K. S.; Amsharov, K. Y.; Jansen, M., Connectivity of the Chiral D-2-Symmetric Isomer of C-76 through a Crystal-Structure Determination $C_{76}Cl_{18}.TiCl_4$. *Angewandte Chemie-International Edition* **2007**, *46*, 8419-8421.
67. Simeonov, K. S.; Amsharov, K. Y.; Jansen, M., Chlorinated Derivatives of C_{78} -Fullerene Isomers with Unusually Short Intermolecular Halogen-Halogen Contacts. *Chemistry-A European Journal* **2008**, *14*, 9585-9590.
68. Simeonov, K. S.; Amsharov, K. Y.; Krokos, E.; Jansen, M., An Epilog on the C_{78} -Fullerene Family: The Discovery and Characterization of an Elusive Isomer. *Angewandte Chemie-International Edition* **2008**, *47*, 2283-6285.
69. Troyanov, S. I.; Kemnitz, E., Synthesis and Structures of Fullerene Bromides and Chlorides. *European Journal of Organic Chemistry* **2005**, (23), 4951-4962.
70. Simeonov, K. S.; Amsharov, K. Y.; Jansen, M., $C_{80}Cl_{12}$ – A Chlorine Derivative of the Chiral D_2-C_{80} Isomer: Empirical Rationale of Halogen Atoms Addition Pattern. *Chemistry-A European Journal* **2008**, *14*, xxxx-xxxx.
71. Hennrich, F. H.; Michel, R. H.; Fischer, A.; RichardSchneider, S.; Gilb, S.; Kappes, M. M.; Fuchs, D.; Burk, M.; Kobayashi, K.; Nagase, S., Isolation and Characterization of C-80. *Angewandte Chemie-International Edition in English* **1996**, *35*, (15), 1732-1734.
72. Dennis, T. J. S.; Kai, T.; Asato, K.; Tomiyama, T.; Shinohara, H.; Yoshida, T.; Kobayashi, Y.; Ishiwatari, H.; Miyake, Y.; Kikuchi, K.; Achiba, Y., Isolation and Characterization by C-13 NMR Spectroscopy of [84] Fullerene Minor Isomers. *Journal of Physical Chemistry A* **1999**, *103*, (44), 8747-8752.

73. Tagmatarchis, N.; Avent, A. G.; Prassides, K.; Dennis, T. J. S.; Shinohara, H., Separation, Isolation and Characterisation of Two Minor Isomers of the [84]Fullerene C-84. *Chemical Communications* **1999**, (11), 1023-1024.
74. Shustova, N. B.; Newell, B. S.; Miller, S. M.; Anderson, O. P.; Bolskar, R. D.; Seppelt, K.; Popov, A. A.; Boltalina, O. V.; Strauss, S. H., Discovering and Verifying Elusive Fullerene Cage Isomers: Structures of C-2-p(11)-(C-74-D-3h)(CF₃)(12) and C-2-p(11)-(C-78-D-3h(5))(CF₃)(12). *Angewandte Chemie-International Edition* **2007**, *46*, (22), 4111-4114.
75. Kareev, I. E.; Kuvychko, I. V.; Shustova, N. B.; Lebedkin, S. F.; Bubnov, V. P.; Anderson, O. P.; Popov, A. A.; Boltalina, O. V.; Strauss, S. H., C-1-(C-84-C-2(11))(CF₃)(12): Trifluoromethylation Yields Structural Proof of a Minor C-84 Cage and Reveals a Principle of Higher Fullerene Reactivity. *Angewandte Chemie-International Edition* **2008**, *47*, (33), 6204-6207.
76. Crassous, J.; Rivera, J.; Fender, N. S.; Shu, L. H.; Echegoyen, L.; Thilgen, C.; Herrmann, A.; Diederich, F., Chemistry of C-84: Separation of Three Constitutional Isomers and Optical Resolution of D-2-C-84 by Using the "Bingel-retro-Bingel" Strategy. *Angewandte Chemie-International Edition* **1999**, *38*, (11), 1613-1617.
77. Kareev, I. E.; Popov, A. A.; Kuvychko, I. V.; et al., Synthesis and X-ray or NMR/DFT Structure Elucidation of Twenty One New Trifluoromethyl Derivatives of Soluble Cage Isomers of C-76, C-78, C-84, and C-90. *Journal of the American Chemical Society* **2008**, *130*, (40), 13471-13489.
78. Shustova, N. B.; Kuvychko, I. V.; Bolskar, R. D.; Seppelt, K.; Strauss, S. H.; Popov, A. A.; Boltalina, O. V., Trifluoromethyl Derivatives of Insoluble Small-HOMO-LUMO-Gap Hollow Higher Fullerenes. NMR and DFT Structure Elucidation of C-2-(C-74-D-3h)(CF₃)(12), C-s-(C-76-T-d(2))(CF₃)(12), C-2-(C-78-D-3h(5))(CF₃)(12), C-s-(C-80-C-2v(5)) (CF₃)(12), and C-2-(C-82-C-2(5))(CF₃)(12). *Journal of the American Chemical Society* **2006**, *128*, (49), 15793-15798.
79. Kikuchi, K.; Nakahara, N.; Wakabayashi, T.; Honda, M.; Matsumiya, H.; Moriwaki, T.; Suzuki, S.; Shiromaru, H.; Saito, K.; Yamauchi, K.; Ikemoto, I.; Achiba, Y., Isolation and Identification of Fullerene Family - C-76, C-78, C-82, C-84, C-90 and C-96. *Chemical Physics Letters* **1992**, *188*, (3-4), 177-180.

- 80.** Kobayashi, K.; Nagase, S., Structures and Electronic States of M@C-82 (M = Sc, Y, La and lanthanides). *Chemical Physics Letters* **1998**, 282, (3-4), 325-329.
- 81.** Kubozono, Y.; Rikiishi, Y.; Shibata, K.; Hosokawa, T.; Fujiki, S.; Kitagawa, H., Structure and Transport Properties of Isomer-Separated C-82. *Physical Review B* **2004**, 69, 165412-7.
- 82.** Sheldrick, G. M., SHELXTL DOS/Windows/NT, version 6.14; Bruker Analytical X-Ray Instruments, Inc.: Madison, WI, **1997**.
- 83.** Frisch, M. J.; et al., Gaussian 03, revision C 02; Gaussian, Inc.: Wallingford, CT, **2004**.
- 84.** Thilgen, C.; Diederich, F., Structural Aspects of Fullerene Chemistry - A Journey through Fullerene Chirality. *Chemical Reviews* **2006**, 106, (12), 5049-5135.
- 85.** Cozzi, F.; Powell, W. H.; Thilgen, C., Numbering of Fullerenes - (IUPAC Recommendations 2005). *Pure and Applied Chemistry* **2005**, 77, (5), 843-923.
- 86.** Toda, F., Naphthocyclobutenes and Benzodicyclobutadienes: Synthesis in the Solid State and Anomalies in the Bond Lengths. *European Journal of Organic Chemistry* **2000**, (8), 1377-1386.
- 87.** Colt, J. R.; Scuseria, G. E., An Abinitio Study of the C-78 Fullerene Isomers. *Chemical Physics Letters* **1992**, 199, (6), 505-512.
- 88.** Schleyer, P. V.; Jiao, H. J., What is Aromaticity? *Pure and Applied Chemistry* **1996**, 68, (2), 209-218.
- 89.** Schleyer, P. V.; Freeman, P. K.; Jiao, H. J.; Goldfuss, B., Aromaticity and Antiaromaticity in 5-Membered C(4)H(4)X Ring-Systems - Classical and Magnetic Concepts may not be Orthogonal. *Angewandte Chemie-International Edition In English* **1995**, 34, (3), 337-340.
- 90.** Wang, C. R., Dennis, T. John S, Inakuuma, M; Shinohara, H. Production, Isolation and Characterization of a New C80 Isomer, *Proceedings Electrochemical Society*, Nagoya University, Japan, **1998**; 1023-1030.
- 91.** Wang, C. R.; Sugai, T.; Kai, T.; Tomiyama, T.; Shinohara, H., Production and Isolation of an Ellipsoidal C-80 Fullerene. *Chemical Communications* **2000**, (7), 557-558.

- 92.** Haddon, R. C., Hybridization and the Orientation and Alignment of Pi-Orbitals in Nonplanar Conjugated Organic-Molecules - Pi-Orbital Axis Vector Analysis (Poav2). *Journal of the American Chemical Society* **1986**, *108*, (11), 2837-2842.
- 93.** Haddon, R. C., Chemistry Of The Fullerenes - The Manifestation of Strain in a Class of Continuous Aromatic-Molecules. *Science* **1993**, *261*, (5128), 1545-1550.
- 94.** Hirsch, A.; Brettreich, M., Fullerenes - Chemistry and Reactions, *Wiley-VCH*, Weinheim **2005**.
- 95.** Thilgen, C.; Herrmann, A.; Diederich, F., The Covalent Chemistry of Higher Fullerenes: C-70 and beyond. *Angewandte Chemie-International Edition* **1997**, *36*, (21), 2269-2280.
- 96.** Herrmann, A.; Diederich, F.; Thilgen, C.; Termeer, H. U.; Muller, W. H., Chemistry of the Higher Fullerenes - Preparative Isolation of C-76 by HPLC and Synthesis, Separation, and Characterization of Diels-Alder Monoadducts of C₇₀ and C₇₆. *Helvetica Chimica Acta* **1994**, *77*, (7), 1689-1706.
- 97.** Hazell, A. C.; Lehmann, M. S.; Larsen, F. K., Neutron-Diffraction Study of Crystal-Structure of Pyrene, C₁₆H₁₀. *Acta Crystallographica Section B-Structural Crystallography and Crystal Chemistry* **1972**, *B 28*, (OCT15), 2977-2984.
- 98.** Grineva, O. V.; Zorky, P. M., Analysis of Molecular Cl...Cl Interactions in Pentachlorobezene and Hexachlorobenzene Crystals. *Crystallography Reports* **2000**, *45*, (4), 633-639.
- 99.** Desiraju, G. R.; Parthasarathy, R., The Nature of Halogen. Halogen Interactions - are Short Halogen Contacts Due to Specific Attractive Forces or Due to Close Packing of Nonspherical Atoms. *Journal of the American Chemical Society* **1989**, *111*, (23), 8725-8726.
- 100.** Ramasubbu, N.; Parthasarathy, R.; Murrayrust, P., Angular Preferences of Intermolecular Forces around Halogen Centers - Preferred Directions of Approach of Electrophiles and Nucleophiles around the Carbon Halogen Bond. *Journal of the American Chemical Society* **1986**, *108*, (15), 4308-4314.
- 101.** Sakurai, T.; Sundaralingam, M.; Jeffrey, G. A., A Nuclear Quadrupole Resonance and X-Ray Study of Crystal Structure of 2,5-Dichloroaniline. *Acta Crystallographica* **1963**, *16*, (5), 354-&.

- 102.** Nyburg, S. C.; Faerman, C. H., A Revision of Vanderwaals Atomic Radii for Molecular-Crystals - N, O, F, S, Cl, Se, Br and I Bonded to Carbon. *Acta Crystallographica Section B-Structural Science* **1985**, *41*, (AUG), 274-279.
- 103.** Price, S. L.; Stone, A. J.; Lucas, J.; Rowland, R. S.; Thornley, A. E., The Nature of Cl...Cl- Intermolecular Interactions. *Journal of the American Chemical Society* **1994**, *116*, (11), 4910-4918.
- 104.** Politzer, P.; Lane, P.; Concha, M. C.; Ma, Y. G.; Murray, J. S., An Overview of Halogen Bonding. *Journal of Molecular Modeling* **2007**, *13*, (2), 305-311.
- 105.** Brisdon, A. K., Halogens and Noble Gases. *Annual Reports on the Progress of Chemistry, Sect. A - Inorganic Chemistry* **2005**, *101*, 128-138.
- 106.** Metrangolo, P.; Neukirch, H.; Pilati, T.; Resnati, G., Halogen Bonding Based Recognition Processes: A World Parallel to Hydrogen Bonding. *Accounts of Chemical Research* **2005**, *38*, (5), 386-395.
- 107.** Fourmigue, M.; Batail, P., Activation of Hydrogen- and Halogen-Bonding Interactions in Tetrathiafulvalene-Based Crystalline Molecular Conductors. *Chemical Reviews* **2004**, *104*, (11), 5379-5418.
- 108.** Ouvrard, C.; Le Questel, J. Y.; Berthelot, M.; Laurence, C., Halogen-Bond Geometry: a Crystallographic Database Investigation of Dihalogen Complexes. *Acta Crystallographica Section B-Structural Science* **2003**, *59*, 512-526.
- 109.** Lommerse, J. P. M.; Stone, A. J.; Taylor, R.; Allen, F. H., The Nature and Geometry of Intermolecular Interactions between Halogens and Oxygen or Nitrogen. *Journal of the American Chemical Society* **1996**, *118*, (13), 3108-3116.
- 110.** Lendvay, G., On the Correlation of Bond Order and Bond Length. *Journal of Molecular Structure-Theochem* **2000**, *501*, 389-393.
- 111.** Paolini, J. P., The Bond Order Bond Length Relationship. *Journal of Computational Chemistry* **1990**, *11*, (10), 1160-1163.
- 112.** Anno, T.; Sado, A., Further Note on the Calculation of Bond Lengths of Carbon-Chlorine Bonds. *Journal of Chemical Physics* **1956**, *25*, (1), 176-177.
- 113.** Dunand, A.; Gerdil, R., X-Ray Structure and Crystal Packing Analysis of Triphenylchloromethane. *Acta Crystallographica Section B-Structural Science* **1982**, *38*, (FEB), 570-575.

7 Appendix

7.1 Isolation of Individual Fullerene Isomers – Chromatograms

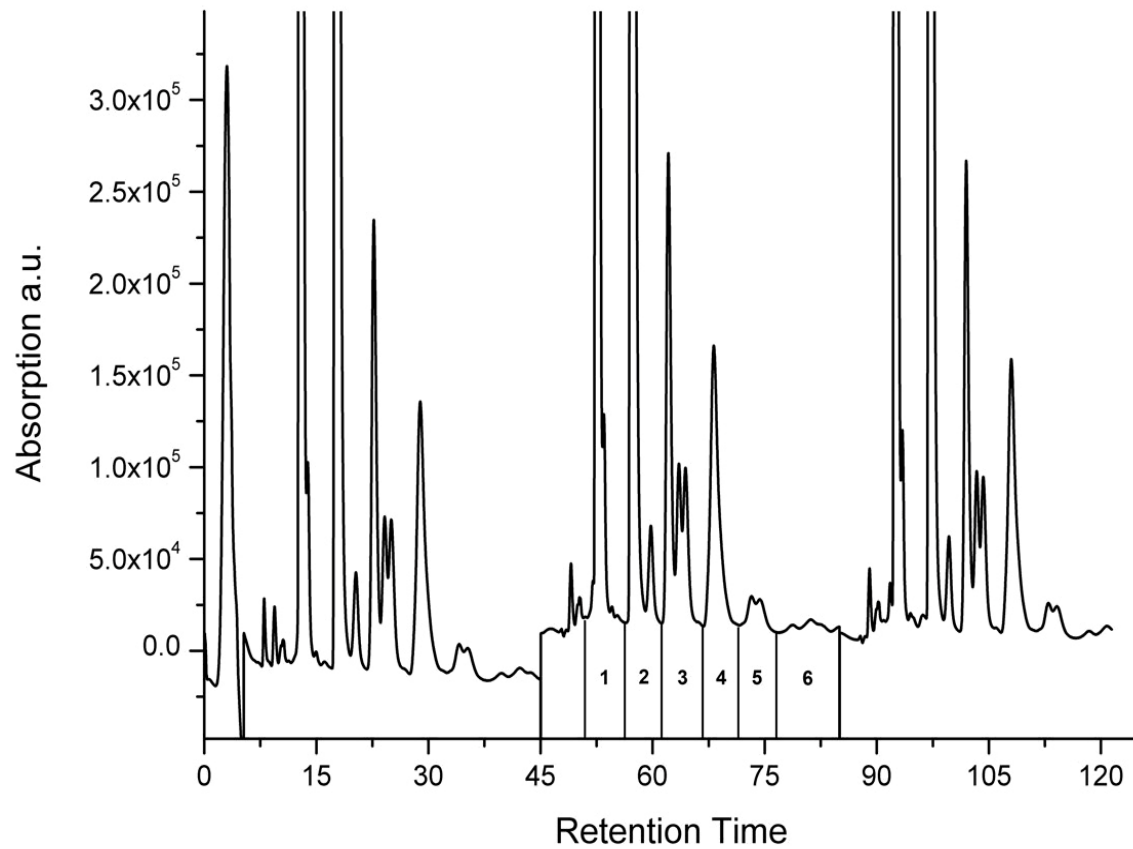


Figure A1 A typical chromatogram showing up three consecutive runs on the fully automated preparative HPLC. Fractions: 1) C_{60} and $C_{60}O_x$, 2) C_{70} and $C_{70}O_y$, 3) C_{76} (first peak), C_{78} -fraction, 4) Major C_{84} -fraction (one D_2 , one D_{2d} , two C_s , one C_2 and one unidentified isomer) 5) C_{86} and two C_{84} isomers (one D_2 and one D_{2d}) 6) Fraction of higher fullerenes (mixture)

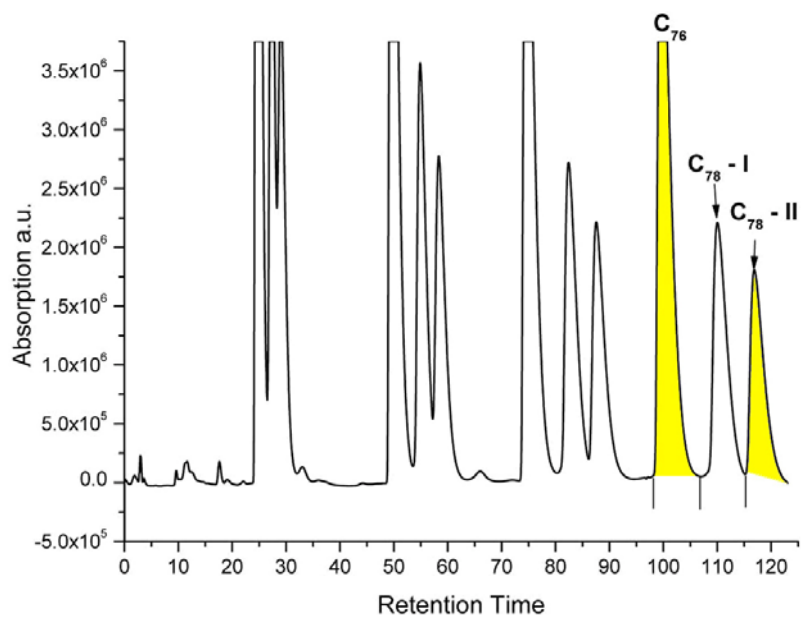


Figure A2 A chromatogram presenting the recycling stage HPLC for C_{76} , C_{78} (subfraction I containing isomers 1 and 2) and $C_{78}(3)$ (subfraction II). The pure species are highlighted.

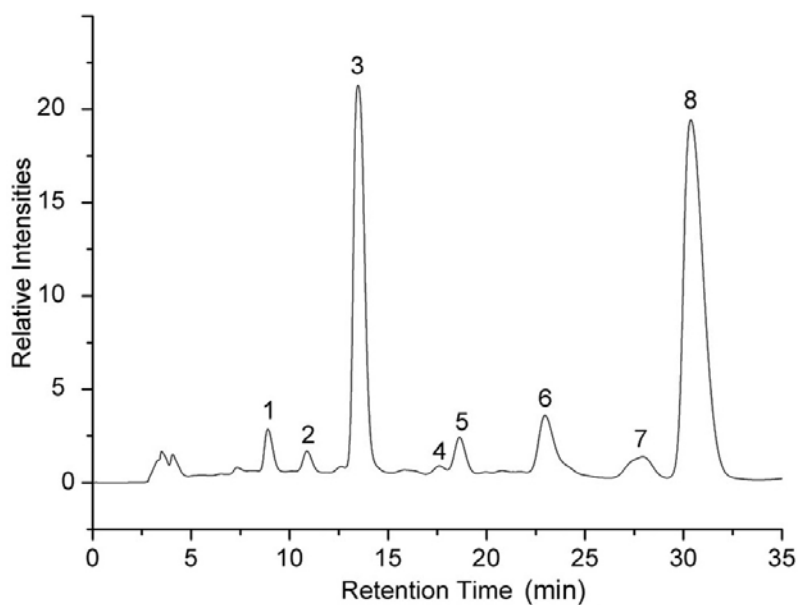


Figure A3 A chromatogram showing the distribution of peaks originating from the different chlorine derivatives of $C_{78}(1)$ and $C_{78}(2)$ upon reacting C_{78} -subfraction I with ICl

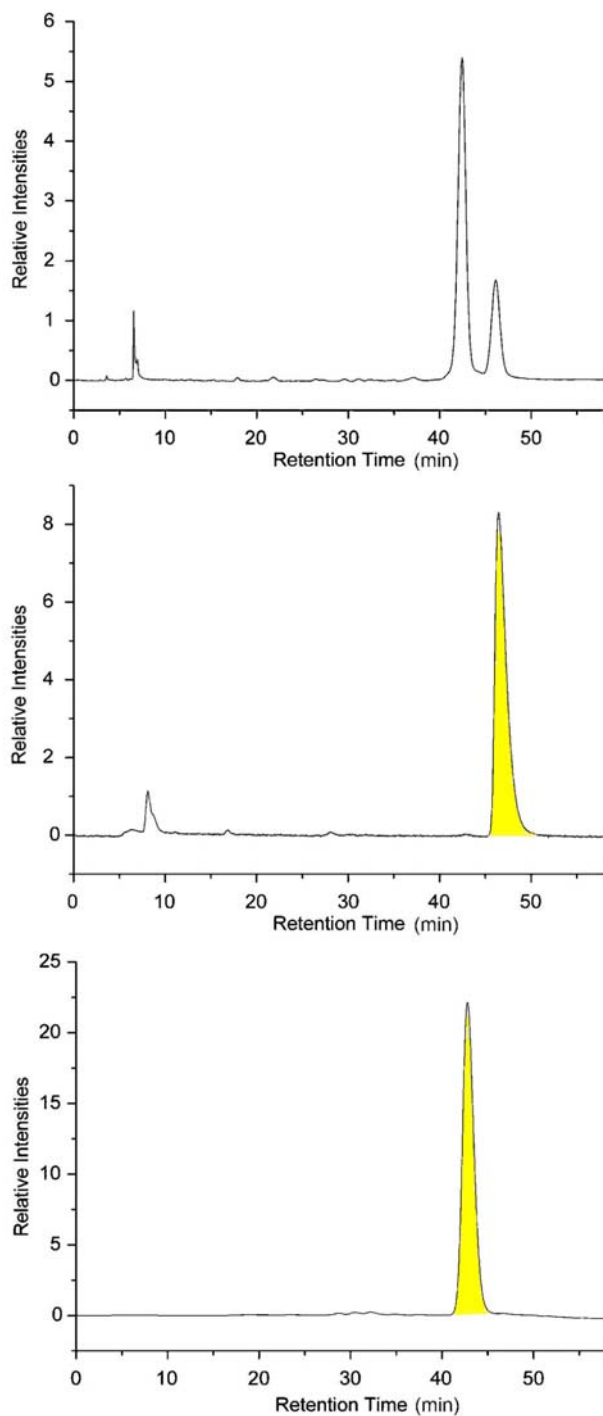


Figure A4 Chromatogram presenting the successful separation between C₇₈ isomers 1 and 2 achieved through their chemical modification (with ICl) and the subsequent retrieval of the parent species by thermal dissociation of their respective chlorine derivatives. Pure C₇₈(1) (middle chromatogram) and C₇₈(2) (bottom chromatogram) are chromatographed on C₁₈-column for confirmation (see the top chromatogram presenting a mixture of the isomers)

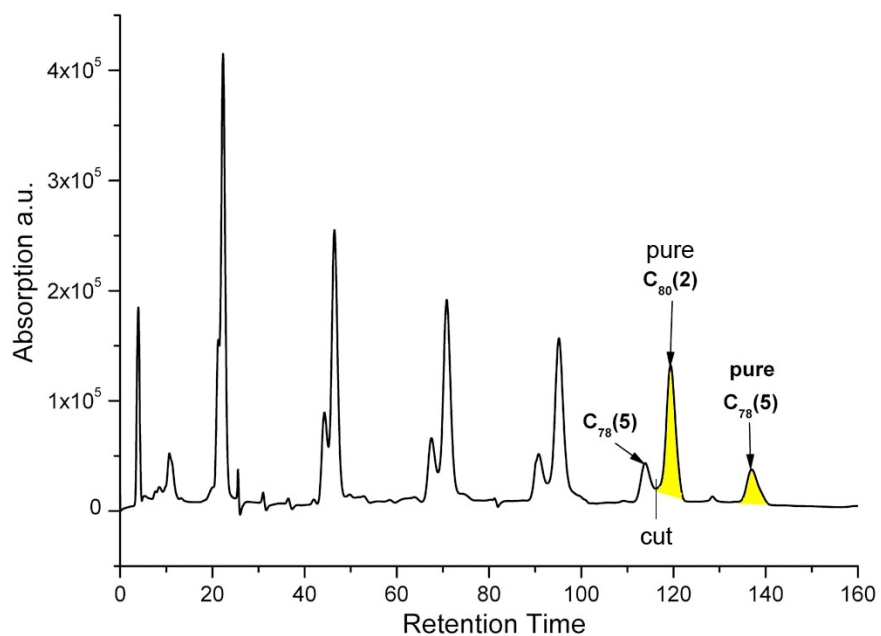


Figure A5 A chromatogram presenting the recycling HPLC for isolation of $C_{78}(5)$ and $C_{80}(2)$. The pure fractions are collected separately. The individual peaks corresponding to a pure fraction are highlighted

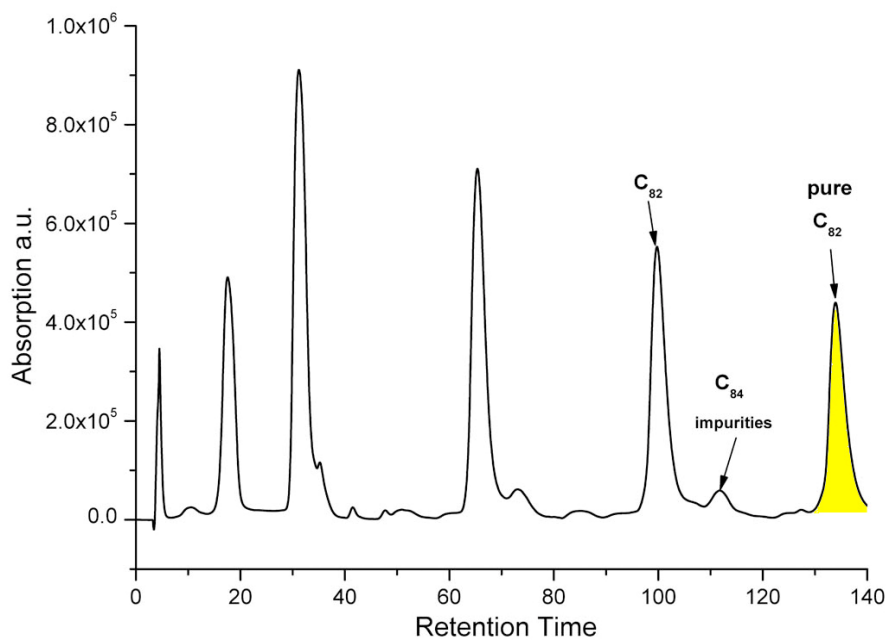


Figure A6 A chromatogram presenting the recycling HPLC for isolation of C_2 - C_{82} . The pure fraction is highlighted

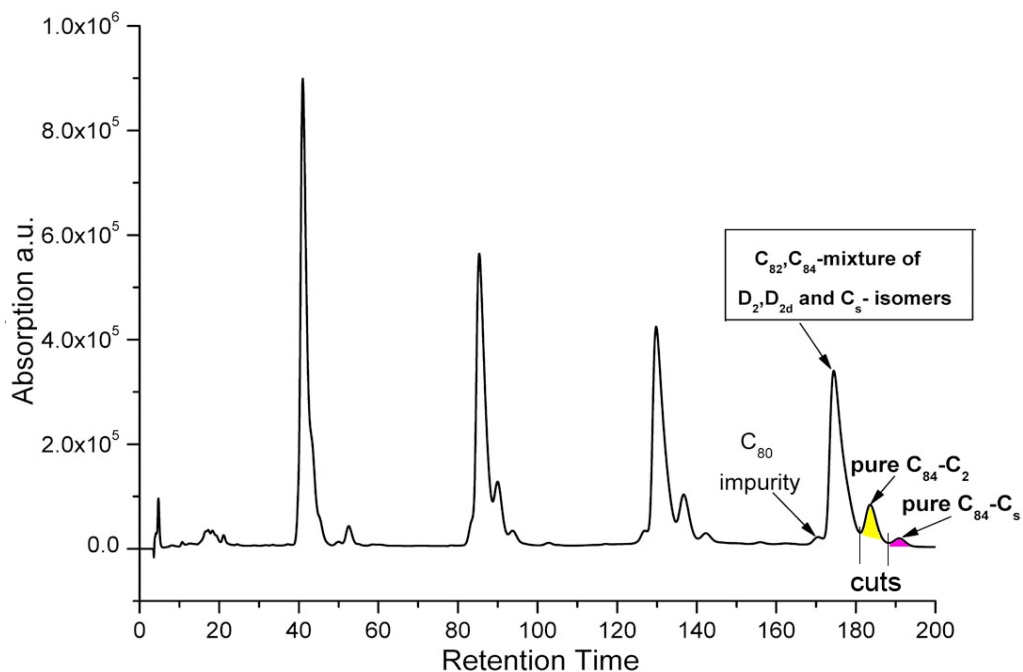


Figure A7 A chromatogram showing the recycling HPLC for isolation of C_2 - C_{84} and C_s - C_{84} (14) isomers. The pure fractions are highlighted in yellow and purple, respectively. The dominant fraction corresponds to the inseparable mixture of three other isomers of C_{84} - D_2 and D_{2d} isomers and C_s .

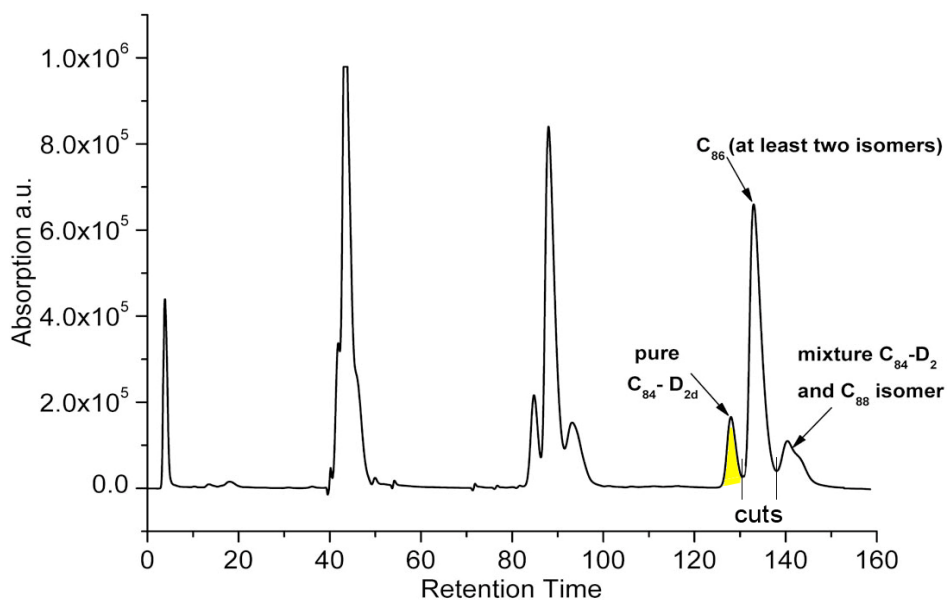


Figure A8 A chromatogram showing the recycling HPLC for isolation of D_{2d} - C_{84} isomer. The pure fraction is highlighted in yellow. The fraction of D_2 - C_{84} is collected for further purification

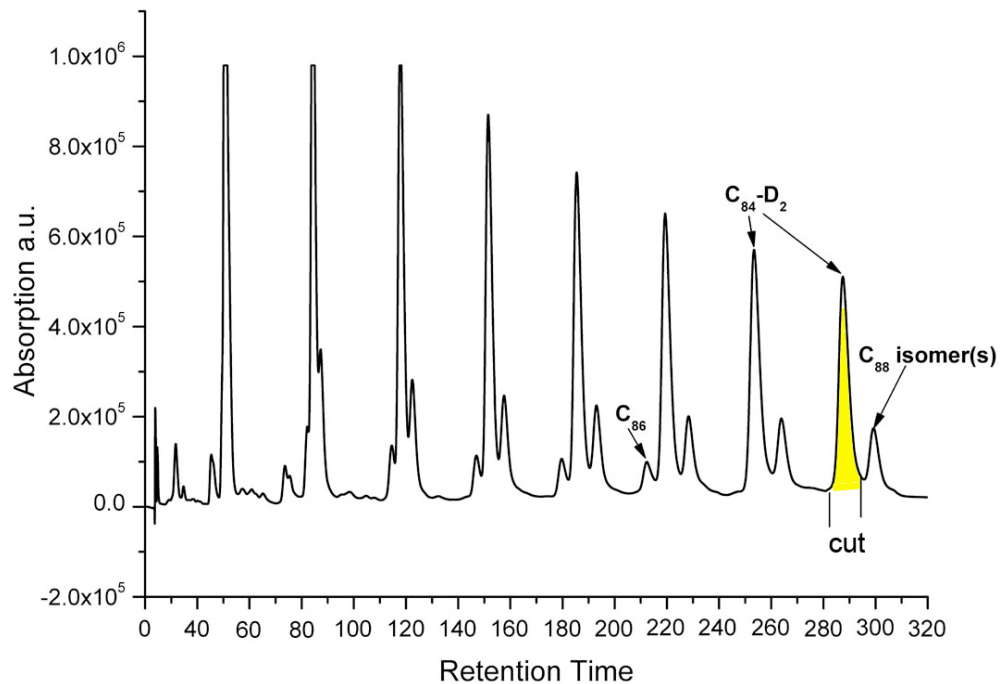


Figure A9 A chromatogram showing the recycling HPLC for isolation of D_2-C_{84} isomer. The pure fraction is highlighted

7.2 UV/VIS Spectra

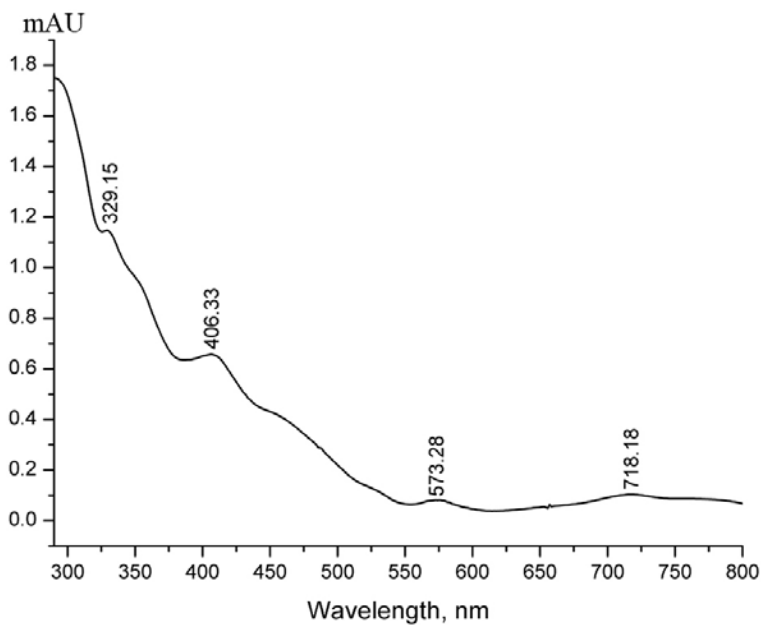


Figure A10 UV/VIS spectrum of $C_{76}(1)$ in toluene

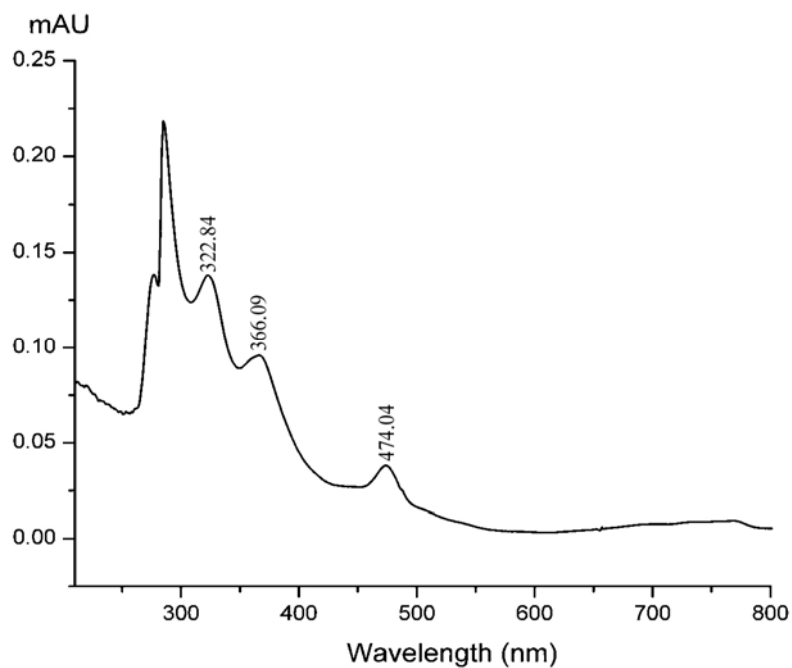


Figure A11 UV/VIS spectrum of C₇₈(1) in toluene

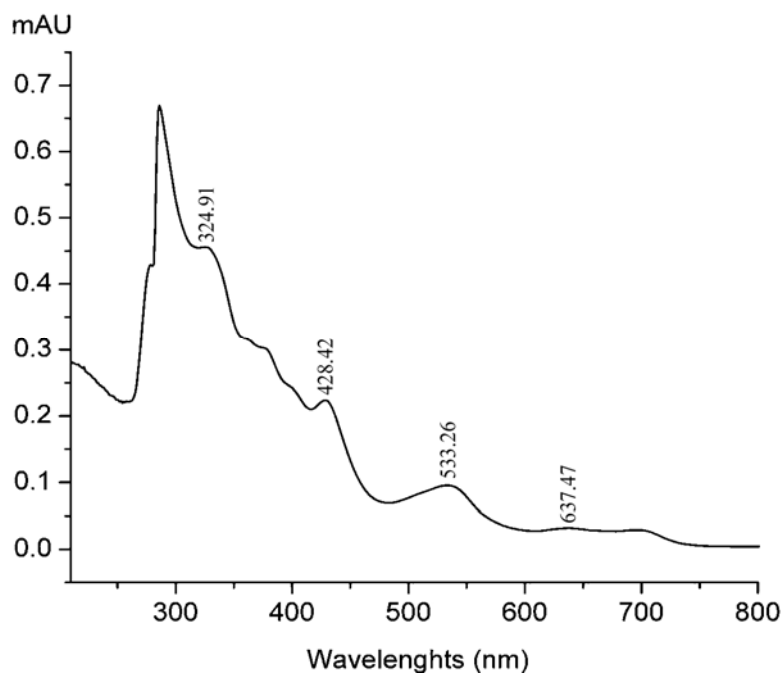


Figure A12 UV/VIS spectrum of C₇₈(2) in toluene

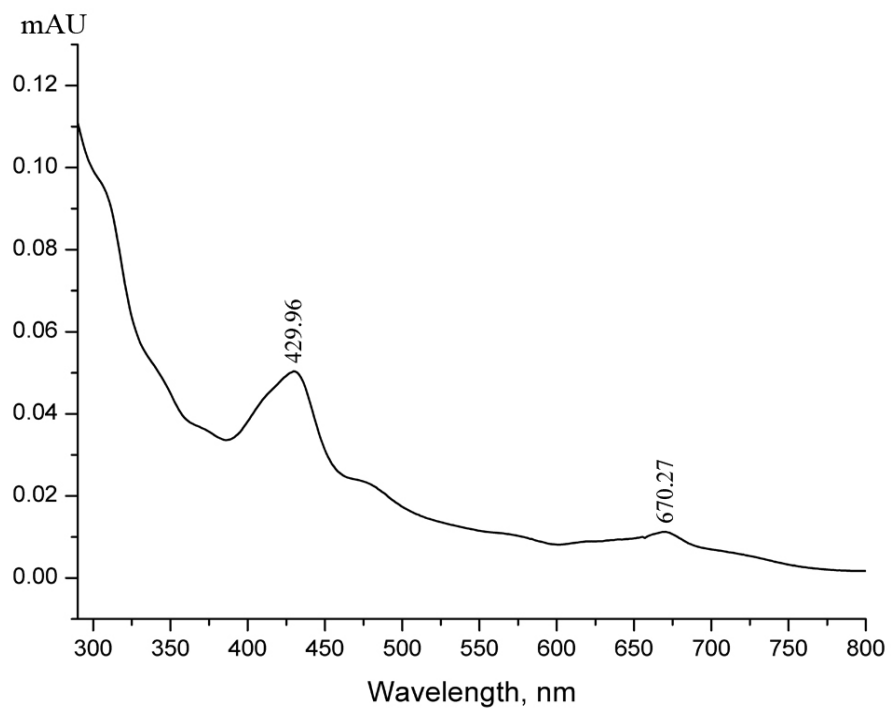


Figure A13 UV/VIS spectrum of C₇₈(3) in toluene

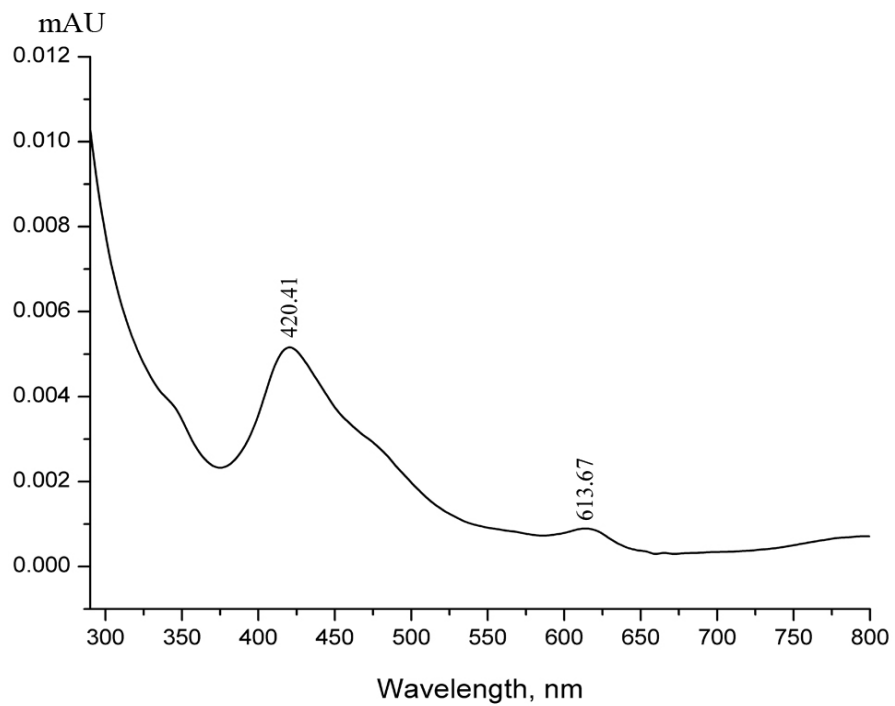


Figure A14 UV/VIS spectrum of C₇₈(5) in toluene

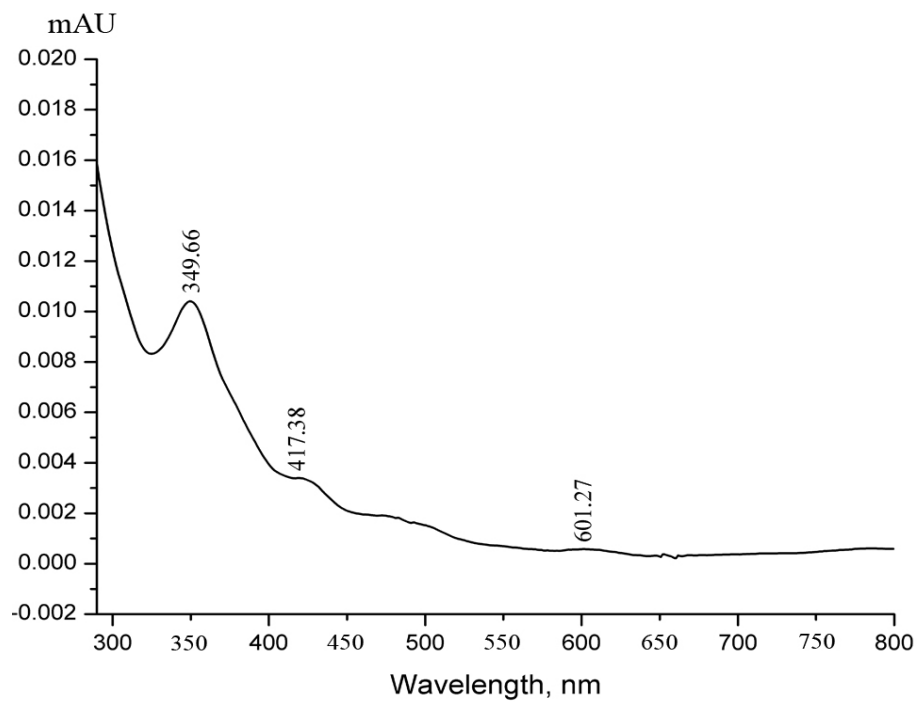


Figure A15 UV/VIS spectrum of C₈₀(2) in toluene

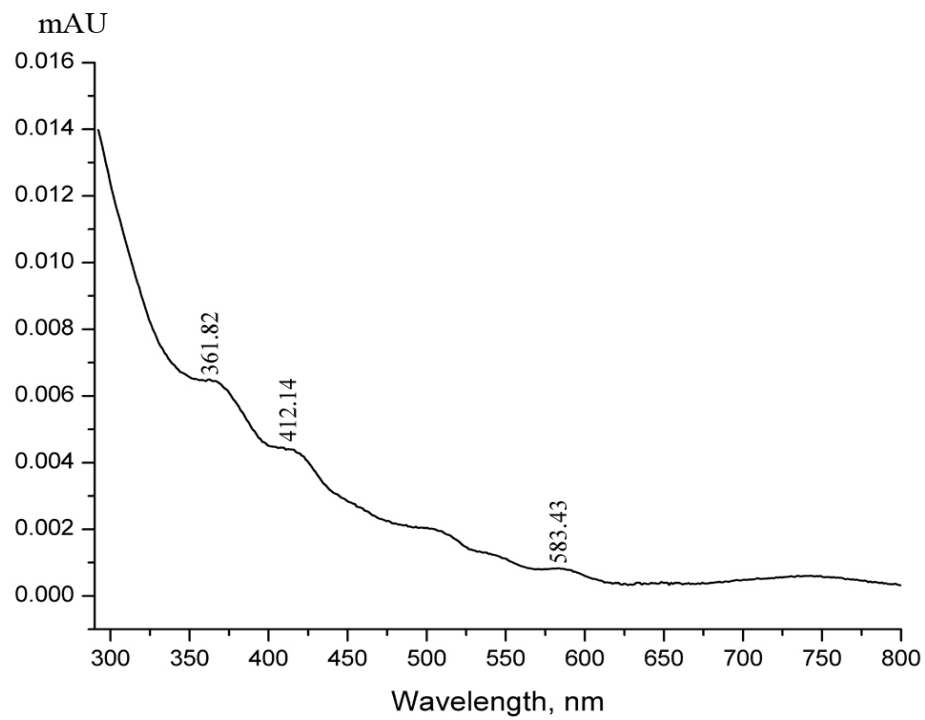


Figure A16 UV/VIS spectrum of C₂-C₈₂ in toluene

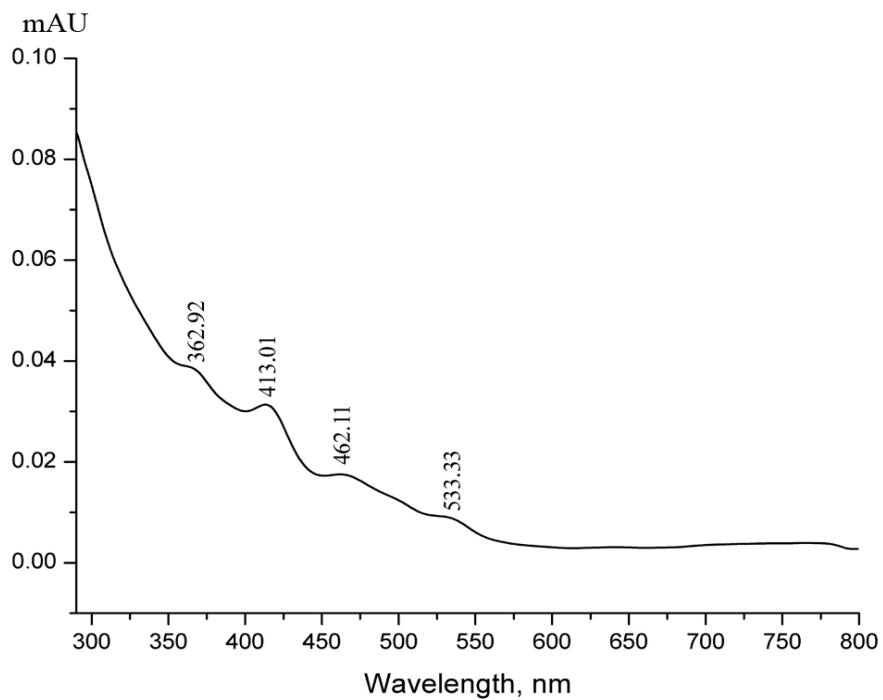


Figure A17 UV/VIS spectrum of C₂-C₈₄ in toluene

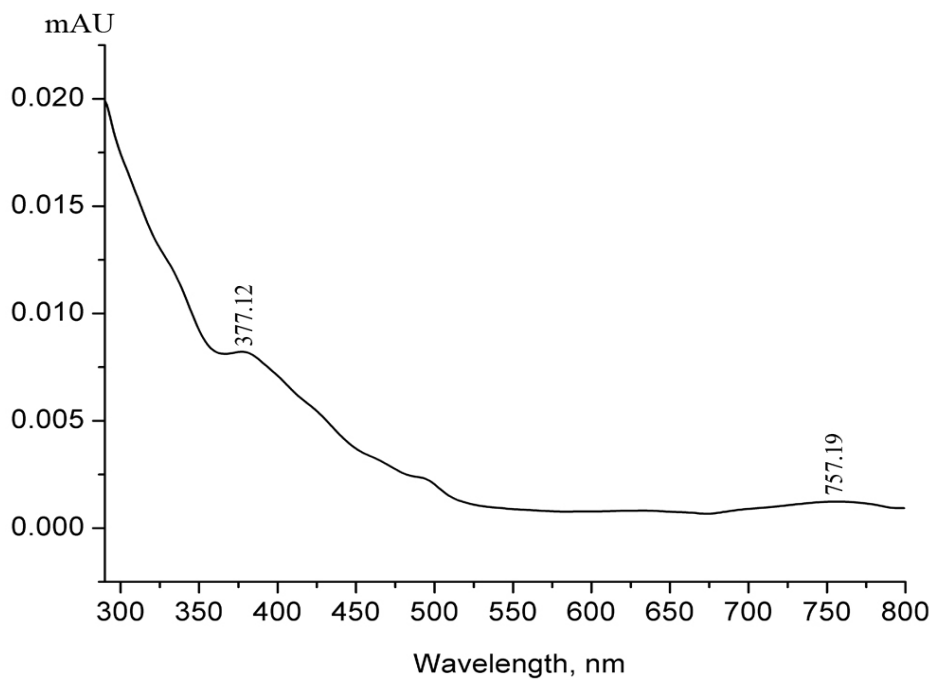


Figure A18 UV/VIS spectrum of C_s-C₈₄ in toluene

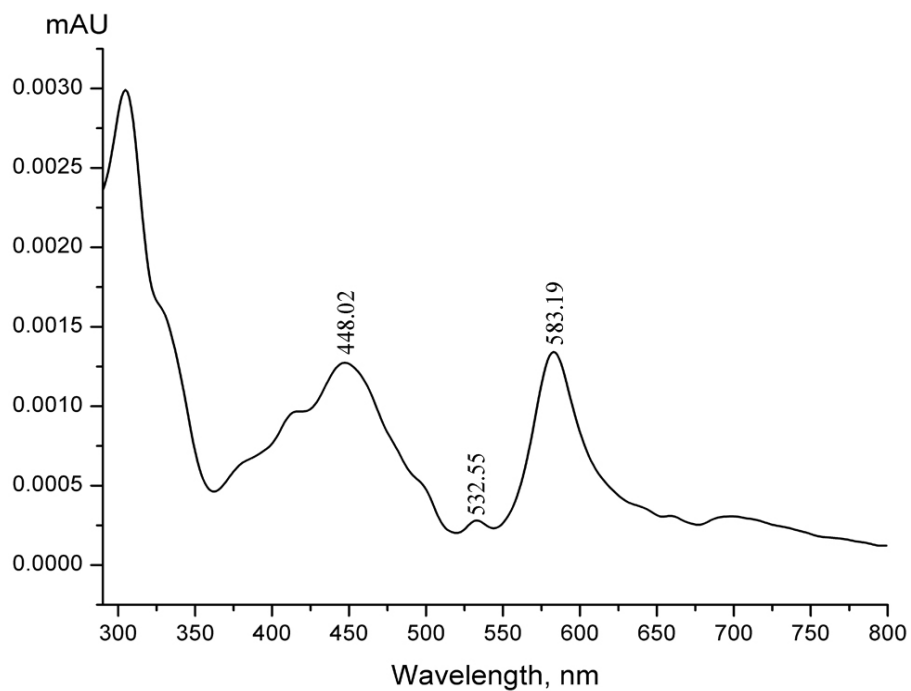


Figure A19 UV/VIS spectrum of D_{2d}-C₈₄ in toluene

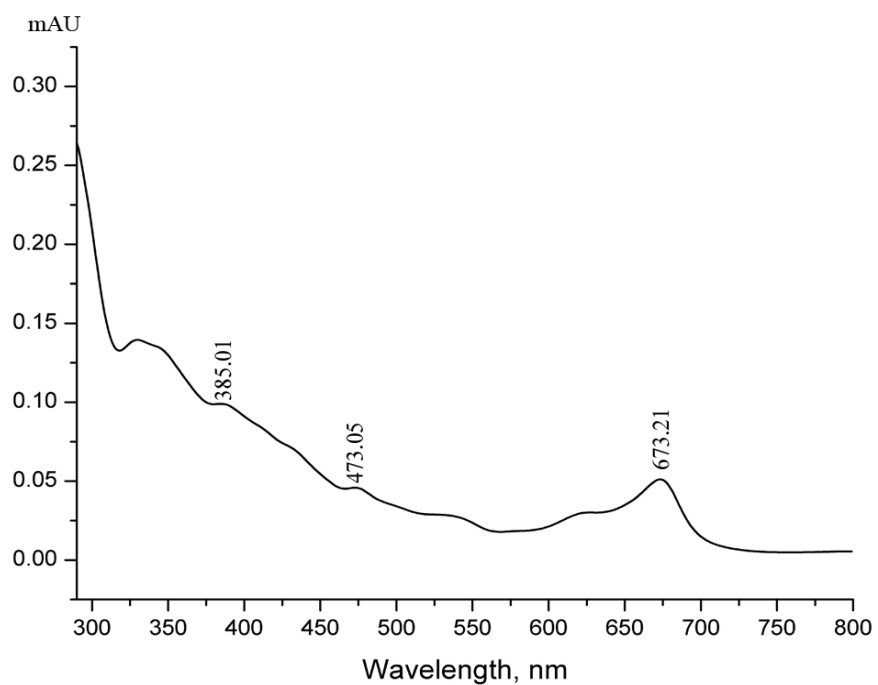


Figure A20 UV/VIS spectrum of D₂-C₈₄ in toluene

8 Acknowledgements

I am truthfully thankful to my supervisor (and advisor) Prof. Dr. Martin Jansen for the help he offered to me throughout the duration of my PhD research in MPI for Solid State Research. He believed in my abilities and gave me the chance to work under his supervision – definitely a great opportunity! Moreover, he has always been at my disposal not only for scientific discussions but also for personal advices. From him I learned the real meaning of the word “motivation”, as well as a valuable package of knowledge.

I would like to thank also my personal supervisor, the leader of the “Fullerene Group” Dr. Konstantin Amsharov for his invaluable help right from the very beginning of my work! Dr. Amsharov is not only a wonderful chemist, but also a great man! He has always been there for me, to give an advice, to help with the work, or even to deal with my temper from time to time! I owe him a great portion of my success as a PhD student. Therefore I must say: “Thank you Kostia for everything”!

I would like to thank Dr. Jürgen Nuss for collecting the X-ray data, Dr. Ulrich Wedig for backing up the experimental results with sound theoretical calculations, Prof. Dr. T. Schleid and Prof. Dr. H. Bertagnolli for being my examiners, and of course all my colleagues for the great three years I spent in Stuttgart.

At last but not least, I want to thank my wife Vanya for being next to me! Thank you Vanya!

9 List of Publications

K. Y. Amsharov, **K. S. Simeonov**, M. Jansen, *Carbon*, **2007**, 45, 337.

K. S. Simeonov, K. Y. Amsharov, M. Jansen, *Angewandte Chemie International Edition*, **2007**, 46, 8419.

K. S. Simeonov, K. Y. Amsharov, E. Krokos, M. Jansen, *Angewandte Chemie International Edition*, **2008**, 47, 33, 6283

K. S. Simeonov, K. Y. Amsharov, M. Jansen, *Chem. Eur J.* **2008**, 14, 9585-9590.

L. Epple, K. Y. Amsharov, **K. S. Simeonov**, I. Dix, M. Jansen, *Chem. Commun.* **2008**, 5610-5612.

K. Simeonov, K. Y. Amsharov, M. Jansen, *Fullerenes, Nanotubes, Carbon Nanostruct.* **2008**:

“A Fast Route towards the Preparative Isolation of Fullerene Isomers – C₇₈(1) and C₇₈(2)” – accepted.

K. Simeonov, K. Y. Amsharov, M. Jansen, *Chem. Eur J.* **2008**:

“C₈₀Cl₁₂ – a Chlorine Derivative of the Chiral D₂-C₈₀ Isomer: Empirical Rationale of Halogen Atoms Addition Pattern” – DOI: 10.1002/chem.200802198.

K. Simeonov, K. Y. Amsharov, M. Jansen, *ECSSC XI – European Conference on Solid State Chemistry*, **2007**: “The Tunnel Crystal Structure of Chlorinated Fullerene C₇₈Cl₁₈”

L. Epple, **K. Simeonov**, K. Y. Amsharov, M. Jansen, *ECSSC XI – European Conference on Solid State Chemistry*, **2007**: “The Crystal Structures of Higher Fullerenes”

K. Simeonov, K. Y. Amsharov, M. Jansen, *NanoteC08 – Nanotechnology in Carbon and Related Materials*, **2008**: “Uncommon Intermolecular Halogen Contacts in Highly Chlorinated Fullerene Derivatives”

K. Simeonov, K. Y. Amsharov, U. Wedig, M. Jansen, *5th European Charge Density Meeting*, **2008**: Gravedona, Italy: “Unusual Short Intermolecular Halogen-Halogen Contacts in Chlorinated Derivatives of Fullerenes”

K. S. Simeonov, K. Y. Amsharov, E. Krokos, U. Wedig, M. Jansen, *44th Symposium on Theoretical Chemistry*, **2008**: Ramsau am Dachstein, Austria: “Unusual Short Intermolecular Halogen-Halogen Contacts in Chlorinated Derivatives of Fullerenes”

10 Curriculum Vitae

Personal

Name	Kalin Stiliyanov Simeonov
Date of birth	23.08.1977
Place of birth	Sofia, Bulgaria
Nationality	Bulgarian
Marital status	married

Educational Background

01/2006 – present	MPI-FKF Stuttgart, PhD Student <u>Doctoral Thesis:</u> Higher Fullerenes-Isolation, Halogenation and Structural Studies
10/1995 – 10/2002	Sofia University St. Kliment Ohridski <u>Master Thesis:</u> Determination of Acetaminophen Levels in Blood Serums of Healthy Volunteers
09/1984-06/1995	Elementary and Secondary School, Sofia